ISTANBUL TECHNICAL UNIVERSITY ★GRADUATE SCHOOL OF SCIENCE ENGINEERING AND TECHNOLOGY

DEVELOPMENT AND CHARACTERIZATION INVESTIGATIONS OF MECHANICALLY ALLOYED AND ACTIVATED SINTERED W-1 WT % Ni MATRIX COMPOSITES REINFORCED WITH TiB_2 AND La_2O_3 PARTICLES

M.Sc. THESIS

Ömer Utku DEMİRKAN

Department of Advanced Technologies

Materials Science and Engineering Programme

NOVEMBER 2011

ISTANBUL TECHNICAL UNIVERSITY ★GRADUATE SCHOOL OF SCIENCE ENGINEERING AND TECHNOLOGY

DEVELOPMENT AND CHARACTERIZATION INVESTIGATIONS OF MECHANICALLY ALLOYED AND ACTIVATED SINTERED W-1 WT % Ni MATRIX COMPOSITES REINFORCED WITH TiB_2 AND La_2O_3 PARTICLES

M.Sc. THESIS

Ömer Utku DEMİRKAN
(521091028)

Department of Advanced Technologies

Materials Science and Engineering Programme

Thesis Advisor: Prof. Dr. M. Lütfi ÖVEÇOĞLU

NOVEMBER 2011

İSTANBUL TEKNİK ÜNİVERSİTESİ ★ FEN BİLİMLERİ ENSTİTÜSÜ

TiB_2 ve La_2O_3 PARTİKÜLLERİ İLE GÜÇLENDİRİLMİŞ W -%1 Ni (AĞIRLIKÇA) MATRİKSLİ KOMPOZİTLERİN MEKANİK ALAŞIMLAMA VE AKTİVE EDİLMİŞ SİNTERLEME YÖNTEMLERİYLE ÜRETİLMESİ VE KARAKTERİZASYONU

YÜKSEK LİSANS TEZİ

Ömer Utku DEMİRKAN
(521091028)

İleri Teknolojiler Anabilim Dalı

Malzeme Bilimi ve Mühendisliği Programı

Tez Danışmanı: Prof. Dr. M. Lütfi ÖVEÇOĞLU

KASIM 2011

Ömer Utku Demirkan, a **M.Sc.** student of ITU **Graduate School of Science, Engineering and Technology** student ID **521091028**, successfully defended the **thesis** entitled "**Development and Characterization Investigations of Mechanically Alloyed and Activated Sintered W-1 wt % Ni Matrix Composites Reinforced with TiB_2 and La_2O_3 Particles**", which he prepared after fulfilling the requirements specified in the associated legislations, before the jury whose signatures are below.

Thesis Advisor : **Prof. Dr. M. Lütfi ÖVEÇOĞLU**
İstanbul Technical University

Jury Members : **Prof. Dr. Şerafettin EROĞLU**
İstanbul University

Assoc. Prof. Dr. Burak ÖZKAL
İstanbul Technical University

Date of Submission : 31 October 2011
Date of Defense : 16 November 2011

FOREWORD

There are many people associated with this thesis deserving recognition. First of all, I would like to thank my supervisor Prof. Dr. M. Lütfi Öveçoğlu for his invaluable guidance, support and training during the course of my thesis and for being my mentor throughout my graduate studies. I would also like to thank Assoc. Prof Dr. Burak Özkal for his guidance and also for keeping his door open and always having an answer. I am also very grateful to Ph.D. student Aziz Genç for his asistance and guidance during my graduate studies.

I would like to express thanks to the members of the Particulate Materials Laboratories (PML), A. Umut Söyler, Hasan Gökçe, Selim Coşkun, Cengiz Hamzaçebi, Ceren Dutdibi, Duygu Yılmaz, Şeyma Duman for their support and help.

I would also like to thank my friends and colleagues Duygu Ağaoğulları and Özge Balcı whose understanding and support made schooling relatively easier.

I would also like to express my thanks to the Scientific and Research Council of Turkey (TÜBİTAK) for providing financial support for the Project 110M130 during my graduate education.

Finally, I owe special thanks to my parents who have given me endless support all my life long.

November 2011 Ömer Utku DEMİRKAN

TABLE OF CONTENTS

Page

ABBREVIATIONS

BPR	**:** Ball-to-powder ratio
CTE	**:** Coefficient of thermal expansion
MA	**:** Mechanical Alloying
MMC	**:** Metal Matrix Composite
ODS	**:** Oxide Dispersoid-Strengthened
OM	**:** Optical Microscope
PCA	**:** Process Control Agent
PM	**:** Powder Metallurgy
PRMMC	**:** Particulate Reinforced Metal Matrix Composite
PSA	**:** Particle Size Analyzer
SEM	**:** Scanning Electron Microscope
TEM	**:** Transmission Electron Microscope

LIST OF TABLES

Page

LIST OF FIGURES

Page

DEVELOPMENT AND CHARACTERIZATION INVESTIGATIONS OF MECHANICALLY ALLOYED AND ACTIVATED SINTERED W-1 WT % Ni MATRIX COMPOSITES REINFORCED WITH TiB_2 AND La_2O_3 PARTICLES

SUMMARY

Tungsten and its alloys are candidate materials for various elevated temperature structural applications due to their excellent properties such as high melting point, high modulus, high resistance of thermal shock, low coefficient of thermal expansion (CTE) and good high temperature strength and stiffness. Recently, tungsten and its alloys have received attention with a view of improving the high temperature mechanical properties.

It is very difficult to fabricate tungsten because of its high melting point and low ductility and even using powder metallurgy techniques, requires very high sintering temperatures up to 2400 – 2800 ^{o}C to get near fully dense tungsten. However, advanced sintering techniques such as hot isostatic pressing or activated sintering offer fabrication of nearly fully dense W composites at lower temperatures (~1400 ^{o}C).

Activated sintering that involves small additions of some transition metals such as Pd, Pt, Ni, Co and Fe enables major reductions in the sintering temperature of W even when the conventional techniques are used.

As dispersion strengtheners, refractory carbide andnitride phases, such as TiC, VC, ZrC, HfC, TiN etc. have been mainly used to improve the mechanical properties of tungsten and its alloys. In addition to these refractory carbide and nitride materials, transition metal diborides are very promising candidates as reinforcements in W due to their high melting point, high hardness, good electrical and thermal conductivities.

Tungsten has high ductile to brittle transition temperature and the strength of tungsten decreases with increasing temperature. The rare-earth oxidesimprove the low-temperature brittleness and decreases ductile to brittle transition temperature in Mo and W materials.

In this study, pre-milled W-1 wt% Ni matrix composites reinforced with pre-milled TiB_2 and/or La_2O_3 particles mechanically alloyed for different durations and fabricated using the activated sintering method. Microstructural and phase characterizations were carried out via PSA, SEM, TEM, OM and XRD analyses. Density measurements, hardness measurements and wear characteristics of sintered samples were also conducted.

According to to powder characterization analyses mean particle size of the powders decrease with increasing MA durations. Submicron particles are observed in SEM investigations of the powders. Crystallite sizes of the powders decrease with increasing MA durations and vary between 6.1 nm and 16 nm. TEM investigations of

the powders which contain TiB_2 reveal the presence of W_2B powders which are formed during MA process.

The sintered samples have relatively high Archimedes'density values which decrease with increasing TiB_2 content. The sintered samples of W1Ni-2TiB_2-1La_2O_3-12h MA'd powders have the highest relative Archimedes' density values of 98.38%.

Vickers microhardness values increase with increased mechanical alloying durations of the powders. The sintered W1Ni-2TiB_2-1La_2O_3-12h MA'd samples have the highest Vickers microhardness value of 5.72 GPa where the value is 4.08 GPa for the sintered samples of W1Ni+12h MA powders.

The sintered W1Ni-2TiB2-12h MA'd sample has the highest wear resistance of all samples. Although La_2O_3 addition contributes to the wear resistance itself for the samples containing TiB_2 the wear resistance of the samples decreases with increasing La_2O_3 addition.

TiB_2 VE La_2O_3 PARTİKÜLLERİ İLE TAKVİYE EDİLMİŞ W-%1 Ni (AĞIRLIKÇA) MATRİKSLİ KOMPOZİTLERİN MEKANİK ALAŞIMLAMA VE AKTİVE EDİLMİŞ SİNTERLEME YÖNTEMLERİYLE ÜRETİLMESİ VE KARAKTERİZASYONU

ÖZET

Toz Metalurjisi, sunduğu çeşitlilik açısından tüm metal işleme teknolojileri içerisinde en kapsamlı şekillendirme ve üretim süreçlerine sahip teknolojidir. Toz Metalurjisini çekici kılan en önemli unsur, yüksek kaliteye sahip karmaşık şekillerdeki parçaların istenilen toleranslarda kayıpsız ya da çok az kayıpla ekonomik olarak imal edilebilmesidir. Wollaston yöntemi ile platin sünger tozundan kompakt platin üretimi modern Toz Metalurjisinin (T/M) başlangıcı olarak kabul edilmektedir. Bu gelişmeyi takiben T/M'nin ilk ticari uygulamaları karbon (C), osmiyum (Os), zirkonyum (Zr), vanadyum (V), tantal (Ta) ve volframın (W) akkor lamba filamanları için kullanılmasıyla gerçekleşmiştir.

Mekanik Alaşımlama yöntemi ise, Toz Metalurjisinde önemli bir yer tutmaktadır. Mekanik Alaşımlama (MA) küçük kristal tanelere ve kontrollü mikroyapılara sahip kompozit metal tozları üretmek amacıyla kullanılan kuru ve yüksek enerjili ortamda bir toz öğütme işlemidir. 80'li yılların ortalarından başlayarak MA yöntemi malzemenin mikroyapısında çok çeşitli kararlı ve yarı-kararlı fazların, aşırı doymuş katı eriyiklerin, nanokristal ve yarı-kristal ara fazların ve amorf alaşımların sentezlenmesinde kullanılmıştır. Bu araştırmalara ek olarak, MA ile elementel toz karışımlarının mekanik olarak aktive edilerek kimyasal tepkimelere yol açabileceği yani oda sıcaklıklarında mekanokimyasal sentezlemenin gerçekleşebileceği bulunmuştur. Bu sayede, ergime ve ısıl işlem gibi yüksek sıcaklık süreçleri yerine oda sıcaklıklarında çeşitli elementel tozlardan kompleks yapılar üretilebilmektedir.

Volfram ve alaşımları yüksek ergime sıcaklıkları, yüksek elastik modülleri, yüksek termal şok dirençleri, düşük termal genleşme katsayıları ve iyi yüksek sıcaklık dayanımları nedeniyle yüksek çalışma sıcaklıklarında yüksek dayanım gerektiren uygulamalar için potansiyel malzemelerdir. Volfram ve alaşımları kinetik enerji penetratörleri, ağırlık dengeleyiciler gibi yüksek yoğunluk gerektiren uygulamalarda 19.3 g/cm^3 yoğunluğu ile en önemli alternatif olarak öne çıkmaktadır. Volfram ve alaşımları ayrıca X-ışını hedefi ve radrasyon kalkanı olarak kullanılmaktadır. Volfram, yüksek ergime sıcaklığı nedeniyle yüksek sıcaklıkta yapısal uygulamalarda da kullanılabilmektedir.

Yüksek ergime sıcaklığı ve düşük tokluğundan dolayı volfram üretmek çok zordur. Toz metalurjisi yöntemi kullanılması durumunda bile yüksek yoğunluklarda volfram üretmek için 2400 – 2800 ˚C sıcaklıklara ihtiyaç duyulmaktadır.Yüksek sinterleme sıcaklığı mekanik alaşımlama işlemniden sonra da ancak 1700-1800 ˚C'ye düşebilmektedir. Volfram üretimindeki bu en önemli sorunu aşmak için önerilen en geçerli teknik aktive edilmiş sinterleme (activated sintering) adı verilen yöntemdir. Genellikle toz bileşimine ya da nadiren sinterleme atmosferinde yapılan küçük

oranlarda katkılar sonucu sinterlenebilme özelliğinin geliştirilmesi işlemine aktive edilmiş sinterleme adı verilmektedir. Aktive edilmiş sinterlemenin oluşabilmesi için yüksek ergime sıcaklığına sahip metalin düşük ergime sıcaklığına sahip metal içerisinde çözünebilmesi gerekmektedir. Bu sayede sinterleme yolu kısalarak işlem kolaylaştırılmaktadır.Aktive edilmiş sinterleme yöntemi sayesinde Pd, Pt, Ni, Co ve Fe gibi bazı geçiş metallerinin düşük miktarlarda eklenmesinde dahi volframın geleneksel sinterleme yönteminde sinterleme sıcaklığının büyük oranda düşürülmesini sağlamaktadır.

Volfram ve alaşımlarının mekanik özelliklerinin geliştirilmesi amacıyla TiC, ZrC, HfC, TiN, Y_2O_3, La_2O_3, Sm_2O_3, ThO_2, ZrO_2 gibi çeşitli refrakter karbürler, nitrürler ve oksit fazları takviye elemanı olarak kullanılmaktadır. Bu refrakter karakterli karbür ve nitrürlere ek olarak yüksek ergime sıcaklığı, yüksek sertlik değerleri ve iyi termal iletkenlikleri göz önünde bulundurularak geçiş metali borürleri de volfram alaşımlarında katkı malzeme olarak kullanılmaya adaydır. Ancak literatüre bakıldığında geçiş metali borürleri ve volfram ile ilgili pek de fazla çalışmaya rastlanmamaktadır.

Volfram, sünek-gevrek geçiş sıcaklığı yüksek olan bir geçiş metalidir ve sıcaklık arttıkça mukavemeti düşmektedir. Nadir toprak oksitleri ise volfram ve molibden gibi malzemelerin yapılarına katılarak bu geçiş sıcaklığını düşürmekte ve bu malzemelerin düşük sıcaklıktaki gevrekliğinden doğan sorunları engellemektedir. Yapılan ilk çalışmalarda ThO_2'in volframın sünek-gevrek geçiş sıcaklığını önemli ölçüde düşürdüğü görülmüştür. Ancak bu malzemenin radyoaktif özellik göstermesi ve kirlenmeye neden olmasından dolayı günümüzde pek fazla tercih edilmemektedir. ThO_2'nin yerine La_2O_3 ve Y_2O_3 gibi nadir toprak oksitlerinin daha çok kullanıldığı gözlemlenebilr.

Bu çalışmada, öncelikle W-%1Ni (ağ), TiB_2 ve La_2O_3tozları farklı ortamlarda ön öğütülmüştür. Ardındanbu ön öğütülmüş tozlar farklı kompozisyonlarda karıştırılarak farklı sürelerde mekanik alaşımlanmış ve ardından aktive edilmiş sinterleme yöntemiyle sinterlenerek üretilmiştir.

Mekanik alaşımlama sonucu elde edilen kompozit tozlardan seçilen numelerinpartikül boyutları laser partikül boyutu cihazı ile ölçülmüş, kompozit tozlarının ve sinterlenmiş numunerelerin mikroyapı ve faz analizleri taramalı elektron mikroskobu (SEM), geçirimli elektron mikroskobu (TEM) ve X-ışınları kırınımı (XRD) teknikleri kullanılarak yapılmıştır.

Sinterlenmiş numunelerin yoğunlukları Arşimet tekniğiyle hesaplanmış ve mikrosertlik deneyleri Vickers mikrosertlik cihazında gerçekleştirilmiştir. Sinterlenen numunelerin faz analizi XRD yöntemiyle yapılmıştır. Elde edilen numunelerden yüksek yoğunluğa ve sertliğe sahip olanlar içerisinden seçilen numulerin mikroyapı analizleri SEM ile yapılmış ve elde edilen sonuçlar doğrultusunda 12 saat mekanik alaşımlanmış numunelere aşınma testi yapılmıştır.

Partikül boyut dağılımı analizi ve SEM çalışmalarında yapılan toz karakterizasyon deneyleri sonunda görülmüştür ki elde edilen kompozit tozlarının boyutları genelde 1 mikronun altındadır. TiB_2 içeren tozlardan yapılan TEM çalışmaları sonucunda yapıda W_2B fazına rastlanmıştır.

Mekanik alaşımlama ile elde edilen tozlarınsinterlenmesi ile oluşan numunelerin analizleri sonucunda mekanik alaşımlama süresinin artmasıyla ölçülen bağıl Arşimet

yoğunluk değerlerinin arttığı görülmektedir. Ancak ilave edilen TiB_2 miktarının artmasıyla bu değerlerde düşüş yaşanmaktadır.

Artan mekanik alaşımlama süresi ve katkı elemanlarının yapıdaki miktarı arttıkça Vickers mikrosertlik değerlerinde artış gözlenmektedir. Toplam 18 saat mekanik alaşımlanmış matriks için mikrosertlik değeri 4.08 GPa iken ağırlıkça %2 TiB_2 ve %1 La_2O_3 içeren numunede bu değer 5.72 GPa'a yükselmektedir.

Aşınma testleri göstermektedir ki ayrı ayrı gerçekleştirilen TiB_2ve La_2O_3 ilavesi malzemenin aşınma direncinde artış oluşturmaktadır. Ancak bu iki malzemenin aynı anda ilavesi durumunda artan La_2O_3 miktarı ile aşınma direnci azalan bir eğilim göstermektedir.

1. INTRODUCTION

Many of our modern technologies require materials with unusual combinations of properties which cannot be met by conventional metal alloys, ceramics, and polymeric materials. Since no single material could fulfill these rising requirements in the last two decades, an increasing interest in developing new materials has been aroused to serve the need for new materials having unique properties for special applications (Song et al., 2003a; Tang et al., 2004).

A composite material which is made by combining two or more materials to givea unique combination of properties can fulfill the requirements of the modern technology have been, and are yet being, extended (Mazumdar, 2002). Composite materials are those comprising, strong and stiff reinforcing fibers—continuous or noncontinuous—surrounded by a weaker matrix material. The matrix serves to distribute the reinforcements and also to transmit the load to the reinforcements. (Gay et al., 2003).The reinforcements can be fibers, particulates, or whiskers, and the matrix materials can be metals, plastics, or ceramics (Mazumdar, 2002).

One simple scheme for the classification of composites is to separate the matrix and reinforcing phase constituents, and divide them into several groups. The first classification is based on the type of the matrix constituent: Polymer-Matrix, Metal-Matrix or Ceramic-Matrix Composites. Composites can also be classified based on the type of reinforcement used: fiber reinforced (continuous or discontinuous) or particulate reinforced (flakes, chopped fibers, shaped particles, and whiskers) (Schwartz, 1984; Coşkun et al., 2004). However, the best way to classify the composites is to include both the reinforcement and matrix constituent, such as particle-reinforced-metal-matrix composites (PRMMC).

A metal matrix composite (MMC) combines into a single material a metallic base with a reinforcing constituent, which is usually non-metallic and is commonly a ceramic. It is also possible to use other materials as reinforcements instead of ceramics, for instance refractory metals or intermetallics (Clyne, 2001). There are

plenty of well-known reasons to add ceramic particles into a metal, such as to give the metal high hardness and wear resistance (Miserez et al., 2004; Shen and Chawla, 2001; Cambronero et al., 2003). Furthermore, MMC's combine metallic properties such as ductility and toughness with the characteristics of ceramics, namely high strength and modulus (Tjong and Ma, 2000). The mechanical properties of the MMC's highly depend on the volume fraction and the type of the reinforcement as well as the type of the matrix (Stjernstoft, 2004). On the other hand, while continuous fiber-reinforcement provides the most effective strengthening in a given direction, particle-reinforcement provides cost-effectiveness and especially isotropic properties to the composite. In addition, the latter one can be processed using similar technology used for monolithic materials (Chawla and Shen, 2001.). Furthermore, MMC's with discontinuous reinforcements are also attractive for their processability into various shapes (Chung, 2001). In overall, there exists a number of variables which determine the characteristics of the composite materials.

Beside all the attention that the composites received for the last 20 years, there is another group of materials which have found applications in various industries, such as defense and aerospace in recent years, namely nanostructured materials or nanomaterials (Cahn, 2001). These materials exhibit unique microstructures and superior mechanical properties (Han et al., 2005). Nanotechnology is regarded world-wide as one of the key technologies of the 21st Century, and nanotechnological products and processes hold an enormous economic potential for the markets of the future (Zweck and Luther, 2003). Thus, the combination of composite materials and nanostructured materials, namely "nanocomposites" with the appropriate matrix and reinforcing phase constituents would be candidate materials for industrial applications, such as defense, aerospace and as cutting tools materials (Coşkun, 2006).

In this last decade, as interesting and appropriate matrix materials with their high melting point, high modulus, high resistance of thermal shock, low CTE and good high temperature strength and stiffness, tungsten and its alloys have received attention with a view of improving the high temperature mechanical properties (Song et. al., 2002). Generally, the fabrication of tungsten is very difficult due to its high melting point, low ductility. The processing requires very high sintering temperatures up to 2400 – 2800 ^{o}C to get nearfully dense tungsten, even using powder metallurgy

techniques (Li and German, 1983). The addition of small quantities of some transition metals such as Pd, Pt, Ni, Co, and Fe makes it possible to greatly reduce the sintering temperature of W (Li and German, 1983; German and Munir, 1976; Vajek, 1959; Hayden and Brophy, 1963).

As dispersion strengtheners, refractory carbide, nitride and oxide phases, such as TiC, VC, ZrC, HfC, TiN, Y_2O_3, La_2O_3, Sm_2O_3, ThO_2, ZrO_2, etc. have been mainly used to improve the mechanical properties of tungsten and its alloys (Song et. al., 2002; Song et. al., 2003b; Lee et. al., 2004). Hardly any reported literature exists on the effects of TiB_2 or TiB_2 and oxide addition on W matrix composites. Keeping the above concepts in mind, the aim of this study has been to develop and characterize nanostructured TiB_2 and La_2O_3 particle-reinforced tungsten composite powders and their consolidated and sintered counterparts. Ni was used as an activation agent to investigate activated sintering of mechanically alloyed W-TiB_2-La_2O_3.

2. LITERATURE REVIEW

2.1 Metal Matrix Composites

Metal matrix composites (MMC's), as well as all composites, consist of at least two chemically and physically distinct phases, suitably distributed to provide properties not obtainable with either of the individual phases. Generally, there are two phases for MMC's, e.g., a fibrous or particulate phase, distributed in a metallic matrix (Chawla and Chawla, 2006). Metals are chosen as the matrix material in MMC structures. Because metals have;

1. higher application temperature ranges,
2. higher transverse stiffnesses and strengths,
3. generally high toughness values,
4. high radiation resistances,
5. high electric and thermal conductivities,
6. higher strength-to-density, stiffness-to-density ratios, as well as better fatigue resistances, lower coefficients of thermal expansion (CTE) and better wear resistances than with monolithic metals,
7. can be fabricated with conventional metal working equipment (Akovali and Uyanik, 2001).

In most cases, the reinforcing material is a ceramic, although there are exceptions to this and MMC's can be taken to encompass materials "reinforced" with relatively soft and/or compliant phases, such as graphitic flakes, lead particles, or even gases. It is also possible to use refractory metals, intermetallics, or semiconductors, rather than true ceramics (Clyne, 2000). Generally, there are three types of MMC's: i) particle reinforced MMC's, ii) short fiber or whisker reinforced MMC's, iii) continuous fiber or sheet reinforced MMC's (Chawla and Chawla, 2006). Figure 2.1 shows the schematic representations of these three major types of metal matrix composites.

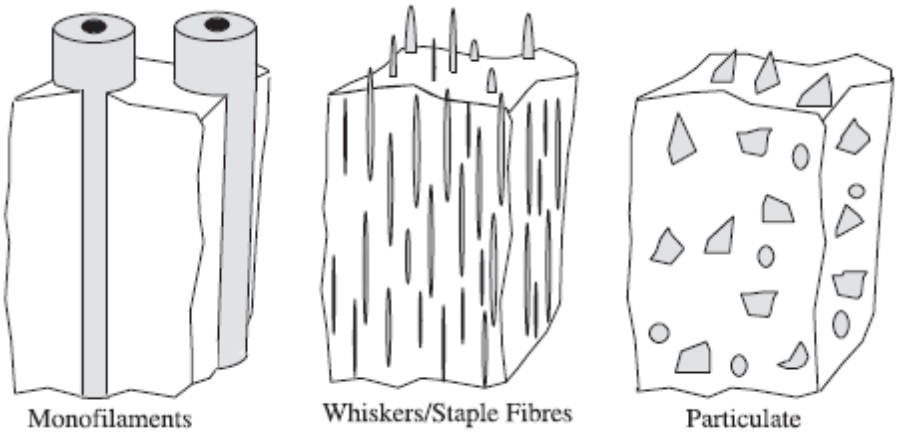

Figure 2.1: Schematic respresentations of three shapes of metal matrix composite materials (Clyne and Withers, 1993).

2.1.1 Particulate reinforced metal matrix composites

Particulate reinforced metal matrix composites (PRMMC's) are comprised of the class of metals containing reinforcement phases having approximately equiaxed geometries, typically referred to as particles or particulates. These differ from composites containing higher aspect ratio reinforcements such as fibers or whiskers in significant and important ways (Hunt, 2000). Recently, PRMMC's are more popular because of their relatively low costs, good formability and machinability as well as characteristic isotropic properties (Ibrahim et al., 1991; Tjong and Ma, 2000; Sun et al., 2003a).

Particle reinforced composite systems can be classified in two sub-classes: 'large particle' and 'dispersion' strengthened composites, by basing on the reinforcement or strengthening mechanisms.

2.1.1.1 Large particle composites

The term 'large' is used to denote that particle-matrix interactions can not be treated on atomic or molecular level and 'continuum mechanics' should be used. For large particle reinforced composites, the reinforcing material is usually harder and stiffer than the matrix and they tend to restrain movement of the matrix. The matrix transfers some of the applied stress to the particles. The efficiency of reinforcement mostly depends on interaction at the particle-matrix interface (Akovali and Uyanik, 2001). These composites are generally used as cutting tools for hardened steels. The hard carbide particles provide the cutting surface but, are not themselves capable of

withstanding the cutting stresses because of their brittleness. Toughness is increased by their inclusion in the ductile metal matrix, which insulate the carbide particles from one another and prevents particle-to-particle crack propagation. Both matrix and particulate phases are quite refractory, to withstand the high temperatures generated by the cutting action on materials that are extremely hard (Askeland, 1984; Schwartz, 1984).

2.1.1.2 Dispersion strengthened composites

In dispersion-strengthened composites, the fine dispersions of oxide, carbide, or boride particles cancel the motion of dislocations so that the matrix is strengthened relatively to the effectiveness of the dispersions as a barrier to the motion of dislocations (Ohring, 1995; Asthana et al., 2006). The applied stress must be sufficiently enough to bend the dislocation line into a semicircular loop to make the dislocation pass through a dispersoid. Calculations show that interparticle separation for effective dispersion hardening should be between 0.01 and 0.3 μm (10 – 300 nm). To achieve this range of spacing between the dispersoid, the particle diameters should be less than 100 nm at volume fractions below 15% (Asthana et al., 2006). Of many dispersion-hardened alloy systems, only a few have reached commercial significance. Aluminum, nickel, and tungsten, copper and titanium, have showed successful results in laboratory and developmental stages (Schwartz, 1984). The development of oxide dispersion-strengthened (ODS) composites has led to considerable improvements in the elevated-temperature strength and creep-resistance of the matrix alloys (Krajnikov et al.,1997; Sakasegawa et al., 2008; Redsten et al., 1995). The ODS composites contain small (< 15%) amounts of fine second-phase particles, which prevent recrystallization and grain coarsening, and act as barriers to the motion of dislocations. Small quantities of fine oxide ceramics improve the strength without degrading the valuable matrix properties (Asthana et al., 2006).

2.2 Fabrication of PRMMC's

MMCs can not be fabricated easily by using conventional methods such as casting due to high cost of processing. There are several techniques to fabricate MMC's which can vary with the choice of the matrix and the reinforcement materials. There are generally three different types of fabrication methods (Huda et al., 1995):

1. Solid phase fabrication methods: Diffusion bonding, hot rolling extrusion, drawing, explosive welding PM route, pneumatic impaction etc (Huda et al., 1995).
2. Liquid phase fabrication methods: Liquid metal infiltration, squeeze casting, compocasting, pressure casting etc (Huda et al., 1995).
3. Two phase processes: Osprey deposition, rheocasting, variable co-deposition of multi-phase materials (VCM) process (Ibrahim et al., 1991).

The selection of one particular process over the others depends on various factors which are types of materials and their properties, final desired properties, size, shape and complexity of the part, subsequent processing and overall cost of the process (Lindroos et al., 2004).

Various processing techniques have been developed to optimize the structure and properties of PRMMC's (Ibrahim et al., 1991; Schwartz, 1997). Among these techniques, there were some luxurious ones to enhance the wettability by, for instance, introducing some kind of surface coating to the particles before fabrication. However, this preprocessing of particles increases the cost of PRMMC's further, which in turn limits their commercial utilization. In addition, some recently developed PRMMC's, using state-of-the-art high performance materials, such as tungsten, molybdenum, niobium and tantalum as the matrix material, are difficult to fabricate by using conventional liquid metallurgy process because these materials have incredibly high melting temperatures (Liu et al., 1994). In these cases, powder metallurgy seems more attractive and has become the most commonly used method for the preparation of PRMMC's (Nieh et al., 1984; Girot et al., 1987; Coşkun, 2006).

2.2.1 Powder metallurgy

The powder metallurgy (PM) route is the most commonly used method for the preparation of PRMMC's (Liu et al., 1994; Huda et al., 1995). Blending of metallic powders with ceramic particles is a versatile technique for the PRMMC production (Clyne, 2001). In the basic process, mixed or prealloyed powders are fed into a die, compacted a desired shape and then this pressed powder is sintered in a controlled atmosphere furnace to convert the mechanical bonds to the metallurgical bonds that link the powder particles (Newkirk and Kohser, 2004).

When higher strength discontinuous MMC's are required, PM processes are often used because segregation, brittle reaction products, and high residual stresses from solidification shrinkage can be minimized (Campbell, 2006). In addition, with the advent of rapid solidification and mechanical alloying technology, the matrix alloy can be produced as a prealloyed powder, rather than starting with elemental blends (Campbell, 2006).

Powder metallurgy method is widely used to produce PRMMC's based on its advantages which of some are listed below:

1. PM method is more economical than many other techniques to produce PRMMC's, since no melting and casting is involved (Huda et al., 1995).
2. The process offers the possibility of using a wide range of reinforcement volume fraction and size (Huda et al., 1995).
3. Production by PM a homogeneous distribution of reinforcements in the matrix material (Huda et al., 1995).
4. PM offers superior mechanical properties as a result of high dislocation density, small subgrain sizes and limited recrystallization during the process (Das et. al., 2002).

2.2.1.1 Starting materials

Starting materials in powder metallurgy processes have very important roles for the success of the process. In addition to the chemistry and the purity of the powders, there are additional issues to concern, such as particle size, size distribution, particle shape as well as the surface texture of the particles (Newkirk and Kohser, 2004). Considering the PRMMC's, mechanical behavior, chemical stability, thermal mismatch and the cost are another factors which play a significant role in the success of the end-product (Liu et al., 1994).

2.2.1.2 Mixing or blending

After selection of the materials, the next step is blending or mixing. Mixing or blending step affects the final distribution of reinforcement particles and porosity in green compacts, which strongly has an influence on the mechanical properties of the PM end-products (Lindroos et al., 2004). After all, there are some problems, such as segregation and clustering. The reasons of these problems include different flow

characteristics between metal powder and reinforcement particles and the tendency of the agglomeration of particles to minimize their surface energy. The segregation behavior of different sized particles is shown in Figure 2.2 (Liu et al., 1994).

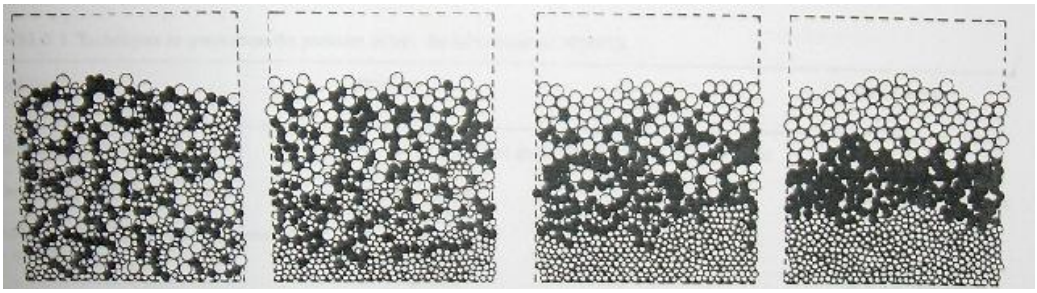

Figure 2.2: Monte Carlo simulations of shaking of a ternary mixture of particles according to number of cycles (Liu et al., 1994).

As seen in Figure 2.2, larger particles rise to top, because they are moved upwards as smaller particles filled the voids beneath the larger particles. Furthermore, the effect of different densities between particles and metal powders of similar size is very important, too. The lighter particles tend to move upwards, while the heavier ones segregate at the bottom (Lindroos et al., 2004). However, these segregation and clustering problems can be overcome by a technique called "Mechanical Alloying (MA)" (Liu et al., 1994). This technique will be discussed in detail in section 2.2.2.

2.2.1.3 Compaction

The next step after blending or mixing operation is the consolidation and pressing of the powder mixture to form the green compacts (Liu et al., 1994). This step is the one of the most critical steps in the PM process, because it sets the density of the powder and the uniformity of the density throughout the product. Because final properties strongly depend on density, uniform properties require uniform density (Newkirk and Kohser, 2004). The compaction process has the following major functions:

1. To consolidate the powders into the desired shape,
2. To impart, as much as possible, the desired final dimensions considering any dimensional changes resulting from sintering,
3. To give the desired level of porosity,
4. To provide sufficient strength for subsequent handling (Upadhyaya, 2000**).**

In the conventional compaction methods, the pressure is usually applied in one direction resulting in a non-uniform distribution of consolidation and even

insufficient densities (Liu et al., 1994). Mostly, mechanical and hydraulic presses and rigid dies are used (Newkirk and Kohser, 2004).

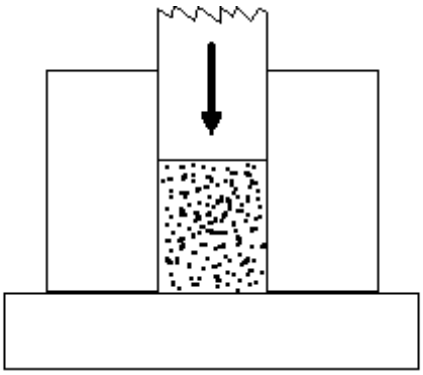

Figure 2.3: Schematic vieew of conventional one-directional pres (Kohser, 2004).

To control the quality of green compacts better, isostatic pressing techniques were developed, such as cold, warm and hot isostatic pressing (Liu et al., 1994).

2.2.1.4 Sintering

The next step after compaction is called sintering where the pressed-powder compacts are heated in a controlled atmosphere environment to the temperature below the melting point but high enough to permit solid-state diffusion, and held for sufficent time to premit bonding of the particles (Degarmo et al., 2003).The sintering process will be discussed in detail in section 2.2.3.

2.2.2 Mechanical alloying

2.2.2.1 History and definition of mechanical alloying

In order to improve the properties and performance of materials, significant developments in mechanical, chemical, and physical properties have been achieved through chemistry modifications and conventional thermal, mechanical, and thermo-mechanical processing methods. (Suryanarayana, 2001). As a result, non-equilibrium processing of materials has attracted the attention of a number of scientists and engineers due to the possibility of producing better and improved materials than it is possible by conventional methods (Suryanarayana et al., 2001; El-Eskandarany, 2001).

The structure and constitution of advanced materials can be better controlled by processing them under non-equilibrium conditions and mechanical alloying (MA) is

such a processing method that materials can be produced under non-equilibrium conditions (Suryanarayana, 2001). MA can be defined as a powder metallurgy process for producing composite metal powders with a controlled fine microstructure by repeated cold welding, fracturing and rewelding of powder particles in a high–energy ball mill (Öveçoğlu, 1987; Benjamin, 1992; Suryanarayana et al., 2001). It utilizes various types of milling machines in which a blend of different powders is subjected to a highly energetic compressive force (Tang et. al., 2004).

The mechanical alloying (MA) process was first employed during the pioneering work of Benjamin at the International Nickel Company's Paul D. Merica Research Laboratory in the late 1960's. It started as an industrial necessity to produce oxide-dispersion-strengthened nickel-based superalloys for gas turbine engine components (Öveçoğlu, 1987; Suryanarayana et al., 2001; Delogu et al., 2003). However, the subsequent discovery of metastable phase formation by MA opened the door to important applications in Materials Science (Delogu et al., 2003). In addition to the metastable phases, equilibrium phases of commercially useful and scientifically interesting materials can be also synthesized by MA (Suryanarayana et al., 2001).

MA is a simple and versatile technique, as well as an economically feasible process with important technical advantages. One of the greatest advantages of MA is in the synthesis of novel alloys, e.g., alloying of normally immiscible elements, which is not possible by any other technique (La Caer et al., 2002). The reason for that is that MA is a completely solid-state processing technique and therefore limitations imposed by phase diagrams do not apply for this process (Suryanarayana et al., 2001). Furthermore, MA holds an advantage over traditional ball milling processes which is to produce a material whose internal homogenity is independent of the initial starting particle size. It is not uncommon to obtain mechanically-alloyed dispersions with less than 1 μm interparticle spacing from initial powder sizes of 50-100 μm average diameters (Goff, 2003).

2.2.2.2 Types of mills

Different types of high-energy milling equipment are used to produce mechanically alloyed powders. These equipment include Spex Mixer/mills, planetary ball mills, attritor mills and commercial mills. They have different capacity, efficiency of

milling and additional arrangements for cooling, heating, etc (Suryanarayana, 2001; Goff, 2003).

Spex Mixer/mills are most commonly used for laboratory investigations and they mill about 10 - 20 g powder at a time depending on the density of starting constituents (Goff, 2003). The common variety of these mills has one vial, containing the sample and grinding balls, secured in the clamp and shakes the milling container in three-mutually perpendicular directions at about 1200 rpm resulting in powder microstructural refinement with time (Suryanarayana, 2001; Goff, 2003). Ball-ball and ball-container collisions continually trap and refine the powder constituents with time ultimately leading to an overall homogeneously dispersed microstructure (Goff, 2003). There are different vial materials available for the Spex mixer/mills, which are hardened steel, alumina, tungsten carbide, zirconia, stainless steel, silicon nitride, agate, plastic, and methacrylate (Suryanarayana, 2001). Typical Spex mill and tungsten carbide vial set can be seen in Figure 2.4.

Figure 2.4: a) A typical Spex shaker mill **b)** Tungsten carbide vial set consisting of the vial, lid, gasket, and balls (Suryanarayana, 2001).

Another popular mill for conducting MA experiments is the planetary ball mill in which a few hundred grams of the powder can be milled at a time. It is called the planetary ball because of its vial's planet-like movement. The centrifugal force produced by the vials rotating around their own axes act on the vial contents,

consisting of material to be ground and the grinding balls. As a result, powders are trapped between the rotating balls and the walls of the vial and refined. Even though the linear velocity of the balls in this type of mill is higher than that in the Spex mills, the frequency of impacts is much more in the Spex mills (Suryanarayana, 2001).

Therefore, compared to Spex mills, planetary ball mills can be considered lower energy mills (Suryanarayana, 2001). In Figure 2.5, a schematic view of ball motion in a planetary ball mill can be seen.

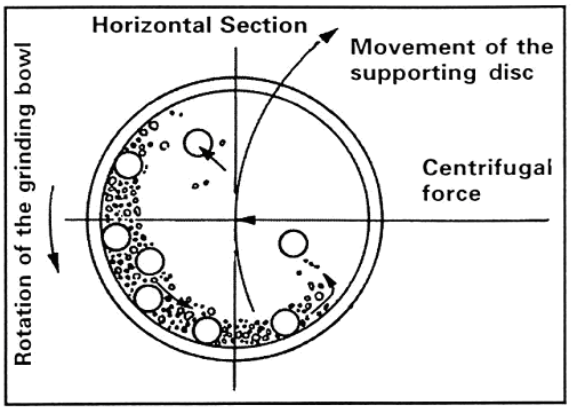

Figure 2.5: A schematic view of ball motion in a planetary ball mill (El-Eskandarany, 2001).

Another type of mills is the attritor mills. In attritor mills, large quantities of powder (from about 0.5 to 40 kg) can be milled at a time (Suryanarayana, 2001). It contains a vertical shaft with a series of impellers that rotates in the tank of about 250 rpm (Goff, 2003). As the shaft rotates, the balls drop on the metal powder that is being ground. The impellers energize the ball charge, causing powder size reduction because of impact between balls, between balls and container wall, and between balls, agitator shaft, and impellers. The rate of grinding increases with the speed of rotation. However, at high speeds the centrifugal force acting on the balls exceeds the force of gravity, and the balls are pinned to the wall of the container. At this point the grinding action stops (Suryanarayana, 2001). Schematic view of an attritor mill is given in Figure 2.6.

Finally, commercial mills for MA are much larger in size than the mills described above and can grind several hundred kilograms of powders at a time. Mechanical alloying for commercial production is carried out in ball mills of up to about 1250 kg capacity (Suryanarayana, 2001). A picture of commercial-size ball mills can be seen in Figure 2.7.

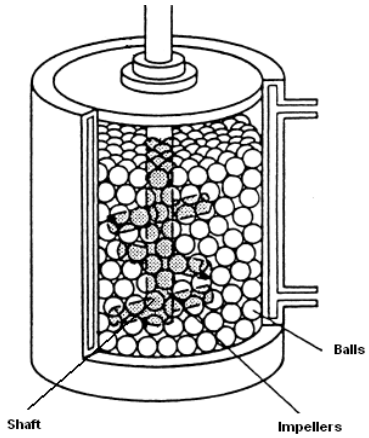

Figure 2.6: A schematic view of an attritor mill (Goff, 2003).

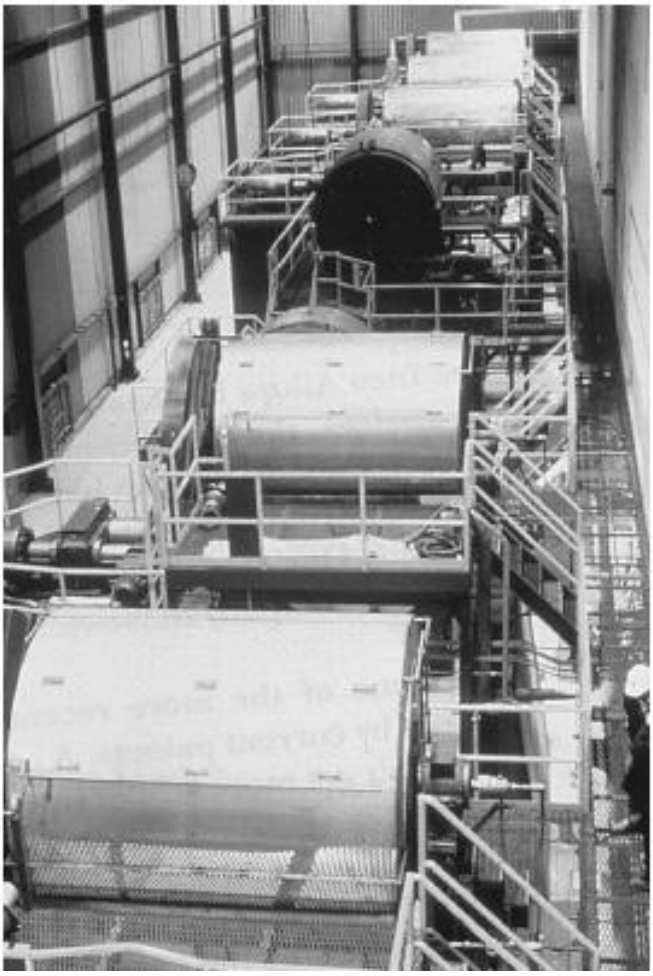

Figure 2.7: Commercial production-size ball mills used for mechanical alloying (Suryanarayana, 2001).

The milling time decreases with an increase in the energy of the mill. Roughly, it can be estimated that a process that takes only a few minutes in the Spex mill may take hours in an attritor and a few days in a commercial mill (Suryanarayana, 2001).

2.2.2.3 Proccess variables in milling

Mechanical alloying is a complex process involving optimization of a number of process variables to achieve the desired product phase, microstructure, and/or properties (El-Eskandarany, 2001). These will decide the nature of the phase formed (solid solution,intermetallic, or amorphous phase, etc.) in the milled powder. For a given composition of the powder, the type (material) of the milling container and the milling medium, ball-to-powder ratio, milling atmosphere, milling time, use of a process control agent (PCA), etc. can be listed as the important variables that have an important effect on the final constitution of the milled powder (Suryanarayana, 2001).

The material used for the milling container (grinding vessel, vial) is important since the impact of the grinding medium on the inner walls of the container will result in tiny fractions of milling material that fracture off and disperse into the composite powder(El-Eskandarany, 2001; Suryanarayana, 2001). These can contaminate the powder or alter the chemistry of the powder. If the material of the grinding vessel is different from that of the powder, then the powder may be contaminated with the grinding vessel material (Suryanarayana, 2001; Goff, 2003). Regardless of the type of MA process, the most appropriate type of container and milling media for the given system should be chosen. Generally, milling media that is made of a similar material as that of the material to be processed is used to reduce contamination during processing (Goff, 2003). Additionally, the density of the grinding medium should be high enough so that the balls create enough impact force on the powder (Suryanarayana, 2001).

Another important issue is the ball-to-powder ratio (BPR). This has been varied by different investigators from a value as low as 1:1 to as high as 220:1. Generally, a ratio of 10:1 is most commonly used while milling the powder in a small capacity mill such as a SPEX mill. The BPR has an important effect on the time required to achieve a particular phase in the powder being milled. The higher the BPR, the shorter is the time required (Suryanarayana, 2001).

Milling atmosphere is also an important variable for the MA process. The major effect of the milling atmosphere is on the contamination of the powder (El-Eskandarany, 2001). The powders are milled in containers that have been either

vacuumed or filled with an inert gas such as argon or helium. However, high-purity argon is the most common used gas to prevent oxidation and contamination of the powder (Suryanarayana, 2001). The presence of air in the vial cause to produce oxides and nitrides in the powder, especially if the powders are reactive in nature. Thus, the loading and unloading of the powders into the vial has to be carried outinside an atmosphere-controlled glove box (Suryanarayana, 2001; Fecht, 2002).

The time of milling is the most important parameter. In most of the cases, the rate of refinement of the internal structure (particle size, crystallite size, lamellar spacing, etc.) is roughly logarithmic with processing time (Figure 2.8) and therefore the size of the starting particles is relatively unimportant (Suryanarayana, 2001). In a few minutes to an hour, the lamellar spacing usually becomes small and the crystallite (or grain) size is refined to nanometer dimensions. Normally, the time is so chosen to achieve a steady state between the fracturing and cold welding of the powder particles (Öveçoğlu, 1987). Furthermore, the times required depend on the type of mill used, the intensity of milling, the ball-to-powder ratio, and the temperature of milling. These times have to be decided for each combination of the above parameters and for the particular powder system. However, it should be realized that the level of contamination increases and some undesirable phases form if the powder is milled for times longer than required. Therefore, the powder has to be milled just for the required duration and not any longer (Suryanarayana, 2001).

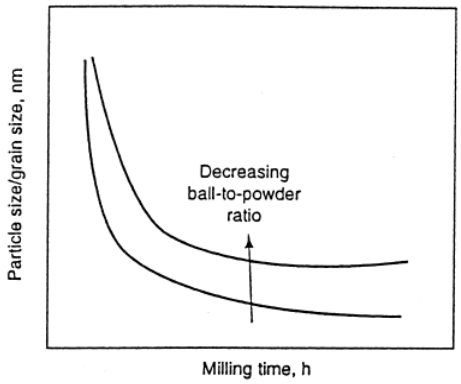

Figure 2.8: Refinement of particle and grain sizes with milling time. Rate of refinement increases with higher milling energy, ball-to powder ratio, lower temperature, etc. (Suryanarayana, 2001).

The use of process control agents (PCA) are another concern in the MA process. Generally, ductile powder particles get cold-welded to each other, due to the heavy plastic deformation during milling. However, true alloying among powder particles

can occur only when a balance is maintained between cold welding and fracturing of particles (El-Eskandarany, 2001). In order to provide, a process control agent (PCA) is added to the powder mixture during milling to reduce the cold welding (Öveçoğlu, 1987; Suryanarayana, 2001; Gilman and Benjamin, 1983). The PCA's can be solids, liquids, or gases. They are mostly organic compounds, which act as surface-active agents by adsorbing on the surface of the powder particles and minimizing cold welding between powder particles and thereby inhibiting the agglomeration (Suryanarayana, 2001).

2.2.2.4 Mechanism of mechanical alloying

MA is an advanced fabrication process that can produce ultra-fine and homogenous powders. Even, nanocrystalline materials (with a grain size of few nanometers, usually<100 nm) are also produced by MA of powder mixtures (Ryu et al., 2000). Additionally, it has been recognized that this technique can be used to induce chemical (displacement) reactions in powder mixtures at room temperature or at much lower temperatures than normally required to synthesize pure metals (Suryanarayana et al., 2001).

In any MA process, starting powder constituents are first mixed or blended according to the required stoichiometry for desired composite batches. Then, they are put in the milling container with the appropriate ball charge and milled until a steady state of homogeneous dispersion is achieved (Goff, 2003). The central event of MA is the ball-powder collisions (Fecht, 2002). Microstructural refinement during the MA process occurs due to the repeated cold-welding, fracturing, and cold-welding of the dry powder constituents during their impact between ball-ball and/or ball-container collisions. Figure 2.9 is a schematic representation of the collided balls. The force of the impact plastically deforms the powder particles leading to work hardening and fracture (Suryanarayana, 2001; Fecht, 2002).

In the early stages of milling, the particles are soft (either ductile-ductile or ductile-brittle material combination), their tendency to weld together and form large particles is high (Suryanarayana, 2001). A broad range of particle sizes develops, with some as large as three times bigger than the starting particles (Suryanarayana, 2001; Goff, 2003). The composite particles at this stage have a characteristic layered structure

consisting of various combinations of the starting constituents (Figure 2.10) (Suryanarayana, 2001).

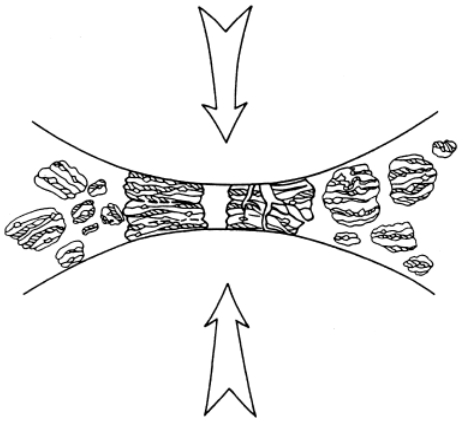

Figure 2.9: Schematic view of a ball-powder-ball collision (Suryanarayana, 2001).

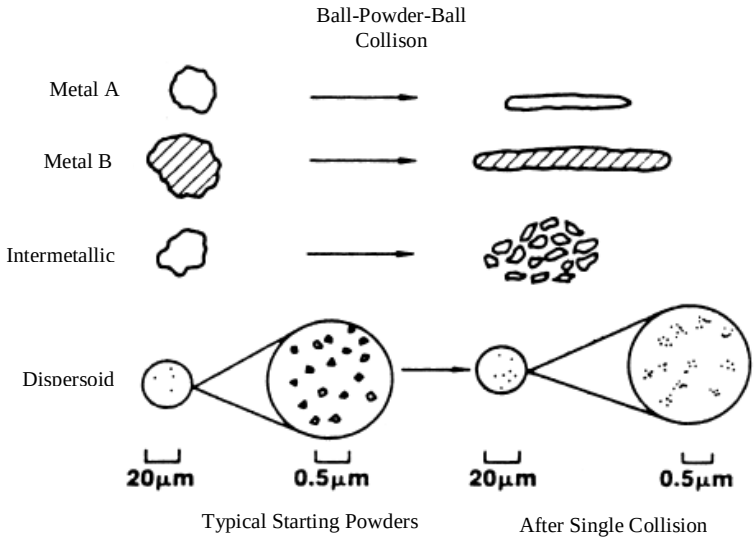

Figure 2.10: Deformation characteristics of starting powders used in a typical MA process (Suryanarayana, 2001).

In order to get better understanding about the physical phenomena that occur during MA processing, it is useful to divide the typical process into three or four stages (Öveçoğlu, 1987; Goff, 2003).

As the metallic phases are flattened and overlap during ball collisions, atomically clean surfaces are placed in contact with one another and subsequently cold-weld together, where brittle constituents (intermetallics and dispersoids) are occluded by the ductile constituents thus becoming trapped along cold-weld interfaces

(Goff, 2003). Figure 2.11 shows early stage of processing in which particles are layered composites of starting constituents.

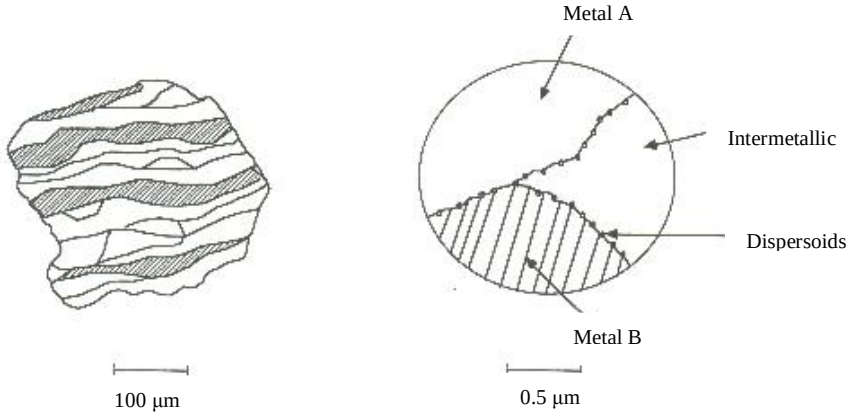

Figure 2.11: Early stage of processing in which particles are layered composites of starting constituents (Suryanarayana, 2001).

In the intermediate stage, the composite powder particles are further refined due to continual welding and fracturing of excessively work-hardened metallic phases and brittle intermetallics and/or dispersoids (Goff, 2003). At this stage, the tendency to fracture predominates over cold welding (Suryanarayana, 2001). The particles consist of convoluted lamellae. The reduction in particle size, increased microstructural mixing, and elevated temperature of the powder constituents due to the adsorbed kinetic energy of milling balls all help to form areas of solute dissolution throughout the metallic powder matrix (Öveçoğlu, 1987). Thus, this potentially may lead to areas where new phases develop which is mainly due to an overall decrease in atomic diffusion distances between individual phases and decreased activation energies for diffusion due to the increase in temperature (Öveçoğlu, 1987; Goff, 2003). Consequently, the inter-layer spacing decreases and the number of layers in a particle increase (Suryanarayana, 2001). Figure 2.12 is a schematic view of the reduced lamellae thickness, solute dissolution, and formation of new phases in the intermediate stage of processing.

In the final stage (Figure 2.13), steady-state equilibrium is attained when a balance is achieved between the rate of welding and the rate of fracturing. As a result, smaller particles are able to withstand deformation without fracturing and tend to be welded into larger pieces, with an overall tendency to drive both very fine and very large particles towards an intermediate size (Suryanarayana, 2001). Furthermore, individual particle compositions are equal to the starting powder blend composition; the lamellae are no longer optically resolvable; and the dispersoid spacing is equal to

the distance between weld interfaces (Öveçoğlu, 1987). At this point, further processing would not improve the dispersoid distribution or serve to enhance the homogeneity of the composite microstructure (Öveçoğlu, 1987; Goff, 2003). The particle size distribution at this stage is narrow, because particles larger than average are reduced in size at the same rate that fragments smaller than average grow through agglomeration of smaller particles (Suryanarayana, 2001).

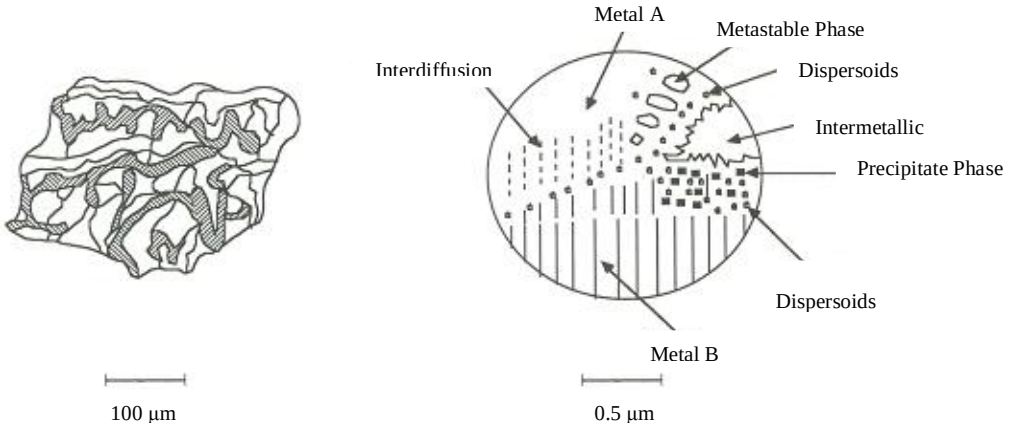

Figure 2.12: Intermediate stage of processing showing reduced lamellae thickness, solute dissolution, and formation of new phases (Suryanarayana, 2001).

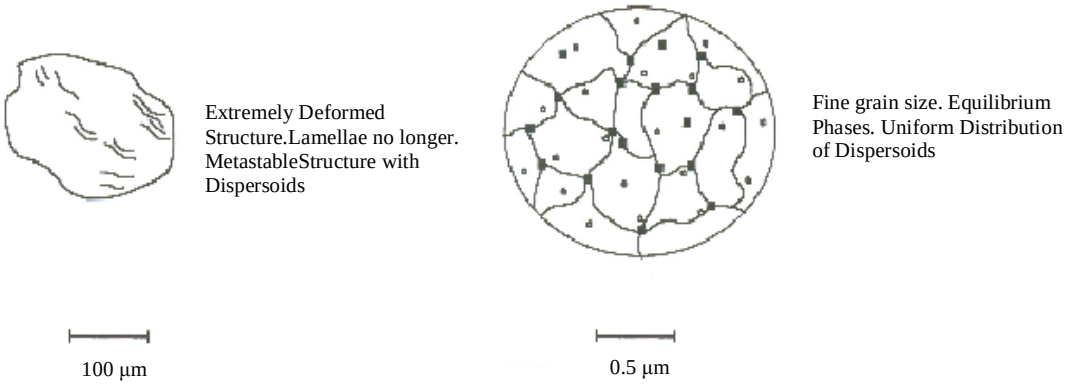

Figure 2.13: The final stage of processing and consolidation (Suryanarayana, 2001).

In order to complete the MA process and obtain a useable bulk composite form, the powders are heated to a temperature greater than half the melting temperature of the composite powder and consolidated. This serves to further homogenize the microstructure (Goff, 2003).

It is possible to conduct MA with three different combinations of metals and alloys, namely ductile-ductile, ductile-brittle and brittle-brittle systems. Therefore, it is convenient to discuss the mechanism of MA also under these categories (Fecht, 2002).

Ductile-ductile combination is thought to be the ideal combination for MA process. It is suggested that it was necessary to have at least 15% of a ductile component for achieving alloying. This was true because alloying occurs due to the repeated action of cold welding and fracturing of powder particles; cold welding cannot occur if the particles are not ductile. In the early stages of MA, the ductile components get flattened to platelet/pancake shapes. A small quantity of the powder, usually one or two particle thickness, also gets welded onto the ball surfaces. This coating of the powder on the grinding medium is advantageous since it prevents excessive wear of the grinding medium and thus preventing the contamination of the powder. However, the thickness of the powder layer on the grinding medium must be kept to a minimum to avoid forming a heterogeneous product (El-Eskandarany, 2001; Suryanarayana, 2001). In the next stage, these flattened particles get cold welded together and form a composite lamellar structure of the constituent metals (Öveçoğlu, 1987). An increase in particle size is also observed at this stage (Suryanarayana, 2001). For instance, it has been found that during MA of a Fe-Cu powder mixture, agglomerates of multilayers are formed leading to microstructures very similar to those obtained by cold-rolling (Fecht, 2002). With increasing MA time, the composite powder particles get work hardened, the hardness and consequently the brittleness increases, and the particles get fragmented resulting in particles with more equiaxed dimensions (Suryanarayana, 2001). With further milling, the elemental lamellae of the welded layer and both the coarse and fine powders become convoluted rather than being linear. Alloying begins to occur at this stage due to the combination of decreased diffusion distances (interlamellar spacing), increased lattice defect density, and any heating that may have occurred during the milling operation (Öveçoğlu, 1987). The hardness and particle size tend to reach a saturation value at this stage, called the *steady-state processing* stage. With further milling, true alloying occurs at the atomic level resulting in the formation of solid solutions, intermetallics, or even amorphous phases. The layer spacing becomes so fine or disappears at this stage that it is no longer visible under an optical microscope (Öveçoğlu, 1987; Suryanarayana, 2001).

Considering ductile-brittle combinations, in the initial stages of milling, the ductile metal powder particles get again flattened by the ball-powder-ball collisions, while the brittle oxide or intermetallic particles get fragmented. These fragmented brittle

particles tend to become occluded by the ductile constituents and trapped in the ductile particles. The brittle constituent is closely spaced along the interlamellar spacings (Figure 2.14a). With further milling, the ductile powder particles get work hardened, the lamellae get twisted, and refined (Figure 2.14b). With continued milling, the lamellae get further refined, the interlamellar spacing decreases, and the brittle particles get uniformly dispersed, if they are insoluble, in the ductile matrix (Figure 2.14c) (Öveçoğlu, 1987; Suryanarayana, 2001). On the other hand, if the brittle phase is soluble, alloying occurs between the ductile and brittle components also and chemical homogeneity is achieved (Suryanarayana, 2001).

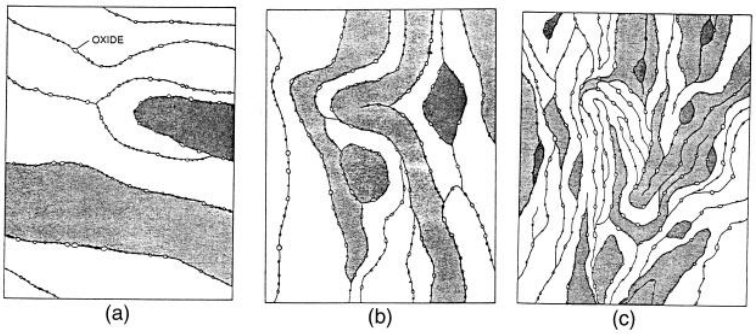

Figure 2.14: Schematics of microstructural evolution during milling of a ductile-brittle combination of powders. This is typical for oxide dispersion strengthened alloys (Suryanarayana, 2001).

If a brittle-brittle combination is the case, it would appear that it is unlikely that alloying occurs in a system consisting of two or more brittle components. The reason for that is that the absence of a ductile component prevents any welding from occurring, and in its absence, alloying is not expected to occur (Coşkun, 2006). However, alloying has been reported to occur in brittle-brittle component systems such as Si-Ge and Mn-Bi or Fe_2O_3-Cr_2O_3 and ZrO_2-Y_2O_3 (Suryanarayana, 2001; Fecht, 2002). During milling, the brittle components get fragmented and their particle size gets reduced continuously. However, at very small particle sizes the powder particles behave in a ductile fashion, and further reduction in size is not possible. This is termed the limit of comminution. Furthermore, during milling of brittle-brittle component systems, it has been observed that the harder (more brittle) component gets fragmented and gets embedded in the softer (less brittle) component (Suryanarayana, 2001).

Nanostructured materials that are defined as materials with grain sizes less than 100 nm have received much attention as advanced engineering materials with improved

physical and mechanical properties (El-Eskandarany, 2001). Because of the extremely small size of the grains, a large fraction of the atoms in these materials is located in the grain boundaries and as a result the material exhibits enhanced combinations of physical, mechanical, and magnetic properties (compared to material with a more conventional grain size, i.e.,>1 μm) (Fecht, 2002; (Suryanarayana, 2001). Nanostructured materials have increased strength, high hardness, extremely high diffusion rates, and consequently reduced sintering times for powder compaction (Suryanarayana, 2001).

Recently, MA process has become a popular method to fabricate nanocrystalline materials due to its simplicity and relatively inexpensive equipment (El-Eskandarany et al., 2000; El-Eskandarany, 2001). The advantage of using MA for the synthesis of nanocrystalline materials lies in its ability to produce bulk quantities of material in the solid state using simple equipment and at room temperature (Suryanarayana, 2001). In this process, lattice defects are produced by pumping energy into powder particles of typically 50 μm particle diameter. This internal refining process with a reduction of the average grain size by a factor of 10^3-10^4 results from the creation and self organization small-angle and high-angle grain boundaries within the powder particles during the mechanical deformation process (Fecht, 2002). Grain sizes with nanometer dimensions have been observed in almost all MA'd pure metals, intermetallics, and alloys (Suryanarayana, 2001). The elemental processes leading to formation of nanostructures include three basic stages. Firstly, the deformation is localized in shear bands which contain a high dislocation density (Fecht, 2002). Their typical width is approximately 0,5-1 μm (Suryanarayana, 2001). At a certain level of strain within the high strained regions, these dislocations annihilate and recombine to small-angle grain boundaries separating the individual grains (Fecht, 2002). This results in a decrease of the lattice strain. With the continuing process, deformation occurs in shear bands located in previously unstrained parts of the material. The grain size decreases steadily and the shear bands unite. The small angle boundaries are replaced by higher angle grain boundaries and, consequently, dislocation-free nanostructured grains are formed (Suryanarayana, 2001).

2.2.3 Sintering

Sintering is a processing technique used to produce density-controlled materials and components from metal or/and ceramic powders by applying thermal energy (Kang, 2005). In sintering, particles bond with one another by atomic diffusion. There are different variables which determine sinterability and the sintered microstructure of a powder compact which given in Table 2.1 (Kang, 2005). All sintering equations contain a number of parameters such as diffusion coefficient, surface tension, particle size, initial pore volume, etc. One can divide these parameters into two classes: a) intrinsic and b) extrinsic (Upadhyaya, 2001).

1. Intrinsic - these specify the intrinsic properties of the materials being sintered, such as surface tension, diffusion coefficient, vapour pressure, viscosity, etc. These properties change when the chemical composition, ambient atmosphere or temperature changes (Upadhyaya, 2001).

2. Extrinsic - these depend on the geometrical or topological details of a system. These include parameters, as average particle size, particle or pore or grain shape and size distribution, etc (Upadhyaya, 2001).

The driving force for sintering is the minimization of the solid-vapor interface area (i.e., the total area of the powders in contact with the surrounding vapor) and elimination of the regions of sharp curvature at powder contacts. In the initial stages of sintering, small necks form and grow between contacting particles by mass transfer via atomic diffusion. Fine powders increase the driving force for sintering because of a larger surface area per unit volume, which increases the total solid-vapor interfacial energy (Asthana et al., 2006).

Basically, sintering processes can be divided into two types: solid state sintering and liquid phase sintering. *Solid state sintering* occurs when the powder compact is densified wholly in a solid state at the sintering temperature, while *liquid phase sintering* occurs when a liquid phase is present in the powder compact during sintering (Kang, 2005).

Table 2.1: Variables affecting sinterability and microstructure (Kang, 2005).

Variables related to raw materials (material variables)	Powder: Shape, size, size distribution, agglomeration, etc. Chemistry: Composition, impurity, homogeneity, etc.
Variables related to sintering conditions (process variables)	Temperature, time, pressure, atmosphere, heatingand cooling rate, etc.

2.2.3.1 Solid state sintering

Solid-state sintering is carried out in protective atmosphere within a furnace at a temperature below the melting point of the base metal. The process leads to a decrease in the surface area, an increase in compact strength and mostly shrinkage in the compact. Sintering for longer durations at high temperature decreases the number of pores and makes the pore shape become smooth. Also, grain growth can be expected (Upadhyaya, 2000).

Various stages and mass transport mechanisms have been proposed to contribute to sintering. The transport mechanisms detail the paths by which mass moves; for solid-state sintering the candidate processes include surface diffusion, volume diffusion, grain boundary diffusion, viscous flow, plastic flow, and even vapor transport from solid surfaces (German, 1996).

The three stages of sintering and and their schematic densification curve of a powder compact can be seen in Figure 2.16 (Kang, 2005). In addition to these three stages, a very first stage occurs when particles come into contact, since there is a weak cohesive cohesive bond at the contacts (German, 1996). The initial sintering stage usually occurs during heating and is characterized by rapid grain growth of the interparticle neck. Although there is a considerable neck growth, the actual volume of the neck is small, so, it takes a small mass to form a neck. In the intermediate stage, the pore structure becomes smooth and develops an interconnected, approximately cylindrical nature. The appearance of isolated pores indicates the final stage of sintering and slow densification (German, 1996).

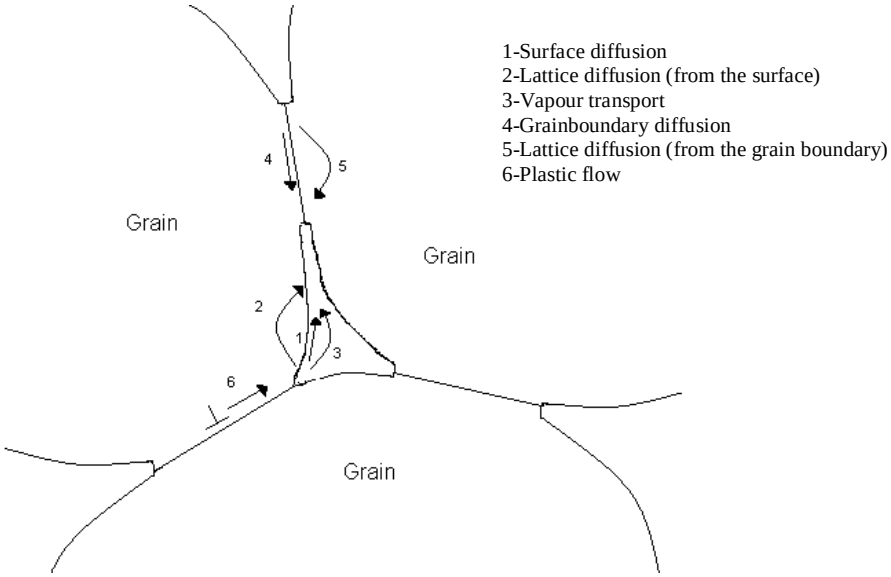

Figure 2.15: Various sintering mechanisms (Uphadhyaya, 2000).

The three stages can be described with the highlights listed below:

Initial Stage: Particle surface smoothing and rounding of pores, grain boundaries form, neck formation and growth, homogenization of segregated material by diffusion, open pores and small porosity decreases <12%(Ring, 1996).

Intermediate Stage: Intersection of grain boundaries, shrinkage of open pores, porosity decreases substantially, slow grain growth and differential pore shrinkage and grain growth in heterogeneous material (Ring, 1996).

Final Stage: Closed pores--density >92 %, closed pores intersect grain boundaries, pores shrink to a limiting size or disappear and pores larger than the grains shrink very slowly (Ring, 1996).

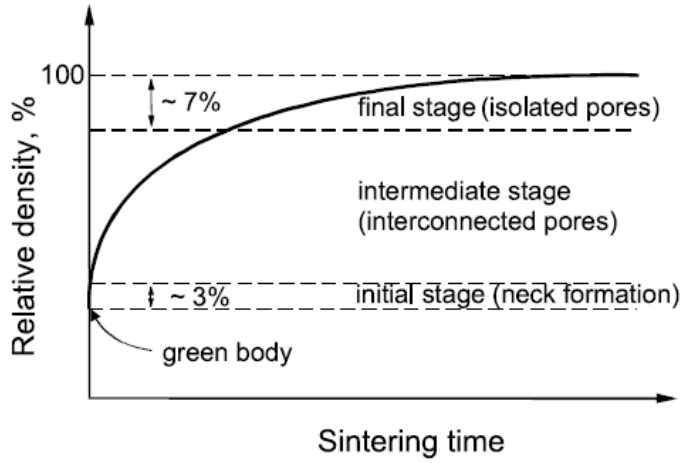

Figure 2.16: Schematic showing the densification curve of a powder compact and the three sintering stages (Kang, 2005).

2.2.3.2 Liquid phase sintering

Liquid phase sintering is a consolidation technique of powder compacts containing more than one component at a temperature above the solidus of the components and hence in the presence of a liquid. Unlike solid state sintering, the microstructure change during liquid phase sintering is fast because of fast material transport through the liquid (Kang, 2005). It is rare that sintering with liquid phase does not imply any chemical reactions, but in the simple case where these reactions do not have a marked influence, surface effects are predominant. The main parameters are therefore: i) quantity of liquid phase, ii) its viscosity, iii) its wettability with respect to the solid, and iv) the respective solubilities of the solid in the liquid and the liquid in the solid (Boch and Leriche, 2001).

There are two kinds of liquid phase sintering namely heterogeneous systems and homogeneous systems. In heterogeneous systems, solid material is heated to sintering temperature and a liquid phase is formed which persists throughout sintering and the liquid solidified during cooling. In case of homogeneous systems, as the consalidated powders are heated to sintering temperatures, a liquid phase is formed which gradually disappears as it is soluble in the matrix. Particle rearrangement stage, dissolution-reprecipitation stage, liquid assimilation and solid state grain growth stage are the four main stages of liquid phase sintering process (Ring, 1996).

Modern liquid-phase sintering is traced to the developement of cemented carbides, bronze bearings and magnetic alloys during 1920s. The developement of W heavy alloys (W-Ni-Fe or W-Ni-Cu) provided an important theoretical basis fort he process. Today, many products are processed by liquid-phase sintering, including dental porcelains, cemented carbide cutting tools, automotive connection rods and refractory ceramics (German, 1996).

2.2.3.3 Activated sintering

Activated sintering involves a small addition to the powder mix or, more rarely, to the sintering atmosphere in order to promote sintering kinetics. The action of the activator may be to remove the surface oxide from the powder particles or to facilitate more rapid diffusion of the metal's atoms (Upadhyaya, 2000). A high-melting-temperature materials material requires a high sintering temperature to

induce significant diffusion. However, a lower-melting-temperature phase will have inherently faster diffusion rates. Activated sintering occurs when the high-melting-temperature material is soluble in the low-melting-temperature phase, resulting is a short-circuit sintering path. Some of the most dramatic examples of activated sintering occur with the refractory metals: molybdenum, tungsten, chromium, rhenium, and tantalum (German, 1996).

Generally, it is very difficult to fabricate tungsten because of its high melting point, low ductility. Even when the powder metallurgy techniques are used, processing of tungsten requires very high sintering temperatures up to 2400 – 2800 ^{o}C to get near fully dense structure (Li and German, 1983). The addition of small quantities of some transition metals such as palladium (Pd), platinum(Pt), nickel(Ni), cobalt (Co), and iron (Fe), provides a major reduce in the sintering temperature of W (Li and German, 1983; German and Munir, 1976; Vacek, 1959; Hayden and Brophy, 1963). This reduction of the sintering temperature is due the decrement of the activation energy between W particles. Activation energy for volume self-diffusion of tungsten, 135 kcal/mol, becomes 68 kcal/mol in the case of Ni activated W (Hayden and Brophy, 1963).

Hayden and Brophy interpreted the mechanism of the activated sintering in terms of three main stage in their study (Hayden and Brophy, 1963). After the appearance on the tungsten particle surface of a “supporting phase”, formed by activating agent, the dissolution of tungsten at the points of contact between particles takes place and the diffusion of tungsten atoms along the interface between the “supporting phase” and the particle provides densification. On this basis, the distance between the centers of adjacent particles decreases and consequently fuller shrinkage occurs (Hayden and Brophy, 1963; Samsonov and Yakovlev, 1967). Figure 2.17 is the schematic representation of sintering nickel-coated tungsten powder which Brophy et. al., indicated during their project prepared in U.S. Navy in M.I.T. laboratories (Brophy et. al, 1963).

Another elucidation of the activated sintering mechanism was accomplished in (Toth and Lockington, 1967) where dissolution of tungsten at the activator-tungsten interface is followed by volume diffusion outwards through the activator layer and subsequent surface diffusion. Diffusion through the activator layer to the contact

point between adjacent particles results in the formation of sintering “necks” (Toth and Lockington, 1967; Corti, 1986).

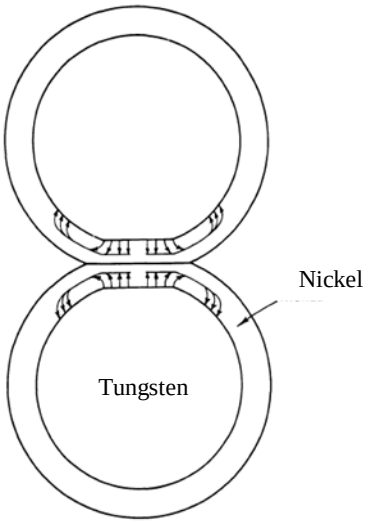

Figure 2.17: Schematic representation of sintering nickel-coated tungsten powder (Brophy et. al., 1963).

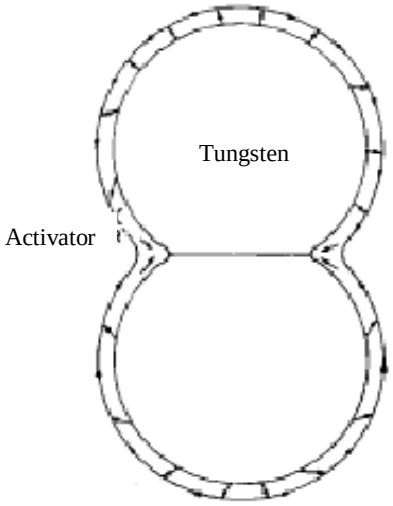

Figure 2.18: Schematic representation of activated sintering of tungsten (Toth and Lockington, 1967).

Samsonov and Yakovlev stated activated sintering in terms of the electron structure of the activators and tungsten; an increase of the stable d-bonds in the system lowers the free energy, activating the sintering process in which diffusion is accelerated by the activators for which tungsten acts as an electron donor and this ease of electron transfer gives rise to the high solubility in the activating element (Samsonov and Yakovlev, 1969).

German and Munir reported that the activator has a role in providing enhanced grain boundary diffusion with the activator layer wetting the interparticle grain boundary. The relative solubility criterion is a prerequisite for enhanced diffusion of the refractory metal. Enhanced mass transport, and hence densification, results from the lowering of the activation energy for the refractory metal in the activator (German and Munir, 1982; Corti, 1986).

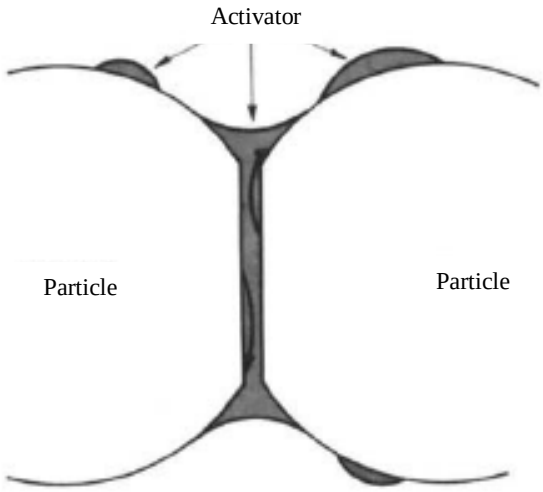

Figure 2.19: Schematic representation of the activated sintering (German and Munir 1982).

3. MATERIALS SELECTION

From the beginning, the selection of a proper combination of matrix and reinforcement has been the main goal of design and production of PRMMC's. The motivation for using MMC materials in current research investigations is that these materials provide a superior combination of different properties of metallic matrix and hard reinforcement. However, these properties can only be obtained with proper selection of the matrix material and the reinforcements (Lindroos et al., 2004).

The matrix of the composites has to be mainly designed for two major tasks, which is firstly to bind and support the reinforcing phase and, secondly, to satisfy special properties based on the requirements in service. Binding strength between the matrix, whose main function is to transfer and distribute the load to the reinforcement, and the reinforcement depend on the type of matrix and reinforcement (Huda et al., 1995; Lindroos et al., 2004). The interface formed between the matrix and the reinforcement is of interest since the characteristics of this region determine load transfer and crack resistance of the composite during deformation. It is now widely acknowledged that in order to maximize interfacial bond strength, it is necessary to promote wetting (when a liquid phase process is present), control chemical interactions and minimize oxide formation (Ibrahim et al., 1991). On the other hand, the hardness of the matrix is the key factor in supporting the reinforcing phase. Furthermore, other considerations such as, cost, weight, fabricability and availability of the matrix materials should also be made (Lindroos et al., 2004). Generally, Al, Ti, Mg, Ni, Cu, Pb, Fe, Ag, Zn, Sn and Si are used as the matrix materials (Huda et al., 1995). In addition to these, tungsten (W) has lately received some attention as a matrix material (Song et al., 2002; Song et al., 2003a).

Reinforcing phase in the composites are mainly used to increase the strength, stiffness, temperature resistance capacity and to lower the density. Generally, ceramics are used as the reinforcement phase, which are typically oxides, carbides and nitrides (Huda et al., 1995). The selection criteria for these ceramic reinforcements include elastic modulus, tensile strength, density, melting

temperature, thermal stability, coefficient of thermal expansion, size and shape, compatibility with matrix material and cost (Ibrahim et al., 1991). Typical reinforcement materials are silicon carbide (SiC), aluminum oxide (Al_2O_3),silicon dioxide (SiO_2), titanium carbide (TiC), boron carbide(B_4C) and silicon nitride (Si_3N_4) (Huda et al., 1995).

3.1 Tungsten

The refractory metals are conveniently described as metals that melt at temperatures above 1850 °C, and for this consideration, twelve metals are in this group namely: tungsten (W), rhenium (Re), osmium (Os), tantalum (Ta), molybdenum (Mo), iridium (Ir), niobium (Nb), ruthenium (Ru), hafnium (Hf), rhodium (Rh), vanadium (V), chromium (Cr). Among these, due to their high melting point, high modulus, high resistance of thermal shock, low CTE and good high temperature strength and stiffness properties, tungsten alloys are potential candidates for service conditions which require high strength at elevated temperatures (Song et al., 2002). Properties of tungsten are listed in Table 3.1 (Lassner and Schubert, 1999).

A large number of W alloys and composites were investigated in literature before, whereas only some of them achieved technical importance. The aim of alloying W is to improve its chemical, physical and mechanical properties at both ambient conditions and at elevated temperatures. However, alloying of W has been relatively less studied than of some of the other refractory metals. W is mainly used in aerospace applications in the unalloyed form which is much easier and cheaper to produce and fabricate. Also, it has been found that, particularly at temperatures above 2200 ˚C, the strengthening effects of many alloying agents decrease disproportionately (Lassner and Schubert, 1999).

W is mainly consumed in three forms, which are tungsten carbide (WC), alloying additions and pure formWC accounts for about 65% of W consumption (Lassner and Schubert, 1999). It is combined with cobalt as a binder to form the so-called cemented carbides, which are used in cutting and wear applications because of their high hardness, good wear resistance, good fracture resistance and high temperature strength (Zhang et al., 2003) Cemented carbides such as WC-Co and WC-Co-TiC are the most widely used material for metalworking. As a consequence, a considerable amount of research effort has been spent to develop alternative cemented carbide

systems in order to improve the microstructure and mechanical properties of these materials (Acchar et al., 2004). Characteristically, most of the carbides used in cermets have high hardness, good electrical and thermal conductivity, and high stability. The brittleness of carbides, however, has prevented their use as single-phase materials in highly stressed structural applications and has led to the development of metal-bonded composites (cemented carbides or cermets) (Coşkun, 2006).

Table 3.1: Properties of W (Lassner and Schubert, 1999).

Period	6
Atomic Number	74
Atomic Mass	183.85
Electronegativity	1.7
Space Group	Im3m
Lattice Parameter	3.16524 Å
Density	19.3 g/cm^3
Melting Point	3422 °C
Boiling Point	5663 °C
Specific Heat	0.0317 cal/gK
CTE	4.32-4.68x10-6 K-1 (25 °C)
Tensile Strength	172.4 MPa
Young's Modulus	390-410 GPa
Shear Modulus	156-177 GPa
Bulk Modulus	305-310 GPa
Poisson' Ratio	0.28-0.30
Hardness	350-450 kg/mm^2

Metallic W and W alloy mill products account for about 16% of consumption. W and W alloys dominate the market in applications for which a high-density material (19.3 g/cm^3) is required, such as kinetic energy penetrators, counterweights, flywheels, and governors. Tungsten and its alloys are also used in radiation shields and X-ray targets.Also in wire form, W is used extensively for lighting, electronic devices, and thermocouples (Lassner and Schubert, 1999; Li and German, 1983).

The high melting point of W makes it an obvious choice for structural applications exposed to very high temperatures. W is also used at lower temperatures for applications that can use its high elastic modulus, density, or shielding characteristics to advantage (Lassner and Schubert, 1999).

3.2 Ni-Activated Sintering and W-Ni System

Activated sintering mechanism is explanied in detail in Section 2.2.3.3, stating that addition of small quantities of some transition metals such as Pd, Pt, Ni, Co, and Fe enables major reductions in the sintering temperature of W. One of the activating agents, Ni, dissolves up to 38 wt % W in its solid solution and the solubility of W into Ni is only about 0.1 wt % which is negligible (Figure 3.1) (Massalski, 1990). Moreover, the volume diffusion of W into Ni is rather more rapid than that of Ni into W (Panichkina, 1967). Hayden and Brophy reported a value of 68 kcal/mole for the activation energy for volume self-diffusion of W in the case of activated sintering with Ni, a value much lower than 135 kcal/mole pertaining to pure W (Hayden and Brophy, 1963).

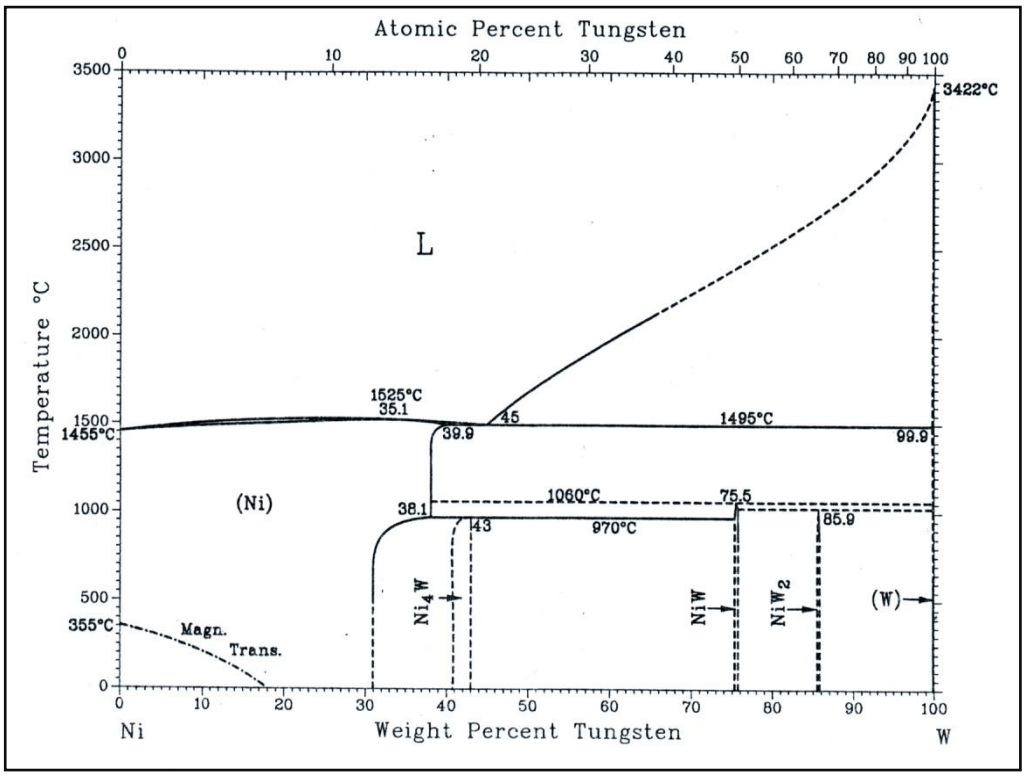

Figure 3.1: Ni-W binary phase diagram (Massalski, 1990).

Activated sintering of W with different transition metal additions have been extensively investigated in the archival literature. German and Munir reported that Pd is the best activator agent for W, and sequentially, Ni, Pt, Co, Fe, Cu addition provides activation (German and Munir, 1976). Even though Pd has been reported as the best activator for W, however its use is limited due to its very high price. Ni is the proper activator agent which can be used instead of Pd, especially at temperature ranges about 1400 ºC (Figure 3.2) (German and Munir, 1976).

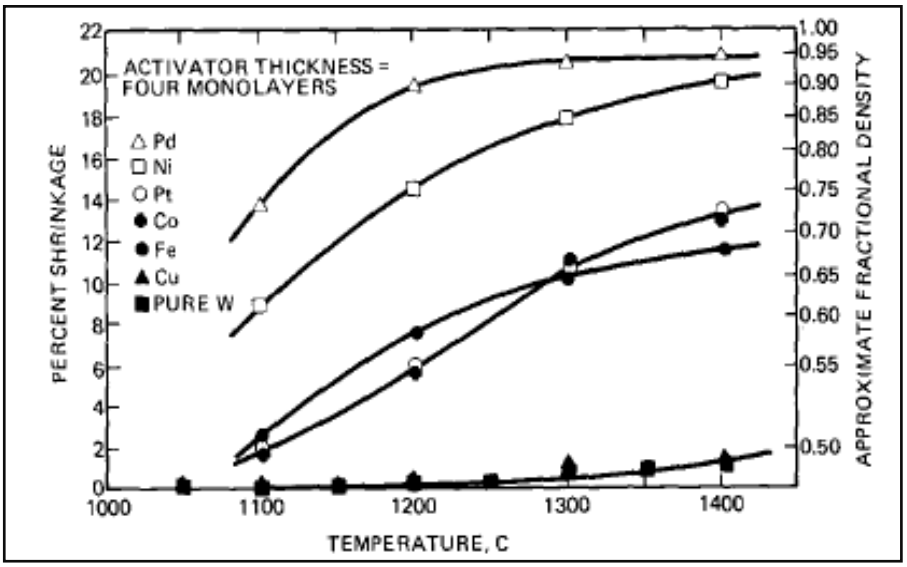

Figure 3.2: Shrinkage dependence on activator type and temperature in activated sintering of W (German and Munir, 1976).

3.3 The Addition of TiB_2 and La_2O_3

In order to improve properties of W, dispersion-strengthened and precipitation hardened composites were developed (Lassner and Schubert, 1999). Investigations regarding the activated sintering of W and W matrix composites reinforced with different refractory carbide, nitride and oxide phases such as TiC, TiN, ZrC, HfC, La_2O_3, Y_2O_3, HfO_2, Sm_2O_3, and ThO_2 have been well documented in the literature (Chen et al., 2009; Genç et al., 2010; Ishijima et al., 2005; Kim et al., 2006; Kurishita et al., 2008; Song et al., 2003b). In addition to these refractory carbide, nitride and oxide materials, transition metal diborides are very promising candidates as reinforcements in W due to their high melting point, high hardness, good electrical and thermal conductivities (Munro, 2000). An important advantage of diborides over carbides and nitrides is that diborides are essentially stoichiometric (Castaing and Costa, 1977). However, there exists no studies in the reported literature on the

microstructural and mechanical properties of transition metal diborides reinforced W matrix composites. Among the transition metal diborides, titanium diboride (TiB_2) comes into prominence with its excellent properties such as high melting point (3225 ˚C), high hardness (25 GPa), good thermal conductivity, high electrical conductivity and considerable chemical stability (Munro, 2000; Genç et al., 2010).

W has a high ductile to brittle transition temperature and its strength decreases with increasing temperature.. For example, the strength of monoclinic W at 1000 ˚C decreases almost 60% compared to its room temperature strength (Chen et al., 2008, Song et al., 2002). A great deal of work has been done on improving the high temperature strength of W. Most studies focused on W strengthened with many finely dispersed particles of carbides, nitrides, oxides (Mabuchi et al., 1996; Mabuchi et al., 1997; Song et al., 2003b; Ryu and Hong, 2003). The particles added can restrict growth of W grain and dislocation motion, both of which lead to high strength and low creep rates at high temperatures. But the volume content of carbide results in low relative density, ductility and strength. However, the rare-earth oxides have some special chemical characteristics. They improve the low-temperature brittleness and decreases ductile to brittle transition temperature in Mo and W materials. (Chen et al., 2008; Mabuchi et al., 1996; Song et al., 2003b). Especially, high temperature oxides, such as ThO_2, La_2O_3, Y_2O_3, and CeO_2 are added to W due to their thermal stability at high temperatures (Kim et al., 2009). Among these oxides, the most common oxide dispersion-strengthened material is the W-ThO_2 alloy which contains a dispersed second phase of 1 wt % thorium. The thorium dispersion enhances thermionic electron emission, which in turn improves the starting characteristics of gas W arc welding electrodes (Mabuchi et al., 1997). It also increases the efficiency of electron discharge tubes and imparts creep strength to wire at temperatures above one-half the absolute melting point of W (Mabuchi et al., 1997; Lassner and Schubert, 1999; Chen et al., 2000). However, it is desirable to replace ThO_2 with non-radioactive activators because of the radioactive pollution of thorium during fabrication, service or handling. In the last decade, considerable efforts have been directed to develop new materials, especially to explore new activators. It has been found that W electrodes activated with rare-earth metal oxides (such as La_2O_3, Y_2O_3, CeO_2, etc.) exhibit superior arc characteristics compared to pure W and W-ThO_2 electrodes (Chen et al., 2000). Particularly, W- La_2O_3

composites with no radioactive potential exhibit good mechanical properties and creep resistance (Mabuchi et al., 1997).

Above mentioned literature review presented the development of dispersion strenghtened W matrix composites and activated sintering of W. However, there are no detailed studies about the sintering behaviour and microstructural properties of dispersion strengthened W-based composites sintered with the presence of both a transition metal diboride and rare-earth oxide. This study aims to fulfill this gap by focusing on sintering behaviour and mechanical properties of mechanically alloyed and Ni activated sintered TiB_2 and La_2O_3 composites. Thus, the objective of the present study is to report on the microstuctural characterization and physical properties of mechanically alloyed and Ni activated W-TiB_2 and W-TiB_2-La_2O_3 composites prepared by mechanical alloying technique.

4. EXPERIMENTAL PROCEDURE

The experimental part of this study was designed in order to provide useful information about sintering, microstructural and mechanical properties of Ni activated W-TiB_2 and W-TiB_2-La_2O_3 composites synthesized by mechanical alloying technique.

The first group of experiments deals with the characterization of W - 1 wt. % Ni. The second and the third group of experiments investigate the effect of TiB_2 and La_2O_3 addition to pre-milled W-Ni matrix. Finally, the fourth group of experiments deals with the effects of TiB_2 and La_2O_3 addition to the pre-milled W-Ni matrix. Additionally, all groups of experiments investigate the effect of mechanical alloying durations on determined composition.

Theexperimental procedure of the present study is summarized in the flow chart shown in Figure 4.1.

4.1 Preparation of Samples

4.1.1 Mechanical alloying and characterization of powders

In this study W (%99.9 purity, 4-7 μm average particle size) and Ni (%99.9 purity, 3-7 μm average particle size) powders were used as matrix materials. TiB_2 (%99.9 purity, 40-44 μm average particle size) and La_2O_3 (%99.99 purity, 25-34 μm average particle size) powders were used as reinforcement materials to avoid the grain growth and improve mechanical properties. Mechanical alloying (MA) experiments were carried out using a Spex™ Duo Mixer/Mill 8000D (Figure 4.2a) with a speed of 1200 RPM in a WC vial with WC balls having a diameter of 6.35 mm (¼ inches). BPR was7:1 in weight. W - 1wt% Ni powders (hereafter referred to as W1Ni) were mixed and pre-milled for 6 hours while TiB_2 and La_2O_3 powders were pre-milled for the same duration. These pre-milled powderswere selected as starting materials in this study. W1Ni (6h MA'd), W1Ni - x wt% TiB_2 (x=2, 3, 4), W1Ni - y wt% La_2O_3 (y=0.5, 1) and W1Ni - 2 wt% TiB_2 - y wt% (y=0.5, 1) powders (hereafter referred to

be as W1Ni-xTiB_2, W1Ni-yLa_2O_3 and W1Ni-xTiB_2-yLa_2O_3) were mixed and alloyed for 6 and 12 hours.

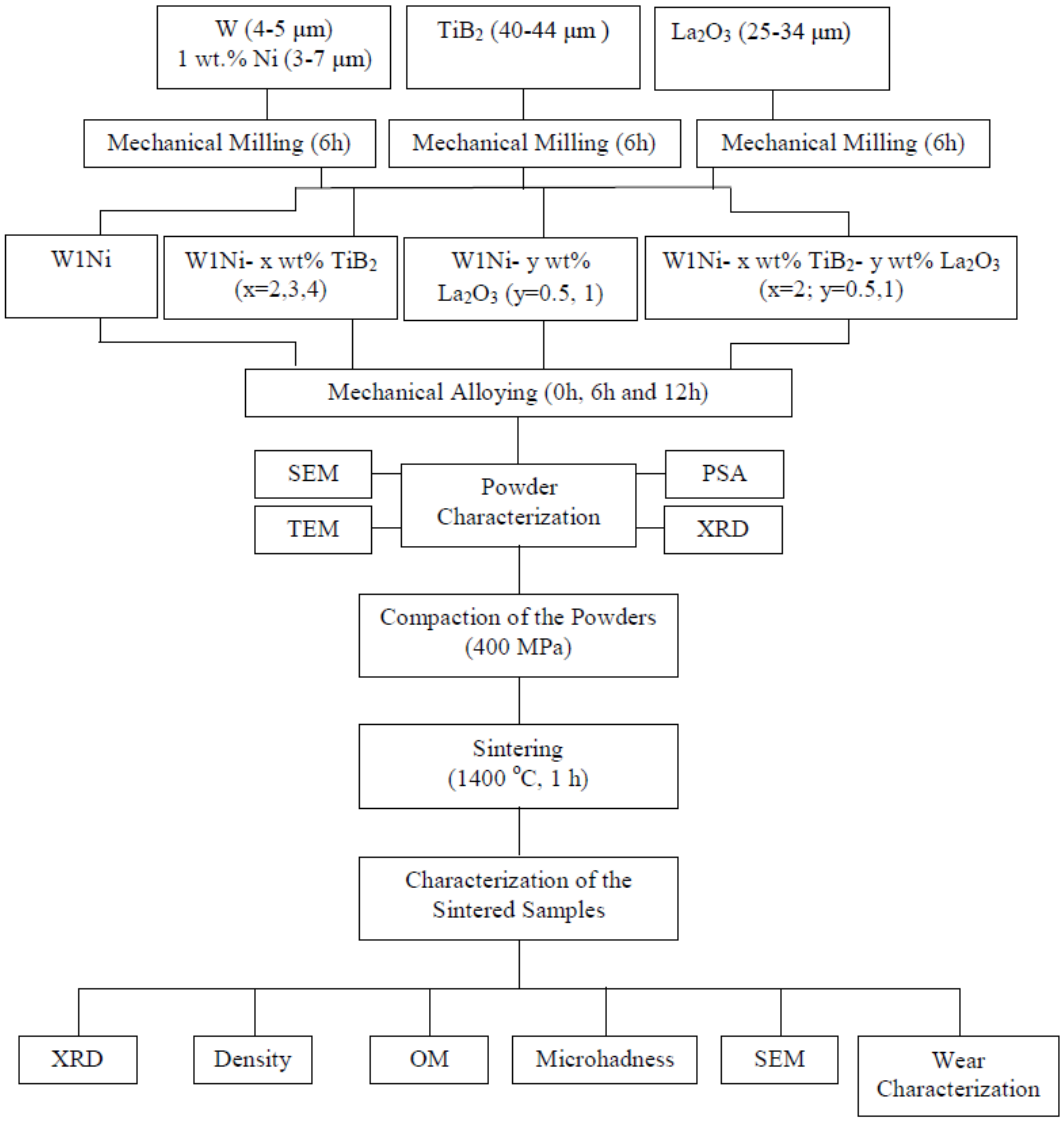

Figure 4.1: The flow chart of the experimental procedure

High-purity argon (Ar) gas was used as the milling atmosphere to prevent oxidation and contamination of the powder in order to prevent the formation of oxides and nitrides in the powder when exposed to air. This is required, especially if the powders are reactive in nature. Thus, the loading and unloading of the powders into the vial was carried out inside a "Pluslabs™" atmosphere-controlled glove box (Figure 4.2b), operated under Ar atmosphere.

Powder particle size measurements were carried out in a Malvern™ Mastersizer Laser particle size analyzer (Figure 4.3a). Microstructural characterization investigations of as-blended and MA'd powders were conducted using a Jeol™-

JSM-T330 (Figure 4.4a) scanning electron microscope (SEM), Jeol™-JEM-EX2000 (Figure 4.4b) transmission electron microscope (TEM) and a Bruker™ X-Ray Diffractometer (Figure 4.3b) (XRD) using CuK_{α} radiation. TOPAS 3 (Bruker AXS) software (Kern and Coelho, 2006) was used to estimate crystallite sizes.

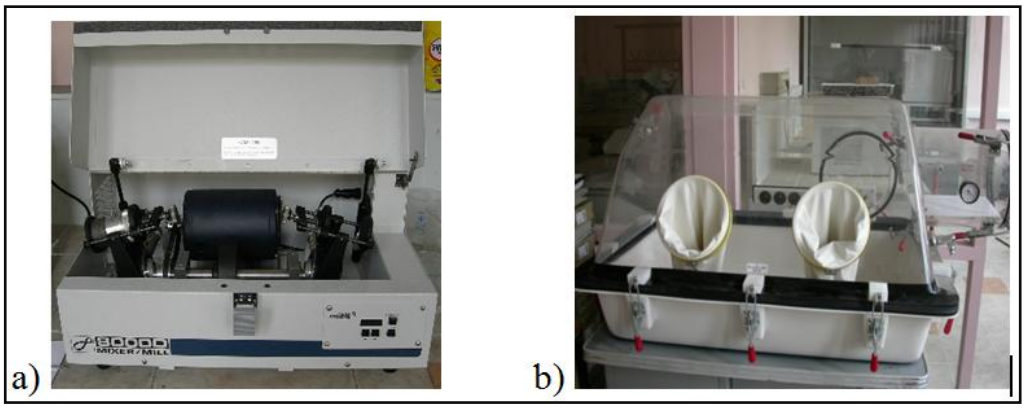

Figure 4.2: a) 8000D™ Spex mill, **b)**Pluslabs™glove box.

Figure 4.3: a) Malvern™ Mastersizer, **b)** Bruker™ X-Ray Diffractomete (XRD).

4.1.2 Compaction

The mechanically alloyed powders were compacted by cold pressing in a tool-steel die at a pressure of 400 MPa into cylinder shaped green compacts with a diameter of ≈6.36 mm for 1 minute by using a 10 tons "MSE" one-action hydraulic pres. Figure 4.5 shows the picture of the MSE hyraulic pres. Liquid paraffin was applied to the walls of the die to take the samples out of the die easily.

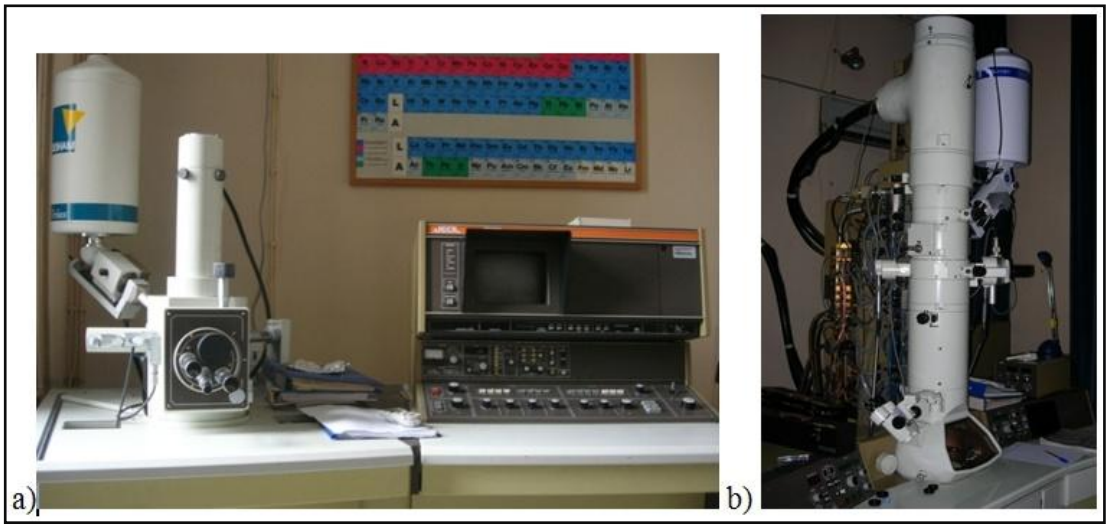

Figure 4.4: **a)** Jeol™-JSM-T330 scanning electron microscope and **b)** Jeol™-JEM-EX2000 transmission electron microscope.

Figure 4.5: MSE one-action hydraulic press.

4.1.3 Sintering

Sintering wasperformed at 1400 ^{o}C for 1 hour in a Linn™ 1800 M Vac Graphite furnace. The furnace works under gas sintering conditions using vacuum and H_2, Ar and N_2 gases as sintering media. The sintering regime is shown in Figure 4.6.

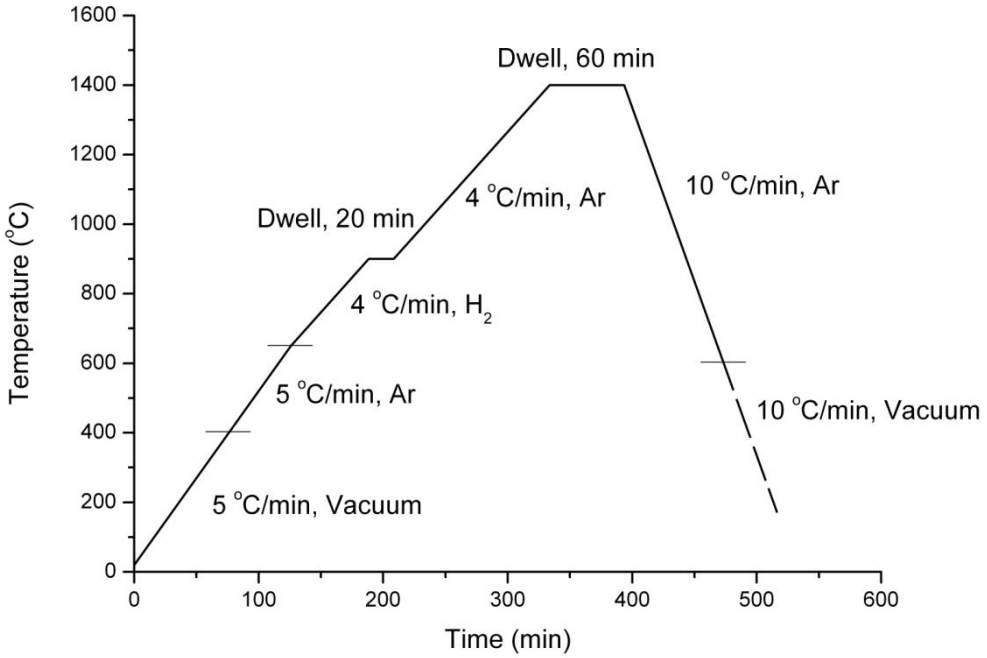

Figure 4.6: The sintering regime in the 1800 M Vac Graphite Linn™ furnace

4.2 Characterization of Sintered Samples

4.2.1 Microstructural and phase characterization

The microstructural and phase characterization investigations of the sintered samples were carried out using optical microscope (OM), scanning electron microscope (SEM) and X-ray diffraction (XRD) techniques. Prior to the characterization investigations, the sintered samples were mounted in bakelite using the Struers™ Labopress-1 machine (Figure 4.7a). After that, samples were polished on the Struers™ Tegrapol-15 automatic polishing machine (Figure 4.7b).

4.2.2 Density measurements

Sintered densities were measured by using the Archimedes method which depends on the relationship between volume and mass. Density results are the arithmetic mean of 5 measurements of the same sample. The Archimedes method mechanism is shown in Figure 4.8.

4.2.3 Hardness measurements

Hardness measurements were carried out on a Shimadzu™ micro hardness tester (Figure 4.9) with a Vickers indenter under a load of 100 g for 15 seconds. Results of hardness tests were averaged out of 15 successive indentations.

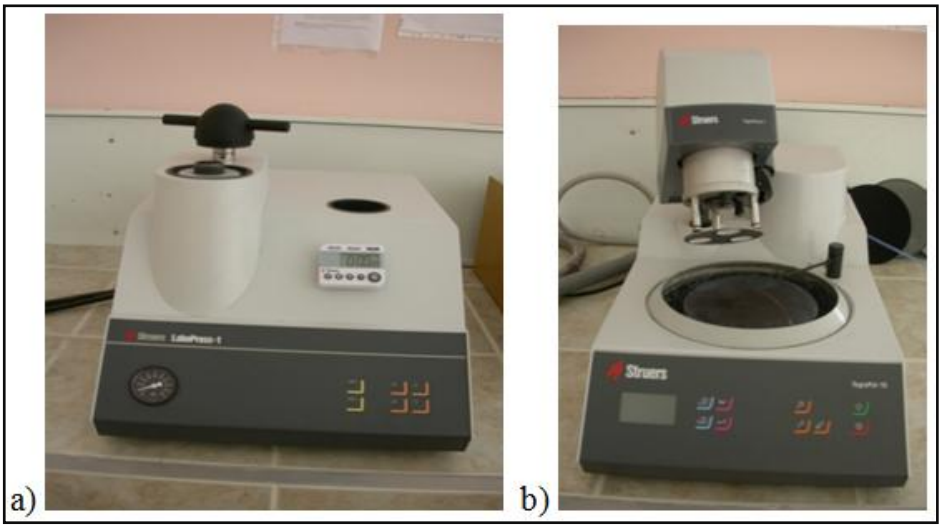

Figure 4.7: a) Struers™ Labopress-1 machine and **b)** Struers™ Tegrapol-15 automatic polishing machine

Figure 4.8: Precisa™ XB220A weighing machine and the Archimedes method mechanism

Figure 4.9: Shimadzu™ micro hardness tester.

4.2.4 Wear characterizations

The sliding wear experiments were conducted on a Tribotech™ Oscillating Tribotester (Figure 4.10a) to the sintered samples of 12h MA'd powders using 6 mm alumina balls under an applied force of 4 N. The tests were conducted at room temperature in a laboratory atmosphere with a sliding speed of 4 mm/s, a stroke length of 2 mm and a sliding distance of 20 m. Abraded surfaces were characterized using a Veeco™ Dektak 6 M Stylus Profiler (Figure 4.10b) and test results are arithmetic mean of three different measurements for each sample which are calculated by integrating the area of the each peak of the surface profile.

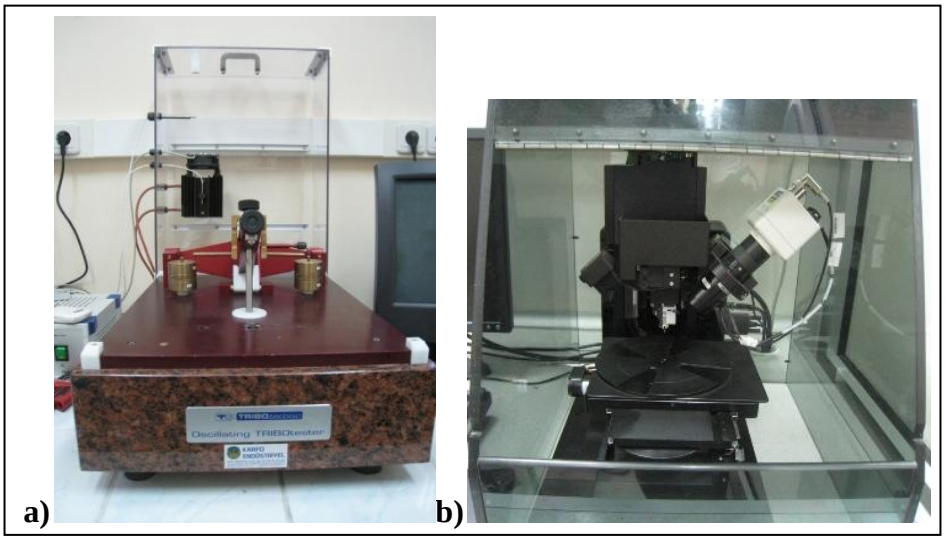

Figure 4.10: **a)**Tribotech™ Oscillating Tribotester **b)** Veeco™ Dektak 6 M Stylus Profiler

5. RESULTS AND DISCUSSIONS

As early mentioned in experimental procedure, the results of this study can be divided into four groups:

1. W1Ni,

2. W1Ni – x wt % TiB_2 (x=2,3,4),

3. W1Ni – y wt % La_2O_3 (y=0.5, 1),

4. W1Ni – x wt % TiB_2– y wt % La_2O_3 (x=2; y=0.5, 1).

Each experimental group contains studies about the fabrication and characterization of the mechanical alloyed and sintered samples. The first group of experiments deal with the characterization of W - 1 wt. % Ni. The second and the third groups of experiments investigate the effect of TiB_2 and La_2O_3 addition to the pre-milled W-Ni matrix, respectively. Finally, the fourth group of experiments deals with the effect of both TiB_2 and La_2O_3 adittions to the pre-milled W-Ni matrix.

In Figure 5.1 andFigure 5.2, XRD patterns and particle size distributions of the powders used in this study are given, respectively.

Figure 5.1a shows XRD patterns of the pre-milled W1Ni powders. As seen in this figure, the peaks of W which has a b.c.c. Bravais lattice and Im $\bar{3}$ m space group with the lattice parameter of a=0.316 nm (ICDD No: 04-0806) can be identified. Figure 5.1b and c are the XRD patterns of 6 hours pre-milled TiB_2 (ICDD No: 35 – 0741, a hexagonal Bravais lattice, with the lattice parameters ofa = b = 0.303 nm, c = 0.323 nm) and La_2O_3 (ICDD No: 83 – 1344, a hexagonal Bravais lattice with the lattice parameters of a = b = 0.394 nm, c = 0.614 nm) powders, respectively.

Figure 5.2a – c show the particle size distributions of the pre-milled W1Ni, pre-milled TiB_2 and pre-milled La_2O_3 powders, respectively. After pre-milling, mean particle size of TiB_2 reduced from 44 μm to 1.20 μm (Figure 5.2b) and that of La_2O_3 from34 μm to 1.79 μm (Figure 5.2c), respectively. The mean particle size of W1Ni matrix was measured as 1.16 μm (Figure 5.2a).

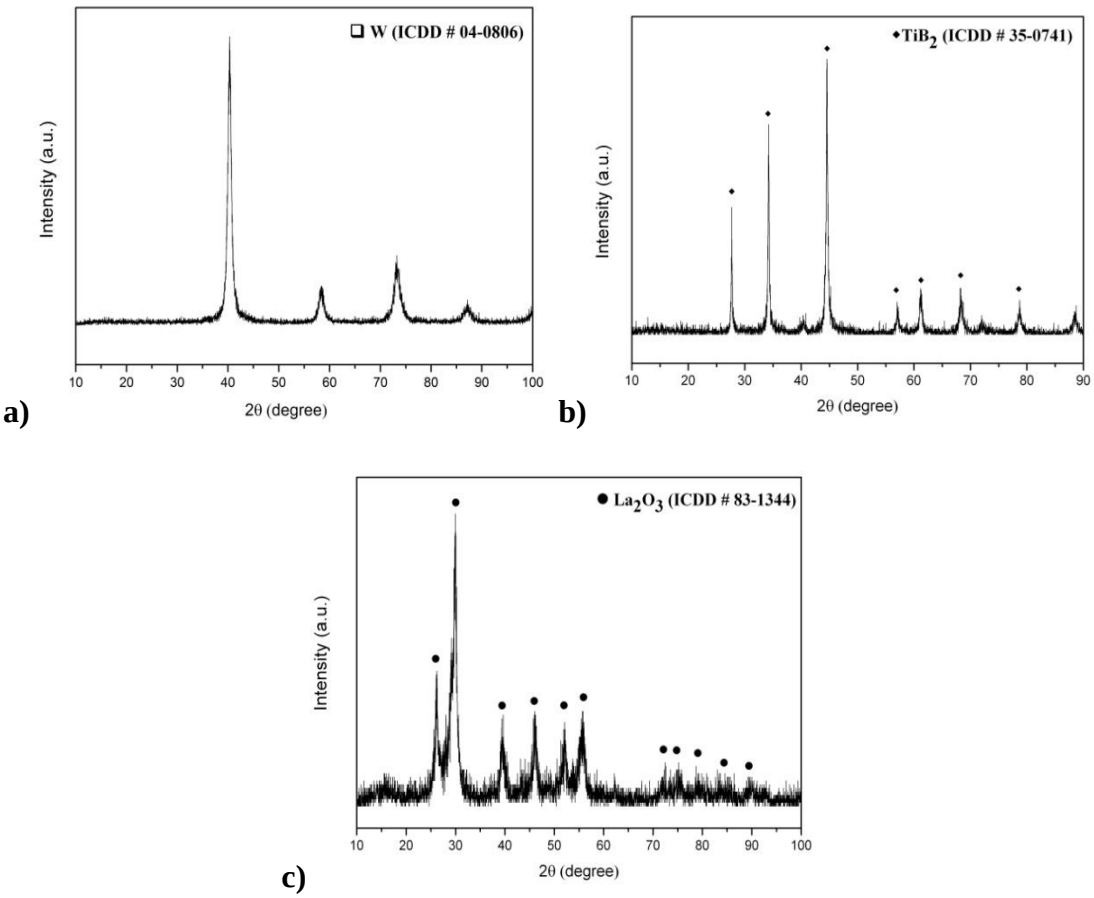

Figure 5.1: XRD patterns of the **a)** pre-milled (6h MA'd) W1Ni **b)** pre-milled TiB_2 **c)** pre-milled La_2O_3powders

5.1 Characterization Investigations of the W1Ni Samples

5.1.1 Characterization of the powders

Figure 5.3 shows the XRD patterns of the W1Ni powders MA'd for different durations. All the peaks seen in the figure belong to W (ICDD No: 04-0806) mentioned before. As seen in the figure peaks were brodened and the peak intensities decreased with increasing MA'd durations.

Crystallite sizes and lattice deformations of the pre-milled W1Ni powders were measured and the results are given in Table 5.1. These calculations reveal that crystallite sizes about 14.7 nm decreased to 6.4 nm with increasing MA duration, whereas lattice deformations increased up to 3.86%.

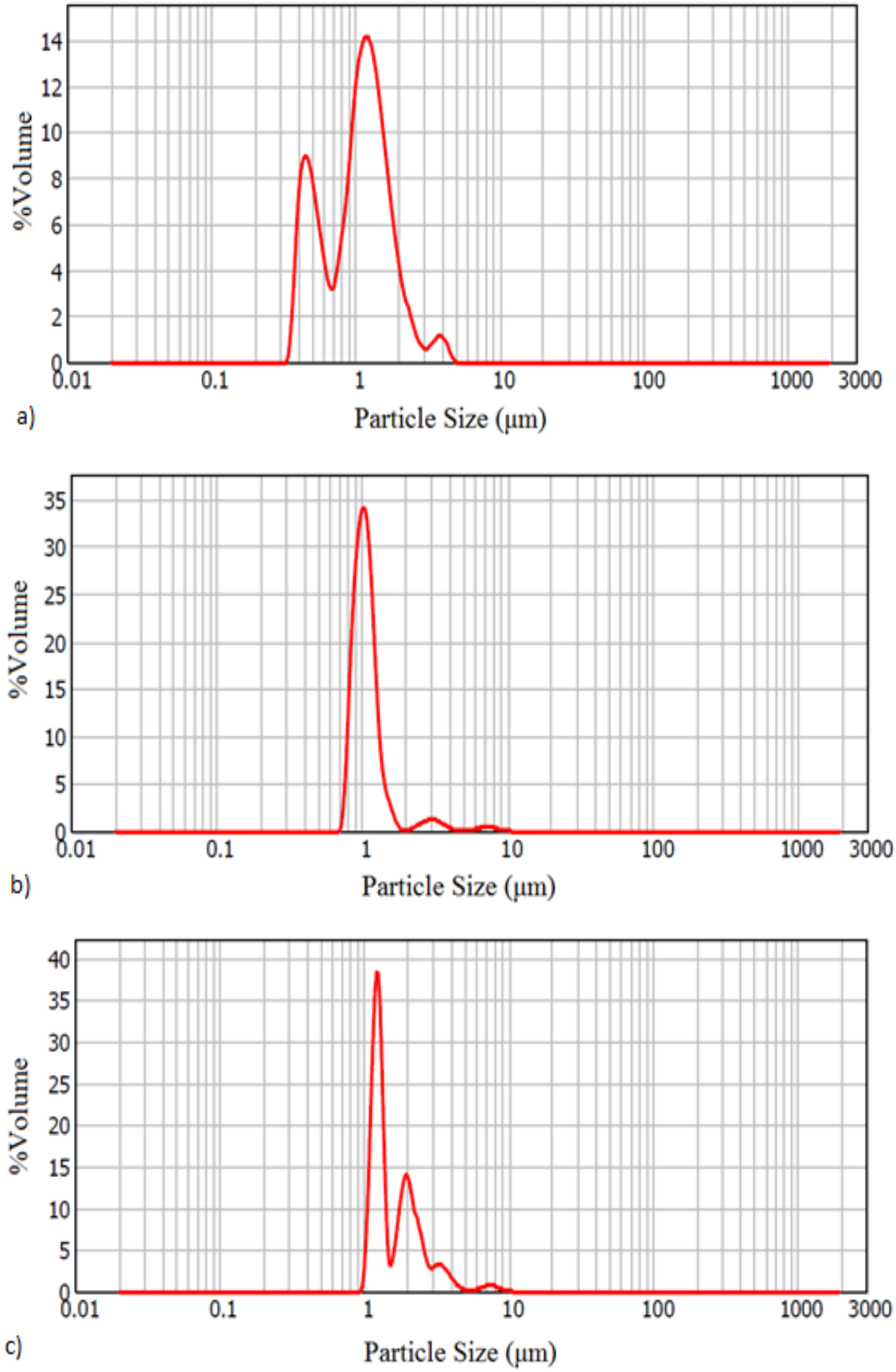

Figure 5.2: Particle size distributions of **a)** pre-milledW1Ni matrix (D_{mean}=1.16µm, D_{50}=1.09µm), **b)** pre-milled TiB_2 (D_{mean}=1.20µm, D_{50}=1.05µm), **c)** pre-milled La_2O_3 (D_{mean}=1.79µm, D_{50}=1.34µm).

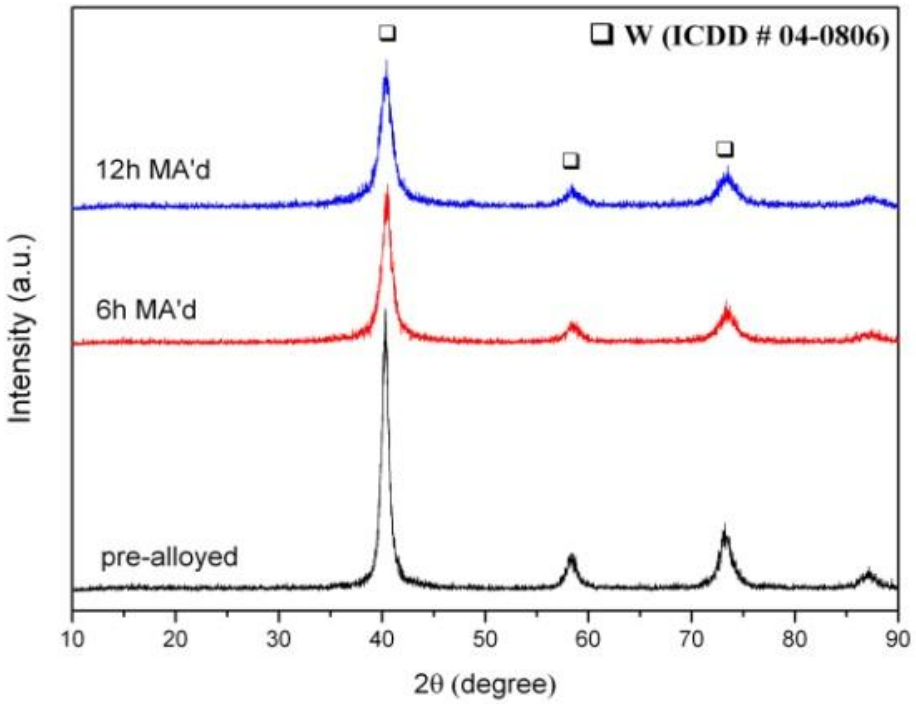

Figure 5.3: XRD patterns of the pre-milled (6h MA'd) and additionally 6h MA'd, 12h MA'd W1Ni powders

Table 5.1: Crystallite sizes and lattice defomations of the MA'd W1Ni powders.

Sample Name	Crystallite Size (nm)	Lattice Deformation (%)
W1Ni pre-alloy (6h MA'd)	14.7	1.75
W1Ni + 6h MA'd	8.1	3.16
W1Ni + 12h MA'd	6.4	3.86

Figure 5.4 shows the representative SEM micrographs taken from the W1Ni pre-milled powder and the W1Ni matrix powders MA'd for 12 h.SEM micrograph of the pre-milled W1Ni powders is shown in Figure 5.4a, revealing that the MA'd powders are mainly consist of submicron particulates, whereas some agglomerates having sizes of about 2 μm are present in the microstructure. SEM micrograph presented in Figure 5.4b is taken from the W1Ni matrix powders MA'd for 12 h. The micrograph shows the presence of submicron (generally a few hundreds of nanometers) sized particles with spherical shapes and some micron sized (1 – 2 μm) agglomerates. By comparing Figure 5.4a and Figure 5.4b, it is possible to state that these powders has almost the same particle sizes but the fraction of the agglomerates decrease with increasing mechanical alloying durations.

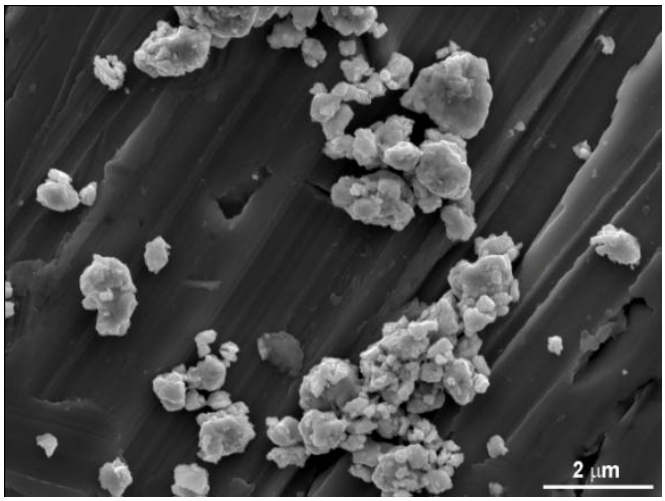

a)

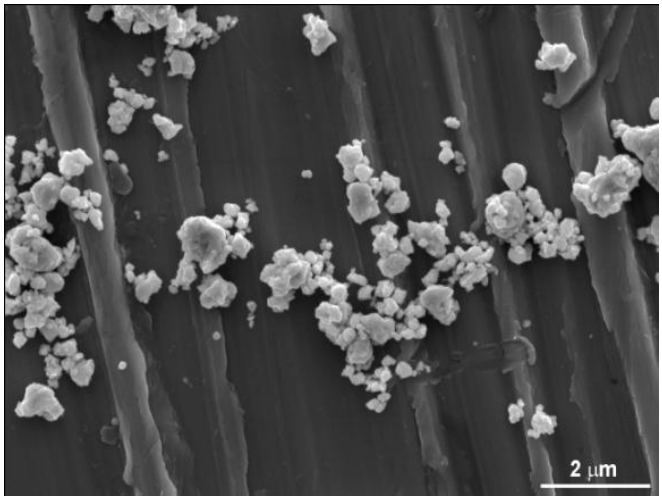

b)

Figure 5.4: SEM micrographs of **a)** pre-milledW1Ni powders **b)**W1Ni matrix powders MA'd for 12h (totaly MA'd for 18h)

5.1.2 Characterization of the sintered W1Ni samples

XRD patterns of the sintered W1Ni powders which were MA'd for different durations are given in Figure 5.5. In this figure, only W phase (ICDD No: 04-0806) is identified in pre-milled W1Ni powders and those MA'd for 6h and 12h.

The relative density measurements and corresponding theoretical density values of the W1Ni samples are given in Table 5.2. The relative density values of W1Ni pre-alloy, W1Ni+6h MA and W1Ni+12h MA samples vary between 97.86 % and 96.51 %. Increasing the mechanical alloying or milling durations results in the decrease of the mean particle size and enables somewhat homogenous distribution of Ni particles in W. After sintering of powders which were milled for longer durations, higher density values were generally obtained. However, it should be mentioned here that there is noremarkable change in the relative density values of the sintered W1Ni

samples with increasing mechanical alloying durations. It is believed that increasing the milling durations causes the contamination of powders by milling media (Chen 2008; Mabuchi 1996), WC, which has a density of 15.8 g/cm^3. As a result of WC contamination theoretical densities decreased, so the relative density remained almost the same with increasing mechanical alloying durations. Thus, relatively high density values (>95%) are reported in the present investigation,after conventionally sintering at a temperature of 1400 °C, indicating the coupled effects of mechanical alloying and Ni activated sintering on the enhanced sinterability of pure W.

Vickers microhardness results of sintered W1Ni samples are given in Table 5.2. The sintered W1Ni-matrix sample MA'd for 6 h has the microhardness value of 4.08 ± 0.28 GPa, which increased to 4.70 ± 0.13 GPa after MA for 12 h. The increase in the microhardness with increasing MA durations can be attributed to grain refinement during MA.

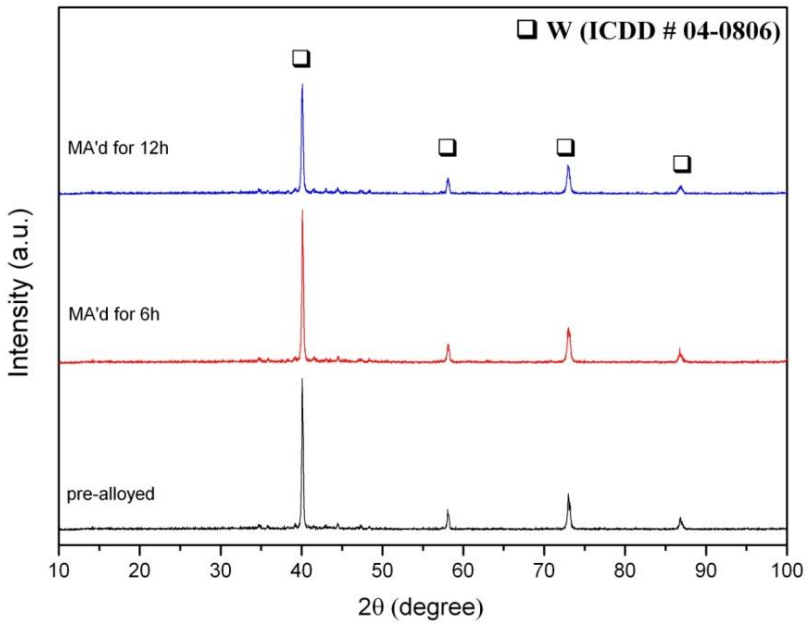

Figure 5.5: XRD patterns of the MA'd and sintered W1Ni samples

Table 5.2: Relative density and microhardness values of the sintered samples

Sample Name	Theoretical Density (gr/cm3)	Relative Archimedes' Density (%)	Microhardness (GPa)
W1Ni pre-alloy (MA'd for 6h)	19.08	96.39	4.08 ± 0.28
W1Ni+ 6h MA		96.51	4.32 ± 0.17
W1Ni+ 12h MA		97.86	4.70 ± 0.13

Figure 5.6 is an optical micrograph taken from the wear tracks of the sintered W1Ni+12h MA sample. The wear amount and friction coefficient weremeasured as 3.26 ± 0.81 ($mm^3N^{-1}m^{-1}$) $x10^{-9}$ and 0.42, respectively. As seen in Figure 5.6, the worn surface of the sintered W1Ni+12h MA sample contains multiple valleys with patches ruptured from the surface and/or the hardfacing alumina balls during sliding wear experiments.

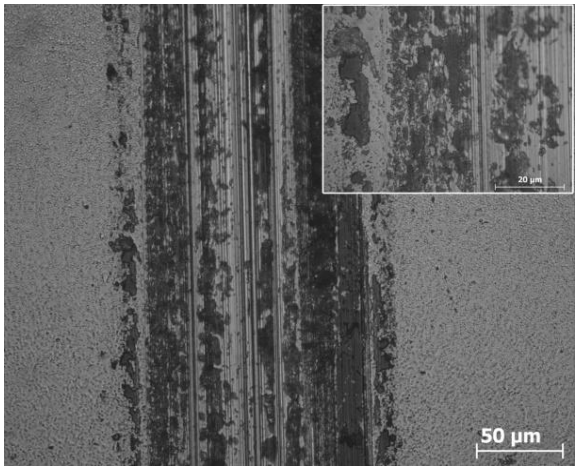

Figure 5.6: Optical micrographs of the wear tracks of the sintered W1Ni+12h MA sample (Insetis a higher magnification image of the wear tracks).

Figure 5.7a and Figure 5.7b arethe back-scatteredelectron micrographs showing the effect of milling of W1Ni matrix powder. Figure 5.7a is taken from W1Ni 6 hours pre-milled and sintered powder where Ni rich areas are located (dark grey particles) at grain boundaries. After miling for 12 hours W1Ni matrix (milled for 18 hours in total), Ni particles are homogenously distributed in the microstructure and can not be observed throughout the microstructure (Figure 5.7b). The average grain size value remains almost the same where the value of 7.03 µm slightly decreased to 6.85 µm.

a) 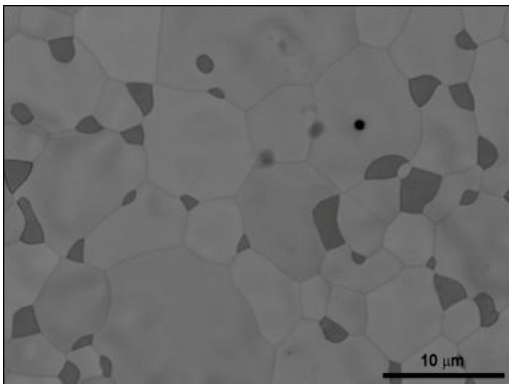

b) 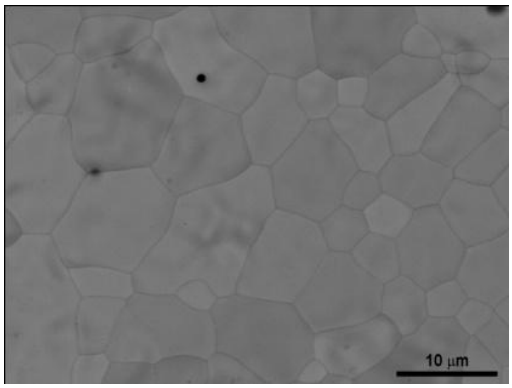

Figure 5.7: Back-scatteredSEM micrographs of sintered **a)** W1Ni pre-alloy **b)** W1Ni+12h MA (totally 18h MA).

5.2 Characterization Investigations of the MA'd and Sintered W1Ni – x wt% TiB_2 (x=2,3,4) Composites

5.2.1 Characterization of the powders

Figure 5.8a-c are the XRD patterns of W1Ni-2TiB_2 (Figure 5.8a),W1Ni-3TiB_2 (Figure 5.8b), W1Ni-4TiB_2 (Figure 5.8c) powders which wereMA'd for different durations. The peaks of W can be identified in all samples. However,in these patterns TiB_2 peaks are not be observed, probably due to the low content in the blends and peak broadening due to MA. All of the peaks diffracted from these phases belong to the W phase (ICDD No: 04-0806), as mentioned before.

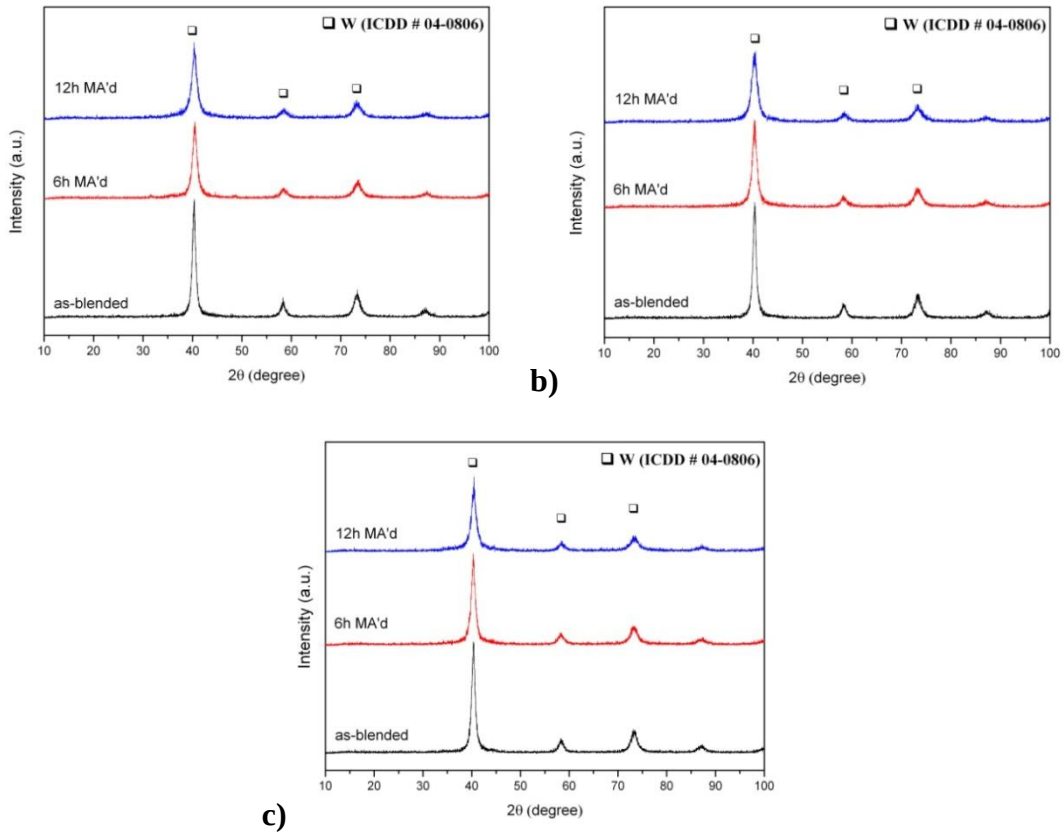

Figure 5.8: XRD patterns of **a)** W1Ni-2TiB_2, **b)** W1Ni-3TiB_2, **c)** W1Ni 4TiB_2powders

Crystallite sizes and lattice deformations of MA'd powders of the W1Ni – x wt% TiB_2 (x=2,3,4) system were measured and the results are given in Table 5.3. These calculations reveal that TiB_2 addition has no remarkable effect on crystallite sizes and lattice deformations within the selected amounts.

All of the as-blended powders (W1Ni-2TiB_2 as-blended, W1Ni-3TiB_2 as-blended, W1Ni-4TiB_2 as-blended) have nanosizes as a result of initial pre-milling step.W1Ni-

$2TiB_2$-12h MA'd powders have the crystallite size about 6.5 nm which is almost the same value for the W1Ni+12h MA powders (about 6.4 nm). As seen in Table 5.3, it is clear to state that crystallite sizes decrease with increasing MA duration, whereas lattice deformations increase.

Table 5.3: Crystallite sizes and lattice defomations of the MA'd powders

Sample Name	**Crystallite Size(nm)**	**Lattice Deformation(%)**
W1Ni-2TiB_2as-blended	14.4	1.78
W1Ni-2TiB_2-6h MA'd	9.3	2.83
W1Ni-2TiB_2-12h MA'd	6.5	3.93
W1Ni-3TiB_2as-blended	15.0	1.71
W1Ni-3TiB_2-6h MA'd	9.3	2.76
W1Ni-3TiB_2-12h MA'd	7.4	3.35
W1Ni-4TiB_2as-blended	13.5	1.90
W1Ni-4TiB_2-6h MA'd	9.6	2.65
W1Ni-4TiB_2-12h MA'd	7.4	3.62

Figure 5.9 a – c show the evolution of particle size distributions of W1Ni-2TiB_2 powders during mechanical alloying. As seen in Figure 5.9, mean particle size distributions decreased with increasing mechanical alloying durations, the mean particle size of as-blended W1Ni-2TiB_2 powders is reduced from 1.27μm (Figure 5.9a) to 1.08 μm (Figure 5.9b) and to 0.94μm (Figure 5.9c) after further MA for 6 h, 12 h, respectively.

SEM micrograph taken from the W1Ni-2TiB_2 powders MA'd for 12 h (Figure 5.10) reveals that spherical like submicron particles exist throughout the microstructure with some micron sized agglomerates. As seen in this figure,powders sizes are consistent with the particle size distributions analysis given in Figure 5.9c

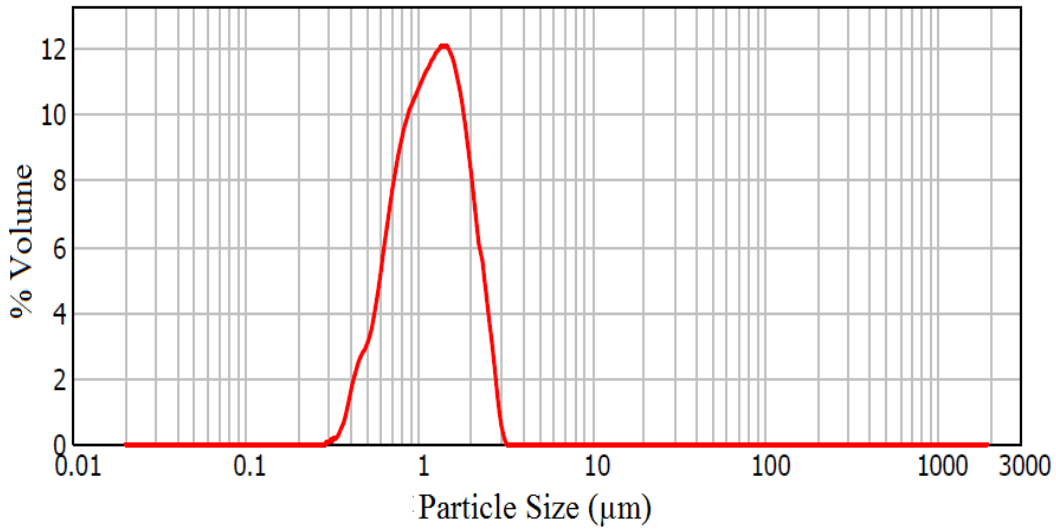

a)

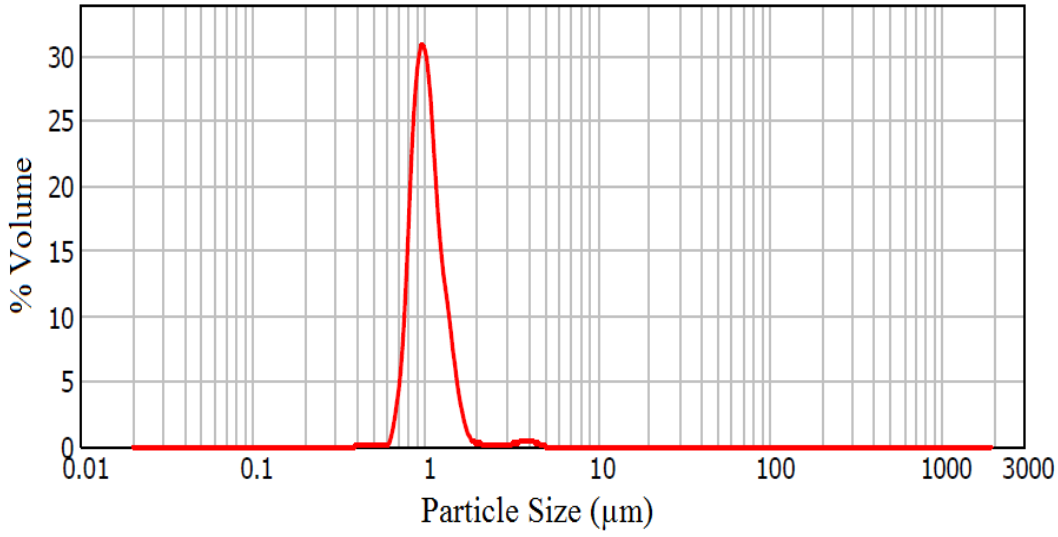

b)

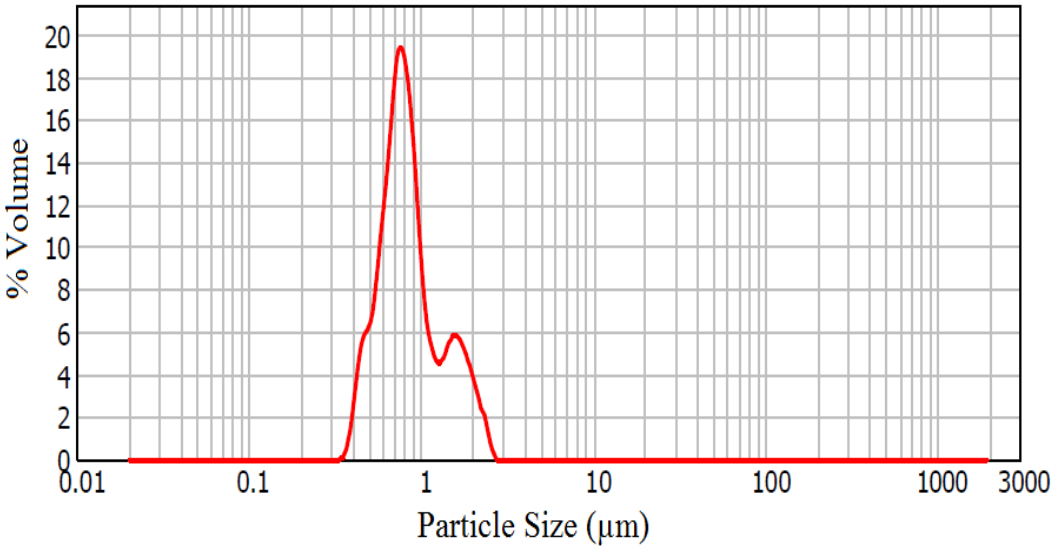

c)

Figure 5.9: Particle size distributions of **a)**W1Ni-2TiB_2as-blended (D_{mean}= 1.27 µm, D_{50}= 1.19 µm), **b)** W1Ni- 2TiB_2- 6h MA'd (D_{mean}= 1.08 µm, D_{50}= 1.01 µm), **c)** W1Ni- 2TiB_2- 12h MA' (D_{mean}= 0.94 µm, D_{50}= 0.80 µm).

Figure 5.11a and Figure 5.11b are bright-field and-dark field TEM micrographs taken from theW1Ni – 2TiB_2 powders MA'd for 12 h showing submicron particles (Accelerating Voltage: 160 kV, L: 100cm). Corresponding electron diffraction pattern taken from the particleslocated on the lower right (indicated with a red circle) in Figure 5.11a is shown in Figure 5.11c indicating that these particles are W_2B phases having a base centered tetragonal Bravais lattice (a = b = 0.557 nm, c = 0.474 nm; ICDD No: 25-0990). As seen in Figure 5.11b, these W_2B phases have nanosizes and are distributed homogeneously throughout the microstructure.

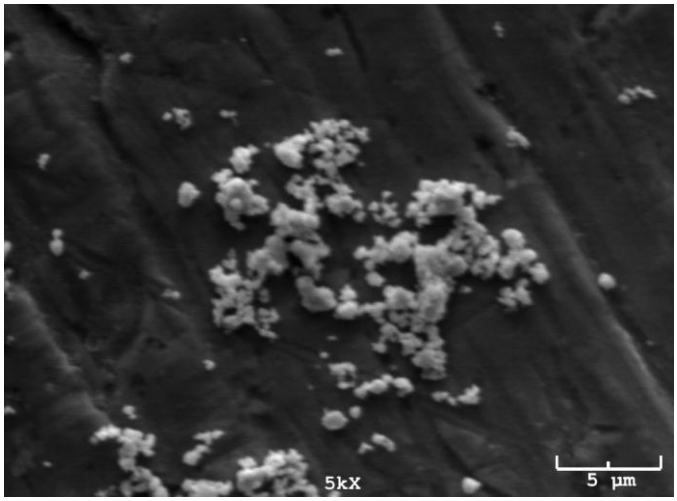

Figure 5.10: SEM micrograph of W1Ni-2TiB_2 powder MA'd for 12h

Figure 5.12a and Figure 5.12b are bright-field and-dark field TEM micrographs taken from the W1Ni – 4TiB_2 powders MA'd for 12 h showing sphereoidal shaped particles up to ~60 nm in size (Accelerating Voltage: 160 kV, L: 100cm). Corresponding electron diffraction pattern from the spheroidal particles is shown in Figure 5.12c, suggesting that these particles are the W phase having a body centered cubic Bravais lattice (a = 0.3122nm,ICDD No: 04-0806).

Figure 5.13a and Figure 5.13b are bright-field and-dark field TEM micrographs taken from theW1Ni – 4TiB_2 powders MA'd for 12 h showing particles between 10 nm and 30 nm in size (Accelerating Voltage: 160 kV, L: 100cm). Corresponding electron diffraction pattern from the spheroidal particles is shown in Figure 5.13c, suggests that these particles are W_2B phases having a base centered tetragonal lattice with a lattice parameter; a = b = 0.557 nm, c = 0.474 nm(ICDD No: 25-0990). W_2B phases are beleived to be formed as a result of decomposition of TiB_2 during mechanical alloying.

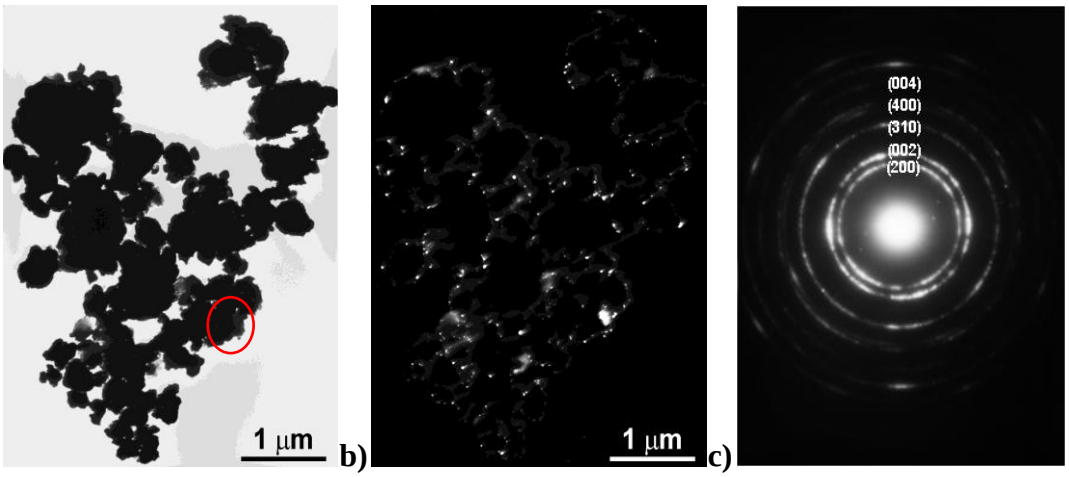

Figure 5.11: a) Bright-field micrograph and **b)** dark-field electron micrograph showing W_2B particles in the W1Ni-2TiB_2 powders MA'd for 12 h **c)** Corresponding selected-area diffraction pattern of W_2B phase (b.c.t., ICDD No: 25-0990; a = b = 0.557 nm, c = 0.474 nm).

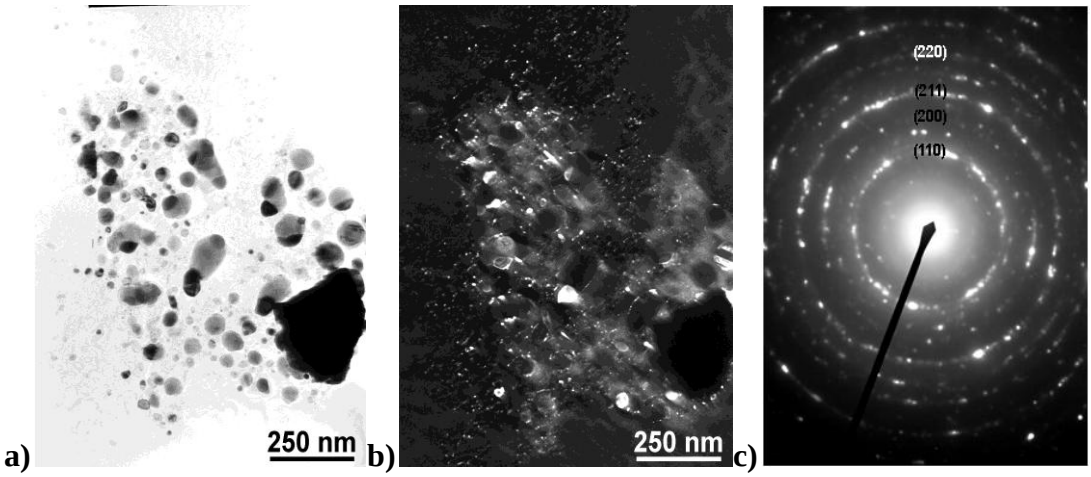

Figure 5.12: a) Bright-field micrograph and **b)** dark-field electron micrograph with the objective aperture on (110) showing spheroidal-shaped particles in the W1Ni-4TiB_2 powders MA'd for 12 h **c)** Corresponding selected-area diffraction pattern of W (b.c.c., ICDD No: 04-0806; a=0.316 nm).

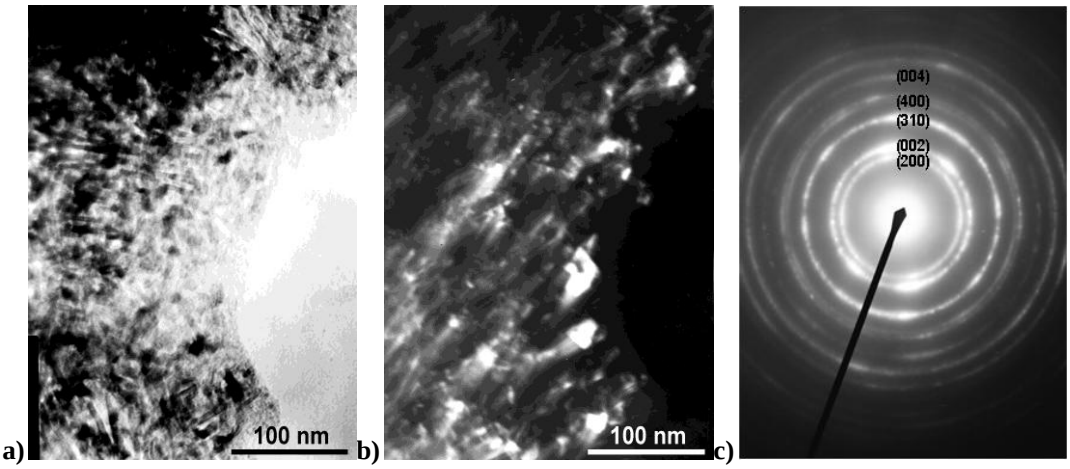

Figure 5.13: a) Bright-field micrograph and **b)** dark-field electron micrograph showing W_2Bparticles in the W1Ni-4TiB_2 powders MA'd for 12 h **c)** Corresponding selected-area diffraction pattern of W_2B phase (b.c.t., ICDD No: 25-0990; a = b = 0.557 nm, c = 0.474 nm).

5.2.2 Characterization of the sintered samples

Figure 5.14 shows the XRD patterns of the sintered W1Ni-xTiB_2 (x=2,3,4) powders which were MA'd for 12h. As seen in Figure 5.14, there are 3 different phases are identified, which of one is W (ICDD No: 04-0806) mentioned before and the others are NiTi (ICDD No: 19-0850) and TiB_2 (ICDD No: 35-0741). NiTi phase has a simple cubic Bravais lattice with a lattice parameter of a = 0.297 nm; and TiB_2 has a hexagonal Bravais lattice with lattice parameters of a = b = 0.303 nm, c = 0.323 nm.

The relative density measurements and corresponding theoretical density values of the samples of the W1Ni – x wt% TiB_2 (x=2,3,4) system are given in Table 5.4. In general, a decreasing tendency in the relative density values are observed with increasing TiB_2 contents. W1Ni-2TiB_2-12 h MA'd sample has a density of 94.88% which is about 3% lower than that of the W1Ni-12 h MA'd sample which has a relative density value of 97.86%. The relative density values of the W1Ni-3TiB_2 samples MA'd for different durations vary between 90% to 93% and samples containing 4 wt% TiB_2 have lower relative density values, which vary between 74% and 90%. However, there is no correlation between these relative density values. Wide disparities between relative density values make them unreliable and can be attributed to the decomposition of TiB_2 during MA and sintering steps.

Vickers microhardness results of sintered W1Ni-2TiB_2 samples are given in Table 5.4. As seen in the table, the microhardness values increased slightly with increasing MA durations as a result of increasing relative density and grain

refinement during MA. The Vickers microhardness measurements were not be carried out on the sintered W1Ni-3TiB_2 and W1Ni-4TiB_2 samples since these samples have inconsistent and unreliable relative density values. Furthermore, the surfaces of these sintered samples could not be polished for subsequent microhardness measurements.

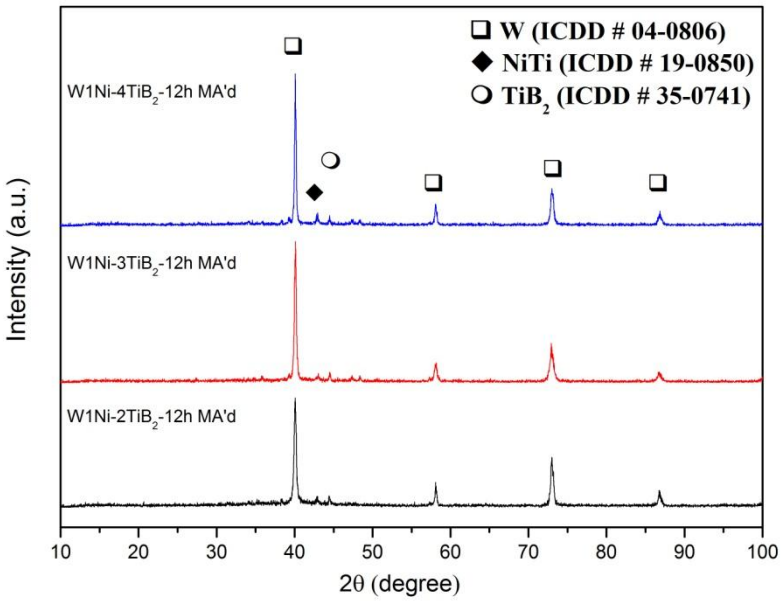

Figure 5.14: XRD patterns of the MA'd and sintered W1Ni-2TiB_2, W1Ni-3TiB_2,W1Ni-4TiB_2 samples

Table 5.4: Relative density and microhardness values of the sintered samples.

Sample Name	Theoretical Density (gr/cm3)	Relative Archimedes' Density (%)	Microhardness (GPa)
W1Ni-2TiB_2as-blended	17.92	91.21	4.11 ± 0.29
W1Ni-2TiB_2-6 h MA'd		93.62	4.46 ± 0.21
W1Ni-2TiB_2-12 h MA'd		94.88	4.58 ± 0.20
W1Ni-3TiB_2as-blended	17.40	90.54	-
W1Ni-3TiB_2-6 h MA'd		93.27	-
W1Ni-3TiB_2-12 h MA'd		88.22	-
W1Ni-4TiB_2as-blended	16.90	74.04	-
W1Ni-4TiB_2-6 h MA'd		86.16	-
W1Ni-4TiB_2-12 h MA'd		90.60	-

Figure 5.15a and Figure 5.15b were taken from the sintered the W1Ni-2TiB_2 and W1Ni-4TiB_2 MA'd for 12 h, respectively, showing the effect of increasing TiB_2

composition. It is clear from the Figure 5.15a that micron/submicron sized TiB_2 particles are homogenously distributed in the microstructure which are mainly located at the grain boundaries. Although the average grain size of the W1Ni matrix decreases from W1Ni-2TiB_2 to W1Ni-4TiB_2 sample, the presence of larger (about 5 μm) TiB_2 particles is observed in the SEM micrograph of the sintered W1Ni-4TiB_2 sample (Figure 5.15b) due to the agglomeration. As seen in Figure 5.15b, the microstructure of the sintered W1Ni-4TiB_2 sample contains a considerable amount of open pores, which is consistent with the reported relative density value of the 90.60 % (Table 5.4).

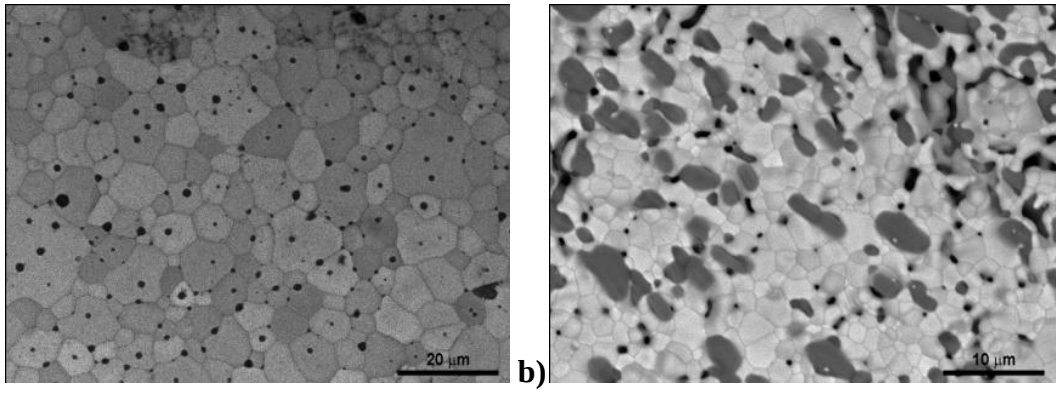

Figure 5.15: Back-scattered SEM micrographs taken from sintered **a)** W1Ni-2TiB_2 12h MA **b)**W1Ni-4TiB_2-12h MA samples.

Optical micrographs presented in Figure 5.16 are taken from polished surfaces of the sintered samples. As seen in these figures, the microstructures of the samples become more porous and relatively rough surfaces as the TiB_2 content increases. The microstructure of the sample containing 4 wt.% TiB_2 (Figure 5.16c) reveals the presence of pores and cracks throughout the microstructures which is consistent with the reported lower relative density values (Table 5.4).

Figure 5.17 shows a typical optical micrograph of the worn surface of the sintered W1Ni-2TiB_2-12h MA'd sample revealing the characteristics of abrasive wear. The wear test was conducted on the sintered sample containing 2 wt% TiB_2 sample because of the porous surfaces of the sintered W1Ni-3TiB_2-12h MA'd and W1Ni-4TiB_2-12h MA'd samples. The wear amount decreased to1.81 ± 0.62 ($mm^3N^{-1}m^{-1}$) $x10^{-9}$ with addition of 2 wt% TiB_2 from a value of 3.26 ± 0.81 ($mm^3N^{-1}m^{-1}$) $x10^{-9}$ for the W1Ni+12h MA sample. Also as seen in Figure 5.17, the width of the wear track is narrower compared to Figure 5.6.

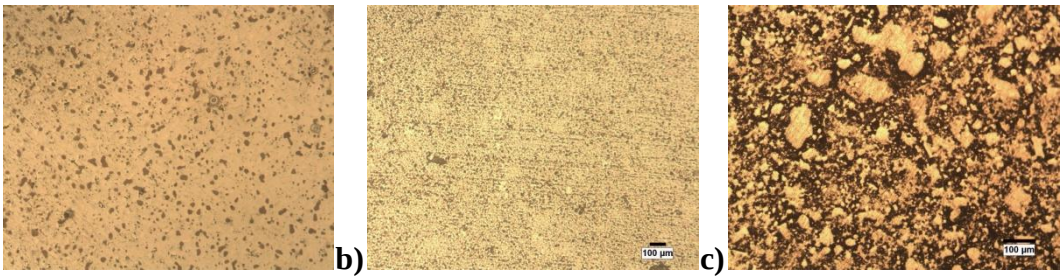

Figure 5.16: Optical micrographs taken from MA'd for 12h and sintered **a)**W1Ni-2TiB_2, **b)** W1Ni-3TiB_2 **c)**W1Ni-4TiB_2 samples

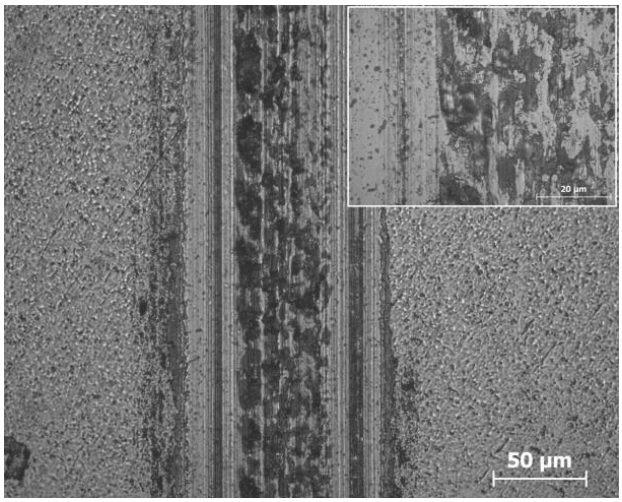

Figure 5.17: Optical micrographs of the wear tracks of the sintered W1Ni-2TiB_2-12h MA'dsample (Inset is higher magnification image of the wear tracks).

5.3 Characterization Investigations of the MA'd and Sintered W1Ni – y wt% La_2O_3 (y=0.5, 1) Composites

5.3.1 Characterization of the powders

XRD patterns of W1Ni-0.5 La_2O_3 (Figure 5.18a) and W1Ni-1 La_2O_3 (Figure 5.18b) powders MA'd for different durations are shown below. All of the peaks belong to W phase (ICDD No: 04-0806).

Crystallite sizes and lattice deformations of MA'd powders were predicted by using TOPAS 3 (Bruker AXS) and the results are given in Table 5.5. These calculations reveal that La_2O_3 addition has no significant effect on crystallite sizes and lattice deformations within the selected amounts. Crystallite sizes decreased with increasing MA duration, whereas lattice deformations increased. As seen in Table 5.5, the pre-milling of the powders decreases the crystallite size of the powders to the nanosizes even for the as-blended ones

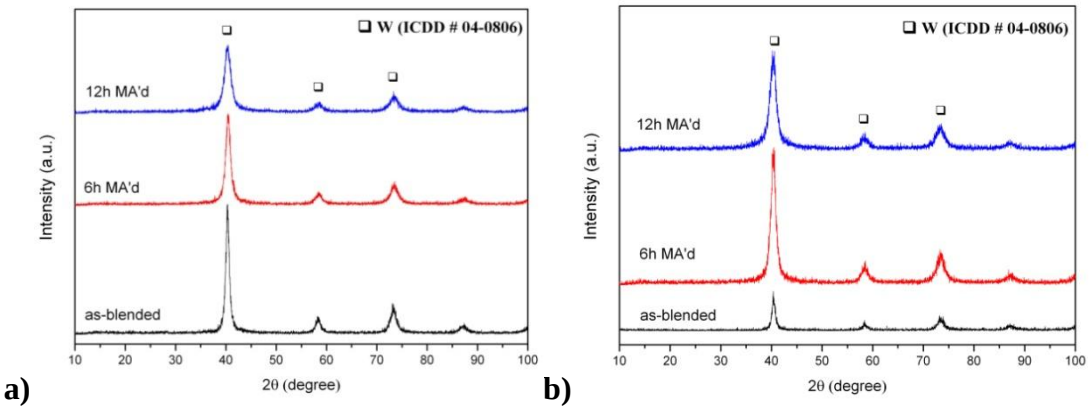

Figure 5.18: XRD patterns of **a)** W1Ni-0.5 La_2O_3**b)** W1Ni-1 La_2O_3 powders

Table 5.5: Crystallite sizes and lattice defomations of the MA'd powders.

Sample Name	Crystallite Size (nm)	Lattice Deformation (%)
W1Ni-0.5La_2O_3as-blended	15.2	1.73
W1Ni-0.5La_2O_3-6h MA'd	9.9	2.71
W1Ni-0.5La_2O_3-12h MA'd	6.3	4.05
W1Ni-1La_2O_3as-blended	16.0	1.32
W1Ni-1La_2O_3-6h MA'd	9.5	2.69
W1Ni-1La_2O_3-12h MA'd	6.7	4.08

Figure 5.19a and b show the particle size distributions of the W1Ni-0.5 La_2O_3 (Figure 5.19a) and W1Ni-1 La_2O_3 (Figure 5.19b) powders MA'd for 12 hours in order to investigate the effect of La_2O_3 addition on particle size distribution. As seen in these figures, W1Ni-0.5 La_2O_3 and W1Ni-1 La_2O_3 powders has almost the same mean particle sizes of about 1 µm revealing that the addition of La_2O_3 powders has no significant effect on particle size distributions. In addition, the smaller peak in the Figure 5.19b reveals that W1Ni- 1La_2O_3- 12h MA'd powders are agglomerated during particle size testing.

The morphology of the W1Ni-1La_2O_3 powders MA'd for 12 h is can be seen in Figure 5.20. Fraction of submicron sized particles seems to increase with the addition of 1 wt.% La_2O_3 particles, probably due to the increased fracturing mechanism with the addition of hard La_2O_3 particles during MA. However, some agglomerates about 2µm in size are present in the microstructure of the W1Ni-1La_2O_3 powders MA'd for 12 h.

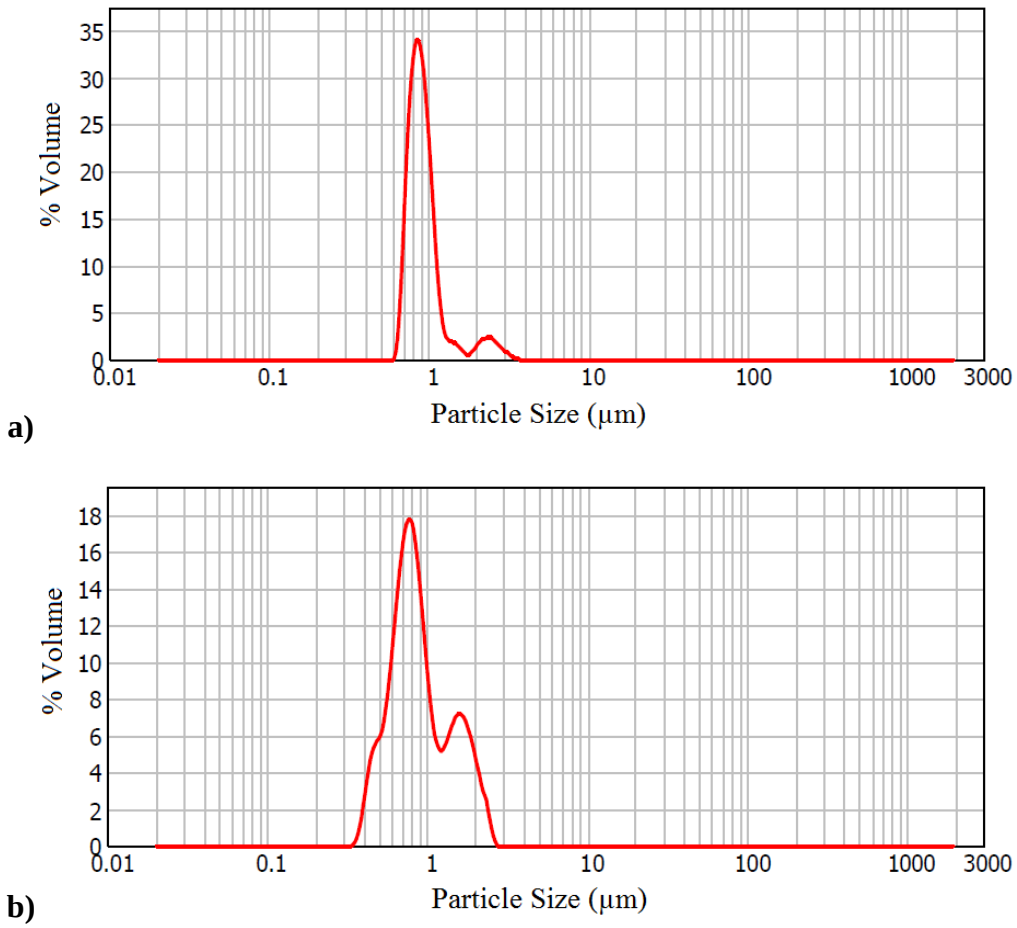

Figure 5.19: Particle size distributions of **a)** W1Ni- 0.5La_2O_3- 12h MA'd (D_{mean}= 1 µm, D_{50}=0.89 µm), **b)** W1Ni- 1La_2O_3- 12h MA'd (D_{mean}= 0.99 µm, D_{50}=0.83 µm).

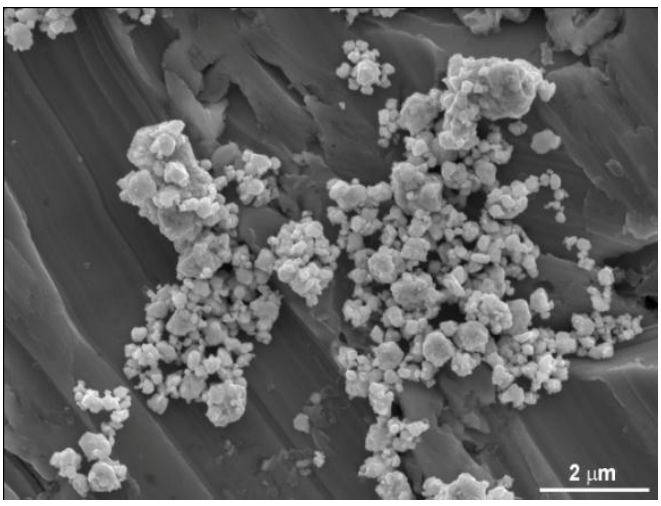

Figure 5.20: SEM micrograph of the W1Ni-1La_2O_3 powders MA'd for 12h

5.3.2 Characterization of the sintered samples

Figure 5.21 shows the XRD patterns of the sintered W1Ni-0.5La_2O_3-12h MA'd and W1Ni-1La_2O_3-12h MA'd samples. All the peaks seen in the figure belong to the b.c.c. W (ICDD No: 04-0806) phases. La_2O_3 phases are not observed due to small additions.

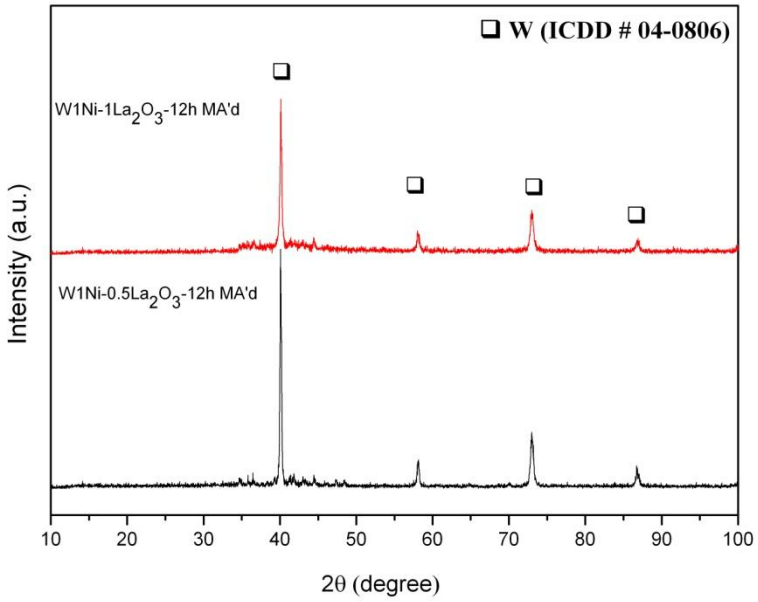

Figure 5.21: XRD patterns of the sintered W1Ni-0.5La_2O_3 and W1Ni-1La_2O_3

Relative density values of the sintered W1Ni – y wt% La_2O_3 (y=0.5, 1) samples are listed in Table 5.6. After sintering of the pre-milled W1Ni matrix, a relative density of 96.39 % was obtained. The relative density value of the pre-milled W1Ni matrix decreased to 94.84 % and 93.53 % with the addition of 0.5 wt % and 1 wt % La_2O_3, respectively. However, sintered samples of the 12 h MA'd powders of these blends, i.e. W1Ni-0.5La_2O_3-12 h MA'd and W1Ni-1La_2O_3-12 h MA'd, have higher relative density values of 97.52 % and 98.09 %, respectively.

Vickers microhardness results of sintered samples are also given in Table 5.6. It is clear to state that sintered samples of the 12h MA'd powders have the highest microhardness values in both groups. The microhardness value of 4.70 GPa of W1Ni+12h MA samle increased to 5.22 GPa and 5.45 GPa with the addition of 0.5 wt% and 1 wt% La_2O_3, respectively. The increase in the microhardness with increasing MA durations can be attributed to the homogenous distribution of La_2O_3 particles throughout the microstructure and successive grain refinement during MA.

Table 5.6: Relative density and microhardness values of the sintered samples

Sample Name	Theoretical Density (gr/cm3)	Relative Archimedes' Density (%)	Microhardness (GPa)
W1Ni-0.5La_2O_3as-blended	18.89	94.84	4.57 ± 0.29
W1Ni-0.5 La_2O_3-6 h MA'd		95.79	4.80 ± 0.23
W1Ni-0.5 La_2O_3-12 h MA'd		97.52	5.22 ± 0.19
W1Ni-1 La_2O_3as-blended	18.72	93.53	4.10 ± 0.22
W1Ni-1 La_2O_3-6 h MA'd		98.18	5.24 ± 0.35
W1Ni-1 La_2O_3-12 h MA'd		98.09	5.45 ±0.29

Figure 5.22a is a SEM micrograph taken from the sintered W1Ni-0.5La_2O_3 sample, showing the homogeneous distribution of micron/submicron sized La_2O_3 particles throughout the microstructure. The presence of larger (about 2 μm) and well-faceted La_2O_3 particles was observed in the SEM micrograph of the sintered W1Ni-1La_2O_3 sample (Figure 5.22b). As seen in Figure 5.22a andFigure 5.22b, size of La_2O_3 particles increased with increasing La_2O_3 amount, where almost the same homogeneous distribution is retrained. The La_2O_3 particles in the microstructure of the sintered W1Ni-0.5La_2O_3 sample are located both at grain boundaries and at grain interiors (Figure 5.22a). The La_2O_3 particles in the microstructure of the sintered W1Ni-1La_2O_3 sample are mainly located at grain boundaries.

a) 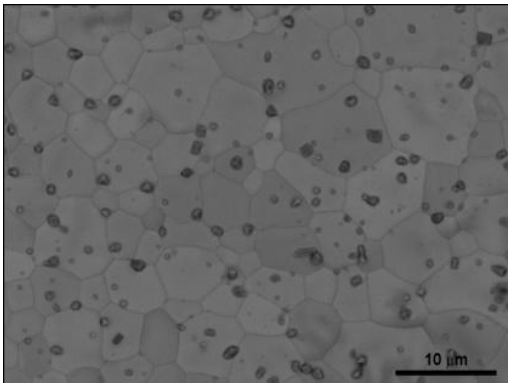

b) 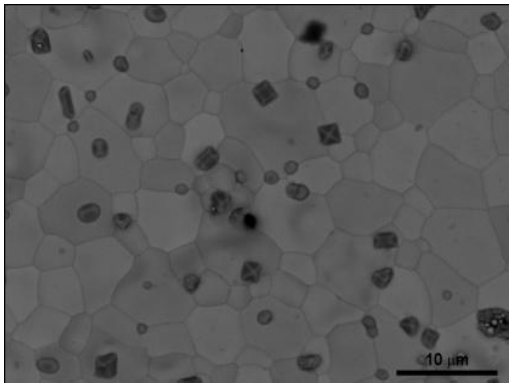

Figure 5.22: Back-scattered SEM micrographs of sintered**a)**W1Ni-0.5La_2O_3-12h MA **b)** W1Ni-1La_2O_3-12h MA samples.

Sliding wear experiments were conducted in order to investigate the effects of La_2O_3 addition on the tribological behavior of the W1Ni matrix composites and the results of the wear experiments are presented in Table 5.7. As seen in Table 5.7, the wear resistance of the sintered W1Ni sample increases significantly with the addition of

La_2O_3 particles. A significant decrease in the wear amount is obtained with the addition of 0.5 wt% La_2O_3 particles, however, the wear resistance of the sintered W1Ni-1La_2O_3 sample is unexpectedly lower than that of the sintered W1Ni-0.5 La_2O_3 sample.The higher wear resistance of the W1Ni-0.5 La_2O_3 sample can be explained with the presence of smaller La_2O_3 particles which are more homogeneously distributed in the microstructure than those in the microstructure of the W1Ni-1La_2O_3 sample (seen in Figure 5.22a).

Table 5.7: Wear amounts and the friction coefficients of the sintered samples

Sample Name	**Wear amount ($mm^3N^{-1}m^{-1}$) x10^{-9}**	**Friction coefficient**
W1Ni+12h MA'd	3.26 ± 0.81	0.42
W1Ni-0.5 La_2O_3-12h MA'd	2.10 ± 0.24	0.38
W1Ni-1La_2O_3-12h MA'd	2.75 ± 0.89	0.42

Figure 5.23 shows the optical micrographs of worn surfaces of the sintered W1Ni-0.5 La_2O_3-12h MA'd (Figure 5.23a) and W1Ni-1La_2O_3-12h MA'd (Figure 5.23b) samples. As seen in these figures, the width and the depth of the wear track increases with the increase in La_2O_3 content. This observation correlates very well with the wear amount values given in Table 5.7. It can be stated that the addition of La_2O_3 decreases the wear resistance of the sintered W1Ni samples.

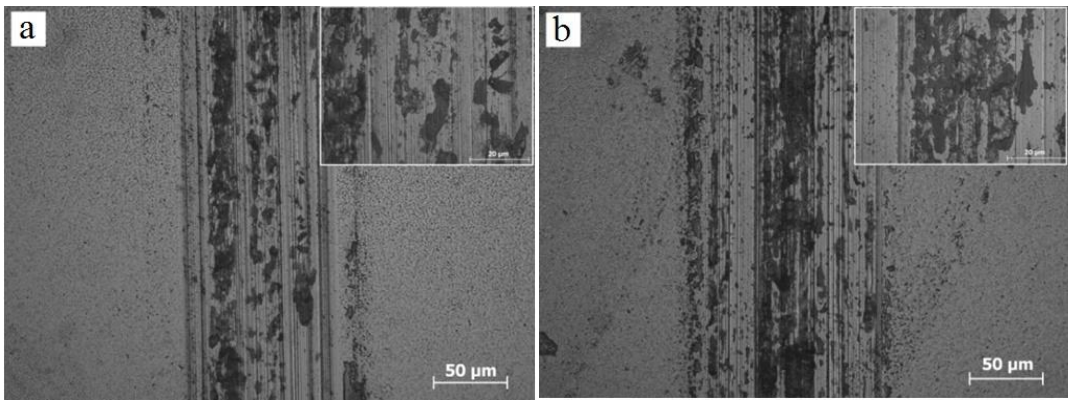

Figure 5.23: Optical micrographs of the wear tracks of the sintered samples**a)**W1Ni-0.5 La_2O_3-12h MA'd,**b)**W1Ni-1La_2O_3-12h MA'd. Insets are higher magnification images of the wear tracks.

5.4 Characterization Investigations of the MA'd and Sintered W1Ni – 2 wt % TiB_2– y wt % La_2O_3(y=0.5, 1) Composites

5.4.1 Characterization of the powders

XRD patterns of mechanically alloyed (MA'd) W1Ni-2TiB_2-0.5La_2O_3 and W1Ni-2TiB_2-1La_2O_3 powders are shown inFigure 5.24a – b, in which only theb.c.c. W phases are identified in all powder samples.It is clear that with increasing MA, peaks are broadened and peak heights are decreased, as a result of grain refinement and due to internal strain buildupduring MA.

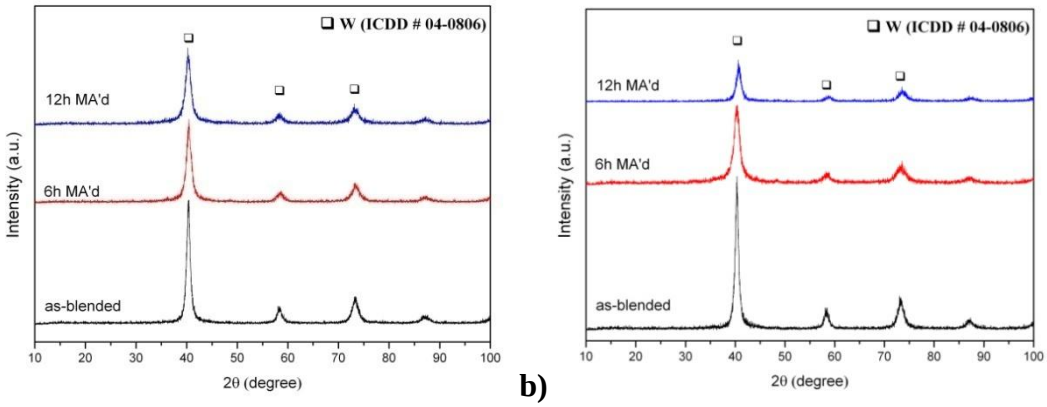

Figure 5.24: XRD patterns of **a)** W1Ni-2TiB_2-0.5La_2O_3**b)** W1Ni-2TiB_2-1La_2O_3 powders

Crystallite sizes and lattice deformations of MA'd powders were measuredand the results are given in Table 5.8. These calculations reveal that crystallite sizes decreased with increasing MA duration, whereas lattice deformations increased.

Average crystallite size of the as-blended powders (~15 nm) is reduced to ~7 nm after MA for 12 h, where lattice deformation is nearly doubled. W1Ni-2TiB_2-1La_2O_3 as-blended powders with average crystallite size of 15 nm and 1.76% lattice deformation have decreased crystallite size of 10.6 and 6.1 nm after 6 and 12 hours of MA, respectively, whereas lattice deformation increases to 4.15 % after MA for 12h.

The effect of La_2O_3 and TiB_2 addition on particle sizes can be seen in Figure 5.25a and Figure 5.25b for he MA'd W1Ni-2TiB_2-0.5La_2O_3 and W1Ni-2TiB_2-1La_2O_3 powders. It can be noted from Figure 5.25a and Figure 5.25b that the mean particle size decreases slightly with increasing La_2O_3 addition. W1Ni- 2TiB_2- 0.5La_2O_3- 12h

MA'd powders have a mean particle size of 1.13µm where W1Ni- 2TiB_2- 01La_2O_3-12h MA'd powders have a mean particle size of 0.93 µm.

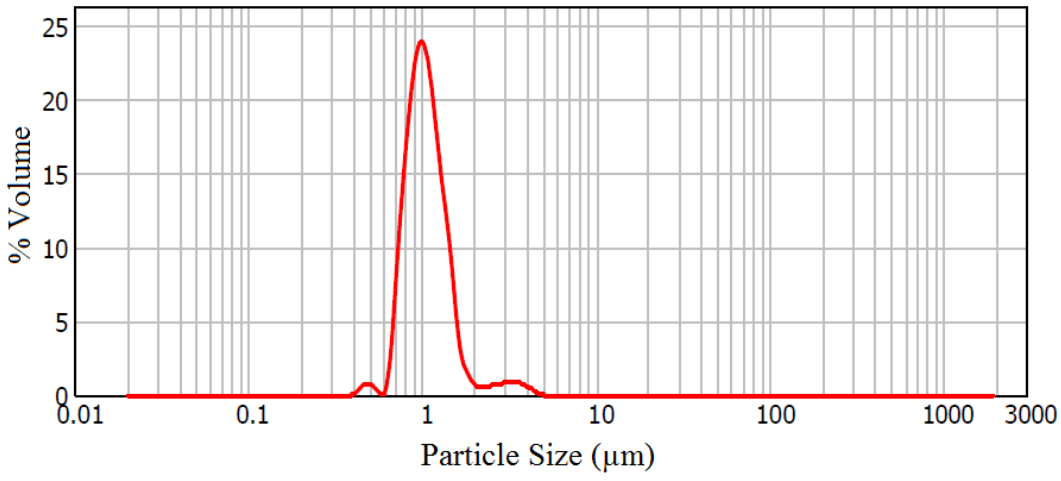

a)

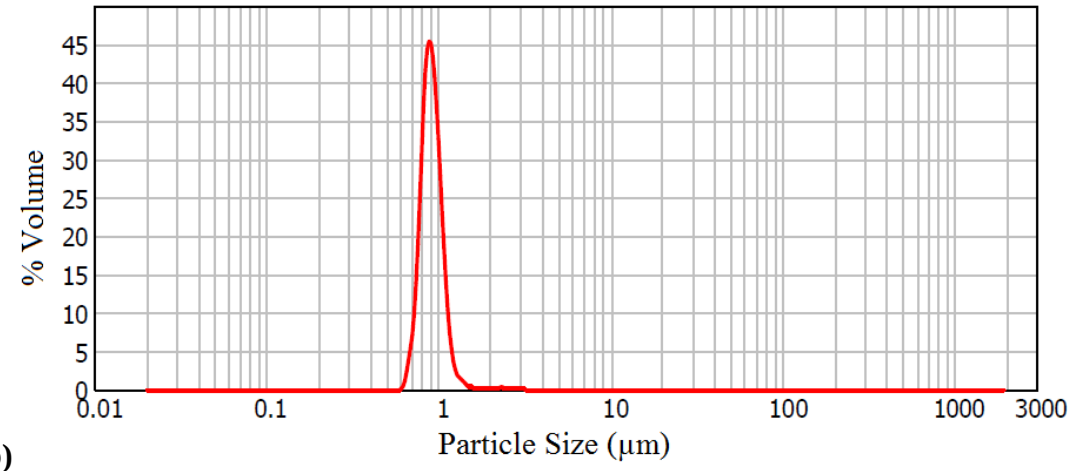

b)

Figure 5.25: Particle size distributions of **a)** W1Ni-2TiB_2-0.5La_2O_3-12h MA'd (D_{mean}=1.13 µm, D_{50}=1.03 µm), **b)** W1Ni-2TiB_2-1La_2O_3-12h MA'd (D_{mean}=0.93µm, D_{50}= 0.90 µm).

Table 5.8: Crystallite sizes and lattice defomations of the MA'd powders.

Sample Name	Crystallite Size (nm)	Lattice Deformation (%)
W1Ni-2TiB_2-0.5La_2O_3as-blended	14.2	1.81
W1Ni-2TiB_2-0.5La_2O_3-6h MA'd	8.6	2.98
W1Ni-2TiB_2-0.5La_2O_3-12h MA'd	6.9	3.74
W1Ni-2TiB_2-1La_2O_3as-blended	15.0	1.76
W1Ni-2TiB2-1La_2O_3-6h MA'd	10.6	2.32
W1Ni-2TiB2-1La_2O_3-12h MA'd	6.1	4.15

Figure 5.26 is a representative SEM micrograph, taken from W1Ni-2TiB_2-1La_2O_3 powdersMA'd for 12h,revealing that the microstructure has spherical like submicron particles with some micron sized agglomerates. Addition of 2 wt.% TiB_2 along with the 1 wt.% La_2O_3 particles resulted in more homogeneous particle size distribution at submicron level.

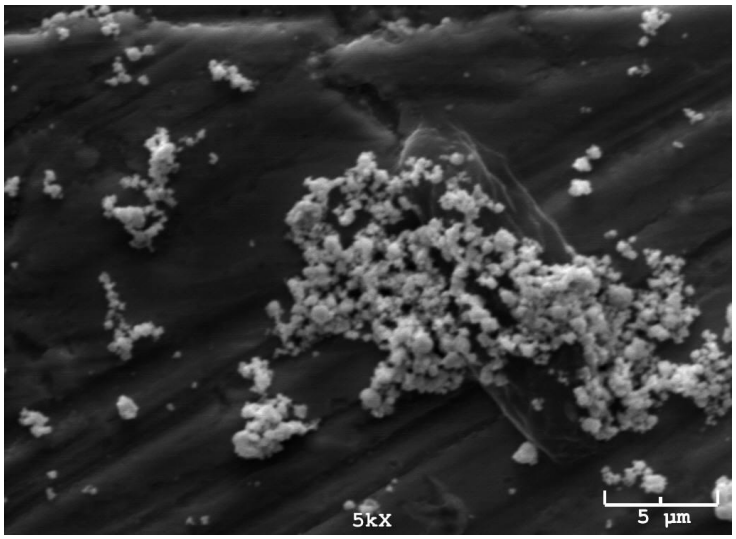

Figure 5.26: SEM micrograph of the W1Ni-2TiB_2-1La_2O_3 powders MA'd for 12h.

5.4.2 Characterization of the sintered samples

Figure 5.27 shows the XRD patterns of the sinteredW1Ni-2TiB_2-0.5La_2O_3 and W1Ni-2TiB_2-1La_2O_3, both MA'd for 12 h. As seen in Figure 5.27, W (ICDD No: 04-0806), Ni (ICDD No: 65-2865) and TiB_2 (ICDD No: 35-0741) phases can be identified. Although these samples contain La_2O_3, no peaks belonging to the La_2O_3 phase were detected due to small additions of La_2O_3.

The relative density measurements and corresponding theoretical density values of the sintered samples of the W1Ni – 2 wt% TiB_2 – y wt% La_2O_3 (y=0.5,1) system are given in Table 5.9. Although a decreasing tendency in the relative density values is observed in Table 5.4 with increasing TiB_2 contents, relative density values increased with La_2O_3 additions. As seen in Table 5.9, relative density and microhardness values increase with MA durations for the sintered samples, containing both 0.5 wt% and 1 wt% La_2O_3. W1Ni-2TiB_2-1La_2O_3-12 h MA'd sample has the highest microhardness value of 5.72 GPa which can be attributed to the highest relative density value of 98.38 %.

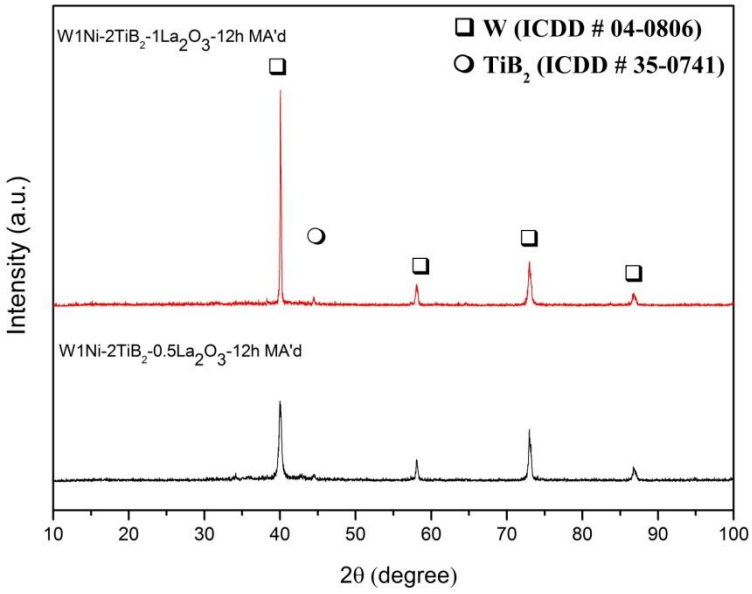

Figure 5.27: XRD patterns of the MA'd and sintered W1Ni-2TiB_2-0.5La_2O_3 and W1Ni-2TiB_2-1La_2O_3 samples

Table 5.9: Relative density and microhardness values of the sintered samples

Sample Name	Theoretical Density (gr/cm3)	Relative Archimedes' Density (%)	Microhardness (GPa)
W1Ni-2TiB_2-0.5 La_2O_3as-blended	17.76	92.00	4.55 ± 0.30
W1Ni-2TiB_2-0.5 La_2O_3-6 h MA'd		93.41	4.60 ± 0.44
W1Ni-2TiB_2-0.5 La_2O_3-12 h MA'd		95.90	5.09 ± 0.28
W1Ni-2TiB_2-1 La_2O_3as-blended	17.60	89.96	4.48 ± 0.11
W1Ni-2TiB_2-1 La_2O_3-6 h MA'd		98.10	5.34 ± 0.18
W1Ni-2TiB_2-1 La_2O_3-12 h MA'd		98.38	5.72 ± 0.19

SEM micrographs taken from the MA'd for 12 h and sintered W1Ni-2TiB_2-0.5La_2O_3 (Figure 5.28a) and W1Ni-2TiB_2-1La_2O_3 (Figure 5.28b) samples exhibit homogeneously distributed micron scale black particles which consist of both TiB_2 and La_2O_3 phases in the W1Ni matrix. As seen in Figure 5.28b, addition of both 2 wt.% TiB_2 and 1 wt.% La_2O_3 particles cause several agglomerations and/or elongated particles throughout the microstructure.

Wear amounts and friction coefficients of the sintered W1Ni, W1Ni-2TiB_2, W1Ni-2TiB_2-0.5La_2O_3 and W1Ni-2TiB_2-1La_2O_3samples all MA'd for 12 h are given in Table 5.10. According to the results, as expected W1Ni+12h MA has the highest wear amount.. These values decreased with addition of TiB_2 and La_2O_3, however, the

sintered W1Ni-2TiB_2-12h MA'd sample is still the most wear resistant sample of all. The increasing La_2O_3 content decreases the wear resistance of the sintered samples which can be explained with the elongated or agglomerated particles throughout the microstructure.

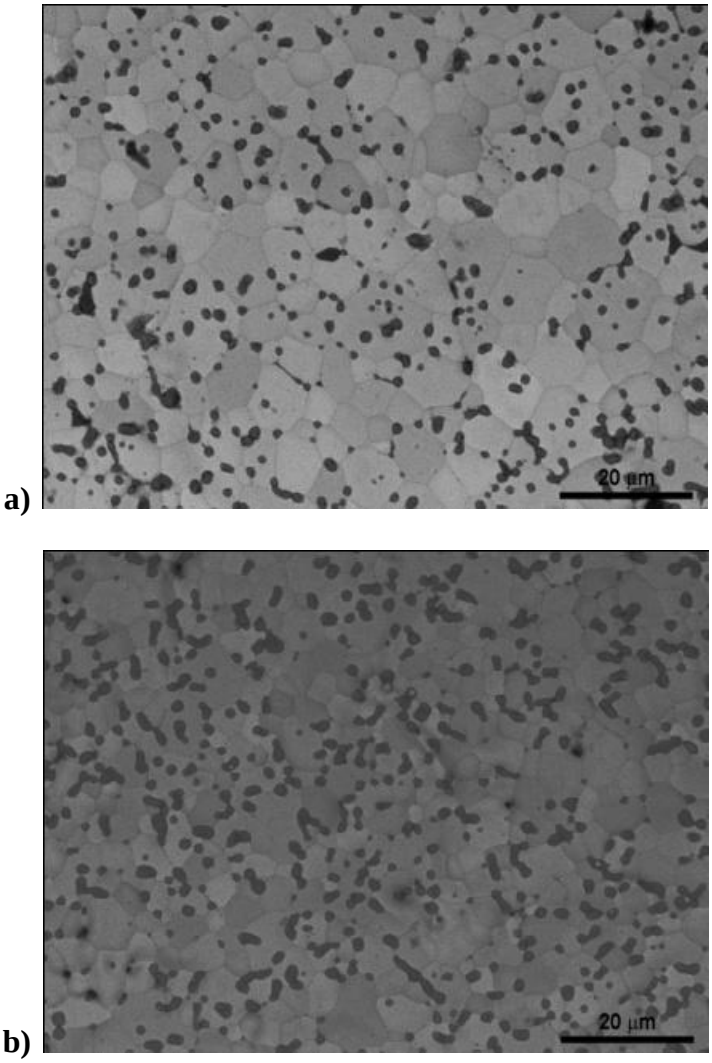

Figure 5.28: Back-scattered SEM micrographs of sintered**a)**W1Ni-2TiB_2-0.5La_2O_3-12h MA **b)** W1Ni-2TiB_2-1La_2O_3-12h MA samples.

Table 5.10: Wear amounts and the friction coefficients of the sintered samples

Sample Name	**Wear amount ($mm^3N^{-1}m^{-1}$) x10^{-9}**	**Friction coefficient**
W1Ni+12h MA	3.26 ± 0.81	0.42
W1Ni-2TiB_2-12h MA'd	1.81 ± 0.62	0.37
W1Ni-2TiB_2-0.5La_2O_3-12h MA'd	2.11 ± 0.28	0.33
W1Ni-2TiB_2-1La_2O_3- 12h MA'd	2.99 ± 0.51	0.41

Sliding wear experiments werecarried out for the sintered samples of W1Ni-2TiB_2-0.5La_2O_3-12h MA'd and W1Ni-2TiB_2-1La_2O_3-12h MA'd powders in order to investigate the effects of TiB_2 and La_2O_3 addition on the tribological behavior of the W1Ni matrix composites. Optical micrographs presented in Figure 5.29 show that the worn surfaces of the sintered samples contain multiple valleys with patches ruptured from the surface and/or alumina balls during sliding wear experiments. As seen in these figures, the sintered samples of the W1Ni-2TiB_2-1La_2O_3 MA'd for 12h have a wider surface area than that of sample containing 0.5 wt% La_2O_3.

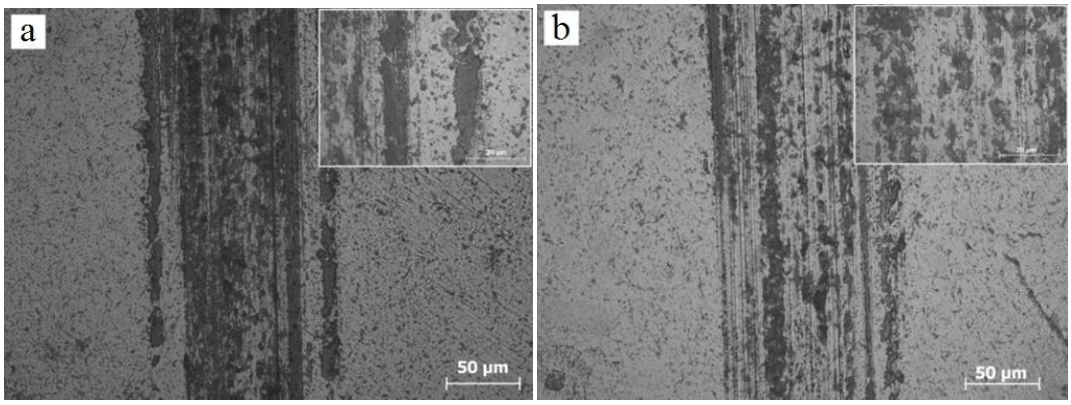

Figure 5.29: Optical micrographs of the wear tracks of the sintered samples: **a)**W1Ni+2TiB_2+0.5La_2O_3 and **b)** W1Ni+2TiB_2+1La_2O_3. Insets are higher magnification images of the wear tracks.

6. CONCLUSIONS

In this study, W – 1 wt% Ni, TiB_2, La_2O_3 powders werepre-milled and these pre-milled powders were selected as starting powders. W1Ni, W1Ni - x wt% TiB_2 (x=2, 3, 4), W1Ni - y wt% La_2O_3 (y=0.5, 1) and W1Ni - 2 wt% TiB_2 - y wt% (y=0.5, 1) powders were MA'd for different durations (6h and 12h) and sintered at 1400 ^oC for 1h where the W1Ni samples are chosen as a control group. XRD, particle size distrubition, SEM, TEM experiments are done to characterize the powders. XRD, Archimedes' density, Vickers microhardness, SEM, sliding wear experiments are conducted to investigate the characteristics of the sintered samples. On the basis of the results of this disseration work, the following conclusions can be made :

1. Mean particle size of the powders decrease with increasing MA durations. Submicron particles and a few micron sized agglomerates are observed in SEM investigations of the powders.
2. W phase (ICDD No: 04-0806) is identified in XRD analyses of all MA'd powders. Crystallite sizes of the powders decrease with increasing MA durations and vary between 6.1 nm and 16 nm.
3. TEM investigations of the powders which contain TiB_2 reveal the presence of W_2B powders which are formed during MA process.
4. W (ICDD No: 04-0806), TiB_2 (ICDD No: 35-0741) and NiTi (ICDD No: 19-0850) phases are identified in XRD analyses of sintered samples which contains TiB_2.
5. Relative Archimedes's density values generally increase with incresing MA durations due to the grain refinement during MA process. Relative Archimedes'density values vary between 91.21% and 98.38% which decrease with increasing TiB_2 content. The sintered samples of W1Ni-2TiB_2-1La_2O_3-12h MA'd powders have the highest relative Archimedes' density values of 98.38%.
6. Vickers microhardness values increase with increased mechanical alloying durations of the powders. The sintered W1Ni-1La_2O_3 samples generally have higher Vickers microhardness values than the sintered W1Ni-0.5La_2O_3

samples. The sintered W1Ni-2TiB_2-1La_2O_3-12h MA'd samples have the highest Vickers microhardness value of 5.72 GPa where the value is 4.08 GPa for the sintered samples of W1Ni+12h MA powders.

7. The sintered W1Ni-2TiB2-12h MA'd sample has the highest wear resistance of all samples. Although La_2O_3 addition contributes to the wear resistance itself for the samples containing TiB_2 the wear resistance of the samples decreases with increasing La_2O_3 addition.

REFERENCES

Acchar, W., Zollfrank, C. and Greil, P., 2004. Microstructure and Mechanical Properties of WC-Co Reinforced With NbC, *Materials Research,***7:** 445-450

Akovali, G. and Uyanik, N.,2001. Introduction in Handbook of Composite Manifacturing, Ed. G. Akovali, Rapra Technology Ltd.

Askeland, D.R.,1984. The Science and Engineering of Materials, Brooks/Cole Engineering Division, CA.

Asthana, R., Kumar, A., Dahotre, N.B., 2006. Composite Materials in Materials Processing and Manufacturing Science: 397-484.

Asthana, R., Kumar, A., Dahotre, N.B., 2006. Powder Metallurgy and Ceramic Forming in Materials Processing and Manufacturing Science: 167-245.

Benjamin, J.S., 1992. Fundamentals of mechanical alloying. *Materials Science Forum*, **88-90,** 1-18.

Boch, P. and Leriche, A.,2001. Sintering and Microstructure of Ceramics in Ceramic Materials Edited by Philippe Boch and Jean-Claude Niepce, HERMES Science Europe Ltd.

Brophy, J.H., Hayden, H.W., Prill, A.L. and Wulff, J., 1963. The Investigation of the Activated Sintering of Tungsten Powder. Final Report, Prepared under U.S. Navy, Bureau of Naval Weapons Contract NO w 61-0326-d, Massachusetts Institute of Technology, Cambridge, Massachusetts.

Cahn, R.W., 2001. The Coming of Materials Science, Pergamon, Amsterdam.

Cambronero, L.E.G., Sanchez, E., Ruiz-Roman, J.M., Ruiz-Prieto, J.M., 2003. Mechanical characterisation of AA7015 aluminum alloy reinforced with ceramics, *Journal of Materials Processing Technology*, **143-144:** 378-384.

Castaing, J., Costa, P., 1977. Boron and refractory borride, Springer-Verlag, New York, p. 390.

Campbell, F.C.,2006. Metal Matrix Composites in Manufacturing Technology for Aerospace Structural Materials: 419-457.

Chawla, N. and Chawla, K.K.,2006. Metal Matrix Composites, Springer, New York.

Chawla, N. and Shen, Y.L.,2001.Mechanical behavior of particle reinforced metal matrix composites, *Advanced Engineering Materials,***3:** 357-370.

Chung, D.D.L.,2001. Materials for thermal conduction, *Applied Thermal Engineering,***21:** 1593-1605.

Chen, L.C.,1993. Dilatometric analysis of sintering of tungsten and tungsten with ceria and hafnia dispersoids,*International Journal of Refractory Metals and Hard Materials*, **1993-1994:** 41-51.

Chen, Z., Zhou, M. and Zuo, T., 2000. Morphological evolution of second-phase particles during thermomechanical processing of W-La_2O_3 alloy, *Scripta mater.*,**43:** 291–297.

Chen, Y., Wu, Y.C., Yu, F.W. and Chen, J.L., 2008.Microstructure and mechanical properties of tungsten composites co-strengthened by dispersed TiC and La2O3 particles, *International Journal of Refractory Metals&Hard Materials,***26:**525-529.

Clyne, T.W..2000. An Introductory Overview of MMC Systems, Types, and Developments in Vol.3 Metal Matrix Composites of Comprehensive Composite Materials, Elsevier.

Clyne, T.W.,2001. Metal matrix composites: matrices and processing, in*Encyclopaedia of Materials: Science and Technology*, Ed. Mortensen, A., Elsevier.

Clyne, T.W. and Withers, P.J.,1993. Introduction to Metal Matrix Composites,Cambridge University Press, Cambridge.

Corti, C.W.,1986. The Role of the Platinium Metals in the Activated Sintering of Refractory Metals.Platinum Metals Rev.,**30:** 184-195.

Coşkun, S., Meydanoğlu, O., Tatar, D., Ozbek, T., Corduk, E., 2004. Building a boot using polymeric-composite materials. *Graduation Project,* I.T.U., Istanbul.

Coşkun, S., 2006. Development and Characterization Investigations of Mechanically AlloyedW-SiC and W-SiC-Y_2O_3 Composites. *M.Sc. Thesis,* I.T.U., Istanbul.

Das, K., Bandyopadhyay, T.K., Das, S., 2002. A Review on the various synthesis routes of TiC reinforced ferrous based composites. *Journal of Materials Science*, **37:** 3881-3892.

Degarmo, E.P., Black, J.T., Kohser, R.A., 2003. Materials and Processes in Manufacturing, John Wiley & Sons, Inc., 344-364.

Delogu, F., Orrù, R. and Cao, G., 2003. A novel macrokinetic approach for mechanochemical reactions, *Chemical Engineering Science,***58:** 815-821.

El-Eskandarany, 2001. Mechanical Alloying for Fabrication of Advanced Engineering Materials, Noyes Publications, New York.

El-Eskandarany, M.S., Mahday, A.A., Ahmed,H.A and Amer, A.H., 2000. Synthesis and characterizations of ball-milled nanocrystalline WC and nanocomposite WC–Co powders and subsequent consolidations, *Journal of Alloys and Compounds,* **312:** 315–325.

Fecht, H.J.,2002. Nanostructured materials and composites prepared by solid state processing, in *Nanostructured Materials: Processing, Properties and Potential Applications*, Ed. Koch, C.C., Noyes Publications, New York.

Gay, D., Hoa, S.V., Tsai, S.W., 2003. Composite Materials Design and Applications, CRC Press LLC, Florida.

Genç, A., Coşkun, S., Öveçoğlu, M.L., 2010. Fabrication and properties of mechanically alloyed and Ni activated sintered W matrix composites reinforced with Y_2O_3 and TiB_2 particles, *Materials Characterization.,* **61:** 740-748.

German, R.M.,1996. Sintering Theory and Practice, John Wiley & Sons, Inc.

German, R.M and Munir, Z.A.,1976. Enhanced Low-Temperature Sintering of Tungsten.Metallurgical Transactions A, **7A:** 1873-1877.

German, R.M and Munir, Z.A.,1982. Activated Sintering of Refractory Metals by Transition Metal Additions.Rev. Powder Metall. Phys. Ceram.,**2:** 9.

Gilman, P.S., Benjamin, J.S., 1983. Mechanical Alloying, *Annual Review of Materials Science,* **13:** 279-300.

Girot, F.A., Quenisset, J.M., Naslain, R., 1987. Discontinuously-reinforced aluminum matrix composites, *Composites Science & Technology,* **30:** 155-184

Goff, A.,2003. Modeling and synthesis of a piezoelectric ceramic-reinforced metal matrix composites. *MS Thesis,* Virginia Polytechnic Institute and State University, Blacksburg, VA.

Han, B.Q., Lavernia, E.J. and Mohamed, F.A., 2005. Mechanical properties of nanostructured materials, *Rev.Adv.Mater.Sci.*,**9:** 1-16.

Hayden, H.W. and Brophy, J.H.,1963.The Activated Sintering of Tungsten with Group VIII Elements, Journal of Electrochemical Society, **110:** 805-810.

Huda, M.D., Hashmi, M.S.J. and El-Baradie, M.A., 1995. MMCs: materials, manufacturing and mechanical properties. *Key Engineering Materials,***104-107:** 37-64.

Hunt, W.H. JR.,2000. Particulate Reinforced MMCs in Vol.3 Metal Matrix Composites of Comprehensive Composite Materials, Elsevier.

Ibrahim, I.A., Mohamed, F.A. and Lavernia, E.J., 1991. Particulate reinforced metal matrix composites – a review. *Journal of Materials Science,* **26:** 1137-1156.

Ishijima, Y., Kurishita, H., Arakawa, H., Hasegawa, M., Hiraoka, Y., Takida, T., et al., 2005.Microstructure and bend ductility of W-0.3 mass % TiC alloys fabricated by advanced powder-metallurgical processing, *Materials Transactions*, **46:** 568-574

Kang, S-J.L.,2005. Sintering Densification, Grain Growth and Microstructure. Elsevier.

Kim, Y., Hong, M.H., Lee, S.H., Kim, E.P., Lee, S., Noh, J.W., 2006. The effect of yttrium oxide on the sintering behaviour and hardness of tungsten, *Metals and Materials International*, **12:** 245-248

Kim, Y., Lee, H.K., Kim, E., Cheong, D., Hong, S.H., 2009 Fabrication of hihg temperature oxides strengthened tungsten composites by spark plasma sintering process, *International Journal of Refractory Metals & Hard Metals.*, **27:** 842-846.,

Kurishita, H., Matsuso, S., Arakawa, H., Hirai, T., Linke, J., Kawai, M., et al., 2009. Development of nanostructured W and Mo materials, *Advanced Materials Research*, **59:** 18-30.

Krajnikov, A.V., Demidik, A.N., Ortner, H.M., 1997. Mechanical properties and interface boundary composition of ferritic steel strengthened by yttrium and titanium disperse oxides, *Materials Science and Engineering A*, **234-236:** 357-360.

La Caer, G., Delcroix, P., Begin-Colin, S. and Ziller, T., 2002. High-energy ball-milling of alloys and compounds, *Hyperfine Interactions*, **141-142:** 63-72.

Lassner, E. and Schubert, W.D.,1999. Tungsten: Properties, Chemistry, Technology of the Element, Alloys and Chemical Compounds, Kluwer Academic, New York.

Lee, K.H., Yoon, J.K., Lee, J.K., Doh, J.M., Hong, K.T. and Yoon, W.Y., 2004.Growth Kinetics of W_5Si_3 Layer in WSi_2/W System, Surface & Coatings Technology, **187:** 146-153.

Lindroos, V.K., Hellman, J.T., Lou, D., Nowak, R., Pagounis, E., Liu, X.W. and Penttiren, I.M., 2004. Designing with metal matrix composites, in *Handbook of Mechanical Alloy Design*, Eds. Totten, G.E., Xie, L. and Funatani, K, M. Dekker, New York.

Li, C. and German, R.M.,1983. The Properties of Tungsten Processed by Chemically Activated Sintering,Metallurgical Transactions A, **14A:** 2031-2041.

Liu, Y.B., Lim, S.C., Lu, L. and Lai, M.O., 1994. Recent development in the fabrication of metal matrix particulate composites using powder metallurgy techniques. *Journal of Materials Science,***29:** 1999-2007.

Mabuchi, M., Okamoto, K., Satio, N., et al., 1996. Tensile properties at elevated temperatures of W-1%La_2O_3, *Materials Science & Engineering A*, **214:** 174-176.

Mabuchi, M., Okamoto, K., Saito, N., Asahina, T. and Igarashi, T., 1997. Deformation behavior and strengthening mechanisms at intermediate temperatures in W-La_2O_3, *Materials Science & Engineering A,***237:** 241-249.

Massalski, T.B.,1990.Binary alloy phase diagrams, 2nd ed., ASM, Metals Park, OH, USA.

Mazumdar, S.K.,2002. Composite Manifacturing, Materials, Product and Process Engineering, CRC Press LLC, Florida.

Munro, R.G., 2008. Material properties of titanium diborride, *Journal of Research of the National Institute of Standarts and Technology*, **105:** 709-720.

Miserez, A., Müller, R., Rossoll, A., Weber, L. and Mortensen, A., 2004. Particle reinforced metals of high ceramic content, *Materials Science and Engineering A*, 387–389: 822–831.

Newkirk, J.W. and Kohser, R.A.,2004. Designing with powder metallurgy alloys, *Handbook of Mechanical Alloy Design*, Eds. Totten, G.E., Xie, L. and Funatani, K, M. Dekker, New York.

Nieh, T.G. and Chellman, D.J.,1984. Modulus measurements in discontinuous reinforced aluminum composites, *Scripta Metallurgica*, **18:** 925-928.

Ohring, M.,1995. Engineering Materials Science, Stevens Institute of Technology, New Jersey, USA, 463-486.

Öveçoğlu, M.L., 1987. Development of a dispersion-strengthened Al-Fe-Ce alloy by mechanical alloying and related theoretical modeling of dislocations in composite materials. *PhD Thesis*, Stanford University, Los Angeles, CA .

Panichkina, V.V.,1967. Activated sintering of tungsten with small additions of nickel, Poroshkovaya Metallurgiya(In Russian), **2:** 1-5.

Powder Diffraction Files: Card No:04-0806, Database Edition, The International Centre for Diffraction Data (ICDD).

Powder Diffraction Files: Card No:19-0850, Database Edition, The International Centre for Diffraction Data (ICDD).

Powder Diffraction Files: Card No:25-0990, Database Edition, The International Centre for Diffraction Data (ICDD).

Powder Diffraction Files: Card No:35-0741, Database Edition, The International Centre for Diffraction Data (ICDD).

Powder Diffraction Files: Card No:62-2850, Database Edition, The International Centre for Diffraction Data (ICDD).

Powder Diffraction Files: Card No:83-1344, Database Edition, The International Centre for Diffraction Data (ICDD).

Redsten, A.M., Klier, E.M., Brown, A.M., Dunand, D.C., 1995. Mechanical properties and microstructure of cast oxide-dispersion-strengthened aluminum, *Materials Science and Engineering A,* **201:** 88-102.

Ring, T.A.,1996. Sintering in Fundamentals of Ceramic Powder Proscessing and Synthesis: 781-874.

Ryu, H.J., Hong, S.H. and Baek, W.H., 2000. Microstructure and mechanical properties of mechanically alloyed and solid-state sintered tungsten heavy alloys, *Materials Science and Engineering A,***291:** 91–96.

Ryu, H.J., Hong, S.H., 2003. Fabrication and properties of mechanically alloyed oxide-dispersed tungsten heavy alloys, *Materials Science & Engineering A*, **363:** 179-184.

Sakasegawa, H., Tamura, M., Ohtsuka, S., Ukai, S., Tanigawa, H.,Kohyama, A., Fujiwara, M., 2008.Precipitation behaviour of oxide particles in mechanically powder of oxide-dispersion-strengthened steel, *Journal of Alloys and Compounds*, **452:** 2-6.

Samsonov, G.V. and Yakovlev, V.I.,1967. Activated Sintering of Tungsten with Nickel Additions.Poroshkovaya Metallurgiya(In Russian), **8:** 10-16.

Samsonov, G.V. and Yakovlev, V.I.,1969. Activation of the Sintering of Tungsten by the Iron-Group Metals.Poroshkovaya Metallurgiya(In Russian), **10:** 32-38.

Schwartz, M.M.,1984.Composite Materials Handbook, McGraw-Hill, New York.

Schwartz, M.M.,1997.Composite Materials-Vol.2., Prentice Hall, Portland, OR.

Shen, Y.L. and Chawla, N. 2001. On the correlation between hardness and tensile strength in particle reinforced metal matrix composites, *Materials Science and Engineering A,* **297:** 44-47

Song, G.M., Wang, Y.J. and Zhou, Y., 2002.The mechanical and thermophysical properties of ZrC/W composites at elevated temperature, *Materials Science and Engineering A,***334:** 223–232.

Song, G.M., Zhou, Y. and Wang, Y.J., 2003a. Effect of carbide articles on the ablation properties of tungsten composites, *Materials Characterization,***50:** 293– 303.

Song, G.M., Wang, Y.J. and Zhou, Y., 2003b. Thermomechanical properties of TiC particle-reinforced tungsten composites for high temperature applications, *International Journal of Refractory Metals & Hard Materials,***21:** 1–12.

Stjernstoft, T., 2004. Machining of some difficult-to-cut materials with rotary cutting tools, *PhD Thesis,* K.T.H., Stockholm.

Sun, L.Z., Liu, H.T. and Ju, J.W., 2003. Effect of particle cracking on elastoplastic behaviour of metal matrix composites, *Int. J. Numer. Meth. Eng,***56:** 2183–2198.

Suryanarayana, C.,2001. Mechanical alloying and milling, *Progress in Materials and Science,***46:** 1-184.

Suryanarayana, C., Ivanov, E. and Boldyrev, V.V., 2001. The science and technology of mechanical alloying, *Materials Science and Engineering A,***304–306:** 151–158.

Tang, H.G., Ma, X.F., Zhao, W., Yan, X.W., Yan, J.M. and Zhu, C.J., 2004. Crystallization of mechanically alloyed amorphous W–Mg alloy under high pressure, *Solid State Communications,***129:** 147–150.

Tjong, S.C. and Ma, Z.Y.,2000. Microstructural and mechanical characteristics of in situ metal matrix composites, Materials Science and Engineering, **29:** 49-113.

Toth, I.J. and Lockington, N.A.,1967. The Kinetics of Metallic Activation Sintering of Tungsten.J. Less-Common Met.,**12:** 353-365.

Upadhyaya, G.S.,2000. Sintered Metallic and Ceramic Materials: Preparation, Properties, and Applications**,** Wiley, New York.

Upadhyaya, G.S., 2001. Some issues in sintering science and technology. Materials Chemistry and Physics, **67:** 1-5.

Vacek, J., 1959. On Influencing the Sintering Behavior of Tungsten. Planseeberiche fur Pulvermetallurgie, **7:** 6-17.

Zhang, F.L., Wang, C.Y. and Zhu, M., 2003. Nanostructured WC/Co composite powder prepared by high energy ball milling, *Scripta Materialia,***49:** 1123–1128.

Zweck, A., Luther, W., 2003. Applications of Nanotechnology in Space Developments and Systems. Technological Analysis, VDI Technology Center Future Technologies Division, Duesseldorf, Germany

CURRICULUM VITAE

Full Name:Ömer Utku Demirkan

Place and Date of Birth:Üsküdar / 08.12.1986

Permanent Address: Selimiye Kışla Caddesi, Daye Kadın Sokak,No:59/2
Üsküdar/İSTANBUL

College: Burak Bora Anatolian High School (2001-2005)

University: Istanbul Technical University
Department of Metallurgical and Materials Engineering (2005-2009)